ELUCIDATING THE RELATIONSHIPS BETWEEN SURFACE-LEVEL OZONE AND METEOROLOGY

by

Gaige Hunter Kerr

A dissertation submitted to The Johns Hopkins University

in conformity with the requirements for the degree of

Doctor of Philosophy

Baltimore, Maryland

May 2020

Abstract

Surface-level ozone (O_3) is associated with respiratory morbidity and mortality, affects vegetation and ecosystems, and impacts the global climate. The cause of day-to-day variations in O_3 remains an open question and is key in interpreting past air quality as well as the ways that future climatic changes will affect air pollution. To this end, we investigate the drivers of O_3 variability on daily timescales across the Northern Hemisphere with a special emphasis on the United States. Using observations and chemical transport model simulations, we show that positive relationships between O_3 and meteorological variables such as temperature and humidity persist only across continental regions in the mid-latitudes ($\sim 35 - 60°$N); elsewhere, these relationships are weak or significantly negative. The covariance of O_3 with meteorology is driven by an association with transport, not a direct dependence on chemistry or emissions. We find that neither stagnation or cyclones can explain day-to-day variations in O_3 or extreme events. Ultimately, we tie spatial and temporal variations in the O_3-meteorology relationships to the jet stream. The jet stream regulates the surface-level mean meridional flow, which affects fluxes of O_3, heat, and moisture. These results provide significant gains in understanding the dominant role of transport on O_3 variability and reconcile

spatial variations in the relationships among O_3, temperature, humidity, and the jet stream.

Thesis Committee

Primary Readers

Darryn W. Waugh (Primary Advisor)
Professor
Morton K. Blaustein Department of Earth and Planetary Sciences
Johns Hopkins Krieger School of Arts and Sciences

Scot M. Miller
Assistant Professor
Department of Environmental Health and Engineering
Johns Hopkins Whiting School of Engineering

Alternate Reader

Benjamin Zaitchik
Associate Professor
Morton K. Blaustein Department of Earth and Planetary Sciences
Johns Hopkins Krieger School of Arts and Sciences

Acknowledgments

My thesis would not have been possible without the unwavering support of my advisor, Darryn Waugh. From him, I have learned everything from atmospheric dynamics to scientific writing to how things worked in the “olden days" (pre-2005). If I am lucky enough to advise students of my own someday, I hope to embody his gentle guidance, open-door policy, and ability to give space and freedom to invigorate scientific inquiry. I would also like to thank Ben Zaitchik and Anand Gnanadesikan, two other members of my committee, for their valuable conversations on research and career directions. Scot Miller, Sarah Strode, Susan Strahan, Luke Oman, and Steve Steenrod all provided support and mentorship in various ways throughout this journey, and I am thankful to each of them for enhancing the breadth and quality of my research and, more importantly, shaping my training as a scientist.

I was supported by by the Water, Health, and Climate Integrative Graduate Education and Research Traineeship Program (IGERT), sponsored by the NSF, and I am grateful not only for the generous financial support from this program but also for the interdisciplinary training I received. Additionally, I appreciate the financial support I received from the Morton K. Blaustein

Department of Earth & Planetary Sciences and NASA's Atmospheric Composition Modeling & Analysis (ACMAP) grant.

Most importantly, I am forever indebted to my friends who balanced the rigors of my PhD with time for leisure and relaxation. To Joe, Mattia, and Mariah: my experience in Olin Hall and Baltimore would be drastically different without the three of you. Your work ethics motivated me to push on when I felt lost or sidetracked, and your company always gave me a reason to look forward to life outside of Olin Hall. Karim and Shane: I'm very thankful that you both, in different ways, encouraged me to leave my desk and spend time hiking, backpacking, running, rock climbing, and biking. Finally, I would like to thank Eric. Your companionship and support mean the world to me.

Table of Contents

List of Tables

List of Figures

Abbreviations

$\mu\mathbf{g\ m}^{-3}$ micrograms per cubic meter.

$\mathbf{CH_4}$ methane.

CO carbon monoxide.

$\mathbf{NO_3^-}$ nitrate.

$\mathbf{NO_x}$ nitrogen oxides (NO+NO_2).

NO nitric oxide.

$\mathbf{O_3}$ ozone.

$\mathbf{SO_2}$ sulfur dioxide.

$\mathbf{^{\bullet}OH}$ hydroxyl.

AQS Air Quality System.

ASI Air Stagnation Index.

CASTNet Clean Air Status and Trends Network.

CEMS Continuous Emission Monitoring Systems.

CTM chemical transport model.

DJF December-January-February.

EPA Environmental Protection Agency.

EW equatorward.

GMI CTM Global Modeling Initiative chemical transport model.

IPCC Intergovernmental Panel on Climate Change.

JJA June-July-August.

MERRA Modern Era Retrospective-Analysis for Research and Applications.

MERRA-2 Modern Era Retrospective-Analysis for Research and Applications, Version 2.

NAAQS National Ambient Air Quality Standards.

NASA National Aeronautics and Space Administration.

PAN peroxyacyl nitrates.

PBL planetary boundary layer.

PBLH planetary boundary layer height.

$PM_{2.5}$ particulate matter with a diameter ≤ 2.5 μm.

ppbv parts per billion by volume.

PW poleward.

$\mathbf{T}_{2m}$ 2-meter temperature.

U.S. United States.

VOC volatile organic compounds.

Chapter 1

Introduction

Ozone (O_3) is instrumental for chemical processes in Earth's troposphere despite its low abundance, which is generally on the order of 10^1 parts per billion by volume (ppbv) (Tarasick and Slater, 2008). At natural background levels, O_3 controls the oxidizing capacity of the troposphere due to its role in the formation of hydroxyl ($^{\bullet}OH$), and, at higher levels, O_3 is an air pollutant with damaging effects on human health, vegetation, and the built environment and acts as a greenhouse gas (Bojkov, 1986; Cooper et al., 2014).

Ozone was formally discovered by Christian Friedrich Schönbein in 1840 (Cooper et al., 2014). Schönbein recognized that the odor associated with O_3 was similar to the odor in the air after lightning and suggested that O_3 was present in the atmosphere (Bojkov, 1986). Using primitive methods, Schönbein began measuring O_3 in the atmosphere. During this time O_3 was the subject of intense public interest and study, and Physician Cornelius Fox remarked, "to the Philosopher, the Physician, the Meteorologist, and the Chemist, there is perhaps no subject more attractive than that of ozone" (Fox, 1873). By the middle of the 1870s, there were around 300 sites routinely measuring O_3,

thus establishing its importance as a constituent in the atmosphere (Stolarski, 2001). Since the time of Schönbein and his contemporaries, the production of O_3 in the troposphere has been linked to photochemical processes, and the significance of O_3 for global atmospheric chemistry, the Earth's climate, and human health has been quantified.

1.1 Global relevance of ozone pollution

The main impacts associated with tropospheric O_3 pollution can be separated into impacts to (1) the global climate, (2) human health, and (3) crop productivity and food security. Here we present a summary of these impacts and motivate the importance of our research on tropospheric O_3.

Tropospheric O_3 is an important climate forcing agent, interacting with both solar and terrestrial radiation (Jacob and Winner, 2009). Reconstructed historical measurements from the 1800s as well as reliable *in-situ* networks, which began recording in the mid-nineteenth century, suggest that baseline tropospheric O_3 levels have increased five-fold between the late 1800s and early 1990s and by a factor of two between the 1950s and early 1990s (Cooper et al., 2014). Accordingly, the Intergovernmental Panel on Climate Change (IPCC) estimates changes in tropospheric O_3 have increased radiative forcing by 0.40 ($\pm$0.2) W m^{-2} since the pre-industrial period (Myhre et al., 2013). To provide additional context, the change in radiative forcing from methane (CH_4), a major greenhouse gas, is estimated to be 0.48 ± 0.05 W m^{-2} (Myhre et al., 2013).

Environmental pollution in all its forms was responsible for $\sim$ 9 million

premature deaths in 2015, and welfare losses from environmental pollution were estimated at $4.6 trillion USD, about 6.2% of global economic output (Landrigan et al., 2017). Of the $\sim$ 9 million premature deaths from environmental pollution, over half is from ambient air pollution. An estimated 4.2 $(3.7 - 4.8)$ million premature deaths annually are attributed to particulate matter with a diameter ≤ 2.5 μm ($PM_{2.5}$), while O_3 results in 0.3 $(0.1 - 0.4)$ million premature deaths annually (Landrigan et al., 2017). O_3 primarily affects morbidity and mortality through respiratory and cardiovascular effects, and the lifetimes of O_3 and its precursors allow for their transport on synoptic to global scales, impacting health in remote regions (Anenberg et al., 2009). Within the United States (U.S.), O_3 and $PM_{2.5}$ are the two pollutants responsible for the most widespread violations of the National Ambient Air Quality Standards (NAAQS) (Fiore et al., 2015).

Ozone poses a major threat to crop productivity. Stomatal leaf uptake of O_3, which reacts within internal plant tissues and interferes with physiological function (Tai and Val Martin, 2017), leads to crop losses totaling $\$11 - 18$ billion USD in the year 2000 alone (Avnery et al., 2011). Future climate and air quality scenarios suggest that the joint effects of O_3 and excess heat could have deleterious effects on crop production and food security; however, future regulatory measures aimed at reducing O_3 may be able to offset some of the warming impacts on agriculture (Tai et al., 2014; Tai and Val Martin, 2017).

1.2 Tropospheric ozone budget

Within the troposphere, O_3 is a secondary pollutant and is therefore not directly emitted. Its production depends on two main groups of precursors: nitrogen oxides ($NO+NO_2$) (NO_x) and volatile organic compounds (VOC). Production of O_3 occurs on the order of seconds to minutes through a chain of photochemical reactions (Monks et al., 2015):

$$NO_2 + h\nu \longrightarrow NO + O(^3P) \tag{1.1}$$

$$O(^3P) + O_2 + M \longrightarrow O_3 + M \tag{1.2}$$

$$NO + O_3 \longrightarrow O_2 + NO_2, \tag{1.3}$$

where the photolysis of Reaction 1.1 occurs at wavelength $\lambda < 424$ nm. Reactions 1.1-1.3 contribute to null O_3 production; however, the presence of oxidant radicals provides additional pathways to convert NO to NO_2 in ways other than Reaction 1.3, and thereby increase O_3. These oxidant radicals are formed from the oxidation of carbon monoxide (CO), methane (CH_4), and non-methane VOC via $^{\bullet}OH$ (e.g., Lu et al., 2019). As such, O_3 production is sensitive to chemical regimes and varies non-linearly with NO_x and VOC. Additional details surrounding tropospheric O_3 can be found in Sillman (1999) and Pusede et al. (2014).

Ozone has a short lifetime, ranging from hours in polluted urban regions to weeks in the free troposphere (Monks et al., 2015). As we will show,

the O_3 budget in the troposphere depends not only on the aforementioned photochemical processes but is also regulated by physical and dynamical processes, which are largely the subject of this thesis.

Over continental regions, loss of O_3 primarily occurs via deposition. During a process known as dry deposition, vertical transport within the atmosphere brings O_3 to Earth's surface; and, as O_3 is a reactive gas, it readily deposits on most surfaces (Monks et al., 2015). During the day when stomata are typically open, dry deposition principally occurs via stomatal uptake (Monks et al., 2015).

Although our primary focus is on O_3, we also discuss particulate matter with a diameter ≤ 2.5 μm ($PM_{2.5}$). Unlike O_3, which is entirely a secondary pollutant in the troposphere, $PM_{2.5}$ is both a primary and secondary pollutant as it is directly emitted from surface source and is formed in the atmosphere through aqueous- and gas-phase reactions (Fiore et al., 2015). $PM_{2.5}$ composition is spatiotemporally varied and is comprised of a variety of chemical components, including black and organic carbon, sulfates, and nitrates (Lippmann, 2012; Fiore et al., 2015). Similar to O_3, loss of $PM_{2.5}$ principally occurs through deposition (both wet and dry). As we will see in Section 1.3, both $PM_{2.5}$ and O_3 are linked to variations in surface-level meteorology.

1.3 Ozone-meteorology relationships

The concentrations of O_3, $PM_{2.5}$, and other pollutants at Earth's surface are regulated by three main groups of processes: transport, chemistry, and emissions (Figure 1.1). These processes are all directly dependent upon or associated

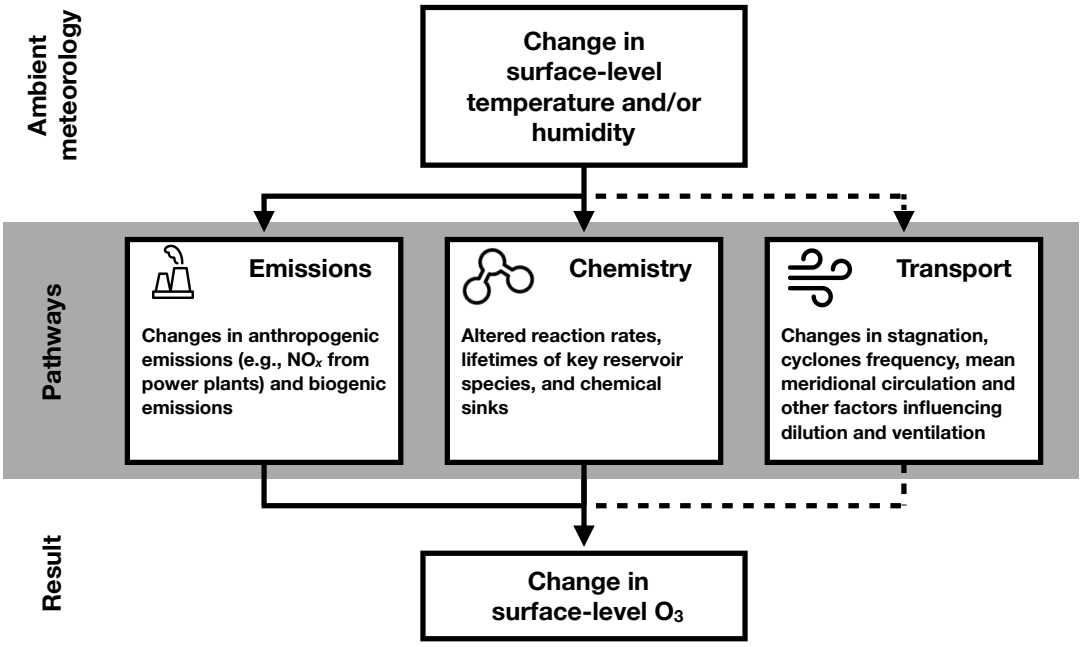

Figure 1.1: Pathways that link changes in the ambient meteorology to surface-level O_3. Solid lines represent a direct dependence, and dashed lines represent an indirect association. Additional discussion is provided in Section 1.3.

with a large number of meteorological variables (Jacob and Winner, 2009). Camalier et al. (2007) found that $\sim$ 80% of the variance of O_3 in the eastern U.S. could be explained by a generalized linear model with ambient temperature and relative humidity. A mechanistic understanding of the drivers of the O_3-temperature and O_3-humidity relationships is key to understanding the basic science of O_3 and needed to effectively regulate air quality and O_3 (and $PM_{2.5}$) pollution in the future (Pusede et al., 2015).

Rates of both natural and anthropogenic emissions are linked to the prevailing weather conditions (Figure 1.1). Higher temperatures increase biogenic VOC emissions (e.g., isoprene and terpenes), which can accelerate O_3 production (Jacob and Winner, 2009; Lu et al., 2019). In the same vein, the biogenic

emission of $PM_{2.5}$ precursors such as agricultural ammonia and VOC increase with temperature (Tai et al., 2012). He et al. (2013) suggested that temperature-dependent emissions of anthropogenic NO_x from air conditioner demand can account for at least one-third of the observed increase of O_3 with temperature in the mid-Atlantic U.S.. Romer et al. (2018) found that the temperature-driven increase of soil NO_x emissions (by soil microbes) yield nearly half the increase of O_3 with temperature for the rural southeastern U.S.. It is an open question as to whether these findings hold over other regions as well as the roles of other sources of natural and anthropogenic emissions relevant to O_3 photochemistry and their connections with meteorology.

The chemistry underpinning O_3 production is largely Arrhenius in form, thereby increasing with higher temperatures (Pusede et al., 2015) (Figure 1.1). The effect of ambient temperatures on O_3 chemistry also reflects, in part, the thermal stability of peroxyacyl nitrates (PAN) and the role of PAN as a reservoir species for NO_x (Jacob and Winner, 2009). The ambient humidity can also alter the efficiency and partitioning of chemical reactions (Lu et al., 2019); however, the exact relationship between O_3 and humidity via chemistry is more complicated and are sensitive to the chemical background condition (i.e., ambient NO_x concentrations; Jacob and Winner, 2009; Lu et al., 2019). The ambient temperature and humidity also influence $PM_{2.5}$ via chemistry. Higher temperature favors faster sulfur dioxide (SO_2) oxidation but lower nitrate (NO_3^-) and VOC concentrations on account of their volatility, and higher humidity promotes aqueous phase ammonium nitrate and sulfate production (Tai et al., 2012)

Variations in ambient temperature and humidity are associated with different meteorological, or transport, patterns that affect O_3 (Figure 1.1). The ventilation and dilution of O_3 and other pollutants from their source region(s) often correlates with temperature and humidity (Fiore et al., 2015). To this end, considerable attention has been given to stagnation, a phenomenon characterized by light winds and stable conditions (Jacob and Winner, 2009; Lu et al., 2019). Shifts of transport patterns influence O_3 by redistributing O_3 and its precursors. Examples of these patterns include synoptic-scale features such as the cold fronts associated with mid-latitude cyclones and subtropical highs (e.g., Bermuda high, West Pacific subtropical high) (Lu et al., 2019). Vertical transport can bring O_3 and $PM_{2.5}$ to Earth's surface where loss can occur via deposition (Monks et al., 2015).

Together, these drivers result in an approximately linear correlation of O_3 with temperature (Pusede et al., 2015), while the O_3-humidity relationship has mixed sign (e.g., Tawfik and Steiner, 2013; Kavassalis and Murphy, 2017). Moreover, some of the O_3-humidity relationship could reflect a joint association of air mass properties rather than cause-and-effect (Jacob and Winner, 2009).

The relative roles of these different drivers on the O_3-meteorology relationships have been the subject of several studies (e.g., Jacob et al., 1993; He et al., 2013; Kavassalis and Murphy, 2017; Romer et al., 2018), but there is little consensus as to which driver dominates the O_3-meteorology relationships, the spatial and temporal scales over which the driver(s) hold, and how future climate changes could affect O_3 (Pusede et al., 2015). As such, the primary

aim of this thesis is to improve the community's qualitative and quantitative understanding of the meteorological drivers of local-to-global O_3 pollution.

1.4 Outline

In Chapter 2 we examine how surface-level O_3 covaries with temperature across the U.S. and isolate how temperature affects transport, chemistry, and anthropogenic NO_x emissions. In doing so, we answer the following:

- How does the Global Modeling Initiative chemical transport model (GMI CTM) perform against *in-situ* observations, especially as temperature dependencies are isolated within the GMI CTM?
- What are the relative roles of transport, chemistry, and anthropogenic NO_x emissions in driving the O_3-temperature relationship?

As we will show, the temperature is linked to O_3 through an indirect association with transport.

Having uncovered this, in Chapter 3 we explore the role of a particular transport-related feature - stagnation - that could be responsible for connecting temperature with O_3, and we uncover the connections between pollutants (both O_3 and $PM_{2.5}$) and stagnation across the contiguous U.S.. In doing so we address these key questions:

- Are ambient concentrations of summer *in-situ* O_3 and $PM_{2.5}$ measurements temporally correlated with temperature and stagnation, as characterized by the Air Stagnation Index (ASI), and do extreme pollution events co-occur with extreme stagnation events?

- What is the relationship between ambient temperature and stagnation, and can stagnation thus provide a transport-related mechanism to tie temperature with pollutant variability?

In Chapter 4 we expand our geographic focus to encompass the entire Northern Hemisphere and explore the roles of large-scale transport features such as the jet stream, cyclones, and mean meridional circulation and their impact on O_3 variability and its covariance with temperature and humidity. We specifically pose and answer the following:

- What is the connection of the jet stream with surface-level O_3, temperature, and humidity?
- Which transport-related feature at the surface both affects the O_3-meteorology relationships and is associated with flow aloft (i.e., the jet stream)?

While Chapter 4 documents the relationship between the jet stream and O_3, it leaves unanswered questions regarding the dynamical source of the O_3-jet relationship and why there are differences in this relationship between continental and maritime regions.

The background O_3 gradient as well as the coupling between the jet stream and the near-surface meridional wind could lead to differences in the O_3-jet relationship. We investigate these potential drivers in Chapter 5 as a follow-up to Chapter 4 and address the following:

- How can idealized tracers lend insight to the correlation between the jet stream and O_3?

- Does the source region of tracers together with the relationship between the jet and near-surface meridional wind influence the sign and strength of the correlation?

Finally, we summarize the major findings of this thesis and discuss future topics of interest regarding the surface-level O_3-meteorology relationships in Chapter 6.

References

Anenberg, Susan Casper, J. Jason West, Arlene M. Fiore, Daniel A. Jaffe, Michael J. Prather, Daniel Bergmann, et al. (2009). "Intercontinental Impacts of Ozone Pollution on Human Mortality". In: *Environmental Science & Technology* 43.17, pp. 6482–6487. DOI: 10.1021/es900518z.

Avnery, Shiri, Denise L. Mauzerall, Junfeng Liu, and Larry W. Horowitz (2011). "Global crop yield reductions due to surface ozone exposure: 2. Year 2030 potential crop production losses and economic damage under two scenarios of O_3 pollution". In: *Atmos. Environ.* 45.13, pp. 2297–2309. DOI: 10.1016/j.atmosenv.2011.01.002.

Bojkov, Rumen D. (1986). "Surface Ozone During the Second Half of the Nineteenth Century". In: *Journal of Climate and Applied Meteorology* 25.3, pp. 343–352. DOI: 10.1029/2019GL084649. URL: https://onlinelibrary.wiley.com/doi/abs/10.1029/2019GL084649.

Camalier, Louise, William Cox, and Pat Dolwick (2007). "The effects of meteorology on ozone in urban areas and their use in assessing ozone trends". In: *Atmos. Environ.* 41.33, pp. 7127–7137. DOI: 10.1016/j.atmosenv.2007.04.061.

Cooper, O. R., D. D. Parrish, J. Ziemke, N. V. Balashov, M. Cupeiro, I. E. Galbally, et al. (2014). "Global distribution and trends of tropospheric ozone: An observation-based review". In: *Elementa: Science of the Anthropocene*, p. 000029. DOI: 10.12952/journal.elementa.000029. URL: http://www.elementascience.org/articles/10.12952/journal.elementa.000029.

Fiore, Arlene M., Vaishali Naik, and Eric M. Leibensperger (2015). "Air quality and climate connections". In: *J. Air Waste Manag. Assoc.* 65.6, pp. 645–685. DOI: 10.1080/10962247.2015.1040526.

Fox, Cornelius B. (1873). *Ozone and antozone: Their history and nature. When, where, why, how is ozone observed in the atmosphere?* London: J. & A. Churchill.

He, Hao, Linda Hembeck, Kyle M. Hosley, Timothy P. Canty, Ross J. Salawitch, and Russell R. Dickerson (2013). "High ozone concentrations on hot days:

The role of electric power demand and NO_x emissions: Ozone and power demand on hot days". In: *Geophys. Res. Lett.* 40.19, pp. 5291–5294. DOI: 10.1002/grl.50967.

Jacob, Daniel J. and Darrell A. Winner (2009). "Effect of climate change on air quality". In: *Atmos. Environ.* 43.1, pp. 51–63. DOI: 10.1016/j.atmosenv.2008.09.051.

Jacob, Daniel J., Jennifer A. Logan, Rose M. Yevich, Geraldine M. Gardner, Clarisa M. Spivakovsky, Steven C. Wofsy, et al. (1993). "Simulation of summertime ozone over North America". In: *Journal of Geophysical Research* 98.D8, p. 14797. DOI: 10.1029/93JD01223.

Kavassalis, Sarah C. and Jennifer G. Murphy (2017). "Understanding ozone-meteorology correlations: A role for dry deposition". In: *Geophys. Res. Lett.* 44.6, pp. 2922–2931. DOI: 10.1002/2016GL071791.

Landrigan, Philip J, Richard Fuller, Nereus J R Acosta, Olusoji Adeyi, Robert Arnold, Niladri (Nil) Basu, et al. (2017). "The Lancet Commission on pollution and health". In: *The Lancet*. DOI: 10.1016/S0140-6736(17)32345-0.

Lippmann, Morton (2012). "Particulate matter (PM) air pollution and health: regulatory and policy implications". In: *Air Quality, Atmosphere & Health* 5.2, pp. 237–241. DOI: 10.1007/s11869-011-0136-5.

Lu, Xiao, Lin Zhang, and Lu Shen (2019). "Meteorology and Climate Influences on Tropospheric Ozone: A Review of Natural Sources, Chemistry, and Transport Patterns". In: *Curr. Pollut. Rep.* 5.4, pp. 238–260. DOI: 10.1007/s40726-019-00118-3.

Monks, P. S., A. T. Archibald, A. Colette, O. Cooper, M. Coyle, R. Derwent, et al. (2015). "Tropospheric ozone and its precursors from the urban to the global scale from air quality to short-lived climate forcer". In: *Atmos. Chem. Phys.* 15.15, pp. 8889–8973. DOI: 10.5194/acp-15-8889-2015.

Myhre, G., D. Shindell, F.-M. Bréon, W. Collins, J. Fuglestvedt, J. Huang, et al. (2013). "Anthropogenic and Natural Radiative Forcing". In: *Climate Change 2013: The Physical Science Basis. Contribution of Working Group I to the Fifth Assessment Report of the Intergovernmental Panel on Climate Change*. Ed. by T.F. Stocker, D. Qin, G.-K. Plaand othersttner, M. Tignor, S.K. Allen, J. Boschung, et al. Cambridge, United Kingdom and New York, NY, USA: Cambridge University Press. Chap. 8, pp. 659–740. DOI: 10.1017/CBO9781107415324.018.

Pusede, S. E., D. R. Gentner, P. J. Wooldridge, E. C. Browne, A. W. Rollins, K.-E. Min, et al. (2014). "On the temperature dependence of organic reactivity, nitrogen oxides, ozone production, and the impact of emission controls in

San Joaquin Valley, California". In: *Atmos. Chem. Phys.* 14.7, pp. 3373–3395. DOI: 10.5194/acp-14-3373-2014.

Pusede, Sally E., Allison L. Steiner, and Ronald C. Cohen (2015). "Temperature and recent trends in the chemistry of continental surface ozone". In: *Chem. Rev.* 115.10, pp. 3898–3918. DOI: 10.1021/cr5006815.

Romer, Paul S., Kaitlin C. Duffey, Paul J. Wooldridge, Eric Edgerton, Karsten Baumann, Philip A. Feiner, et al. (2018). "Effects of temperature-dependent NO_x emissions on continental ozone production". In: *Atmos. Chem. Phys.* 18.4, pp. 2601–2614. DOI: 10.5194/acp-18-2601-2018.

Sillman, Sanford (1999). "The relation between ozone, NO_x and hydrocarbons in urban and polluted rural environments". en. In: *Atmos. Environ.* P. 25.

Stolarski, Richard S. (2001). "History of the study of atmospheric ozone". In: *Ozone: Science & Engineering* 23.6, pp. 421–428. DOI: 10.1080/01919510108962025.

Tai, A. P. K., L. J. Mickley, D. J. Jacob, E. M. Leibensperger, L. Zhang, J. A. Fisher, et al. (2012). "Meteorological modes of variability for fine particulate matter (PM2.5) air quality in the United States: implications for PM2.5 sensitivity to climate change". In: *Atmos. Chem. Phys.* 12.6, pp. 3131–3145. DOI: 10.5194/acp-12-3131-2012.

Tai, Amos P. K., Maria Val Martin, and Colette L. Heald (2014). "Threat to future global food security from climate change and ozone air pollution". In: *Nature Climate Change* 4.9, pp. 817–821. DOI: 10.1038/nclimate2317.

Tai, Amos P.K. and Maria Val Martin (2017). "Impacts of ozone air pollution and temperature extremes on crop yields: Spatial variability, adaptation and implications for future food security". In: *Atmos. Environ.* 169, pp. 11–21. DOI: 10.1016/j.atmosenv.2017.09.002.

Tarasick, D.W. and R. Slater (2008). "Ozone in the troposphere: Measurements, climatology, budget, and trends". In: *Atmosphere-Ocean* 46.1, pp. 93–115. DOI: 10.3137/ao.460105.

Tawfik, Ahmed B. and Allison L. Steiner (2013). "A proposed physical mechanism for ozone-meteorology correlations using land-atmosphere coupling regimes". In: *Atmos. Environ.* 72, pp. 50–59. DOI: 10.1016/j.atmosenv.2013.03.002.

Chapter 2

Disentangling the Drivers of the Summertime Ozone-Temperature Relationship Over the U.S.

This chapter is published by the *Journal of Geophysical Research* (Kerr et al., 2019).

Summertime surface-level O_3 is known to vary with temperature, but the relative roles of different processes responsible for causing the O_3-temperature relationship are not well quantified. In this study we use simulations of National Aeronautics and Space Administration (NASA)'s GMI CTM to isolate and assess the relative impact of atmospheric transport, chemistry, and emissions on large-scale O_3 variability, events, and its covariance with temperature. Using observations from CASTNet in the contiguous U.S., we show that the GMI CTM reproduces the spatiotemporal variability of O_3 and its relationship with temperature during the summer. We use the change in O_3 given a change in temperature (dO_3/dT) along with other metrics to understand differences

between our simulations. In regions with moderate to strong positive correlations between temperature and O_3 such as the Northeast, Great Lakes, and Great Plains, temperature's association with transport yields a majority of the total O_3-temperature relationship ($\sim$ 60%), while temperature-dependent chemistry and anthropogenic NO emissions play smaller roles ($\sim$ 30% and $\sim$ 10%, respectively). There are regions, however, with insignificant correlations between temperature and O_3, and our findings suggest that transport is still an important driver of O_3 variability in these regions, albeit not correlated with temperature. Transport is not directly dependent on temperature but rather is linked through an indirect association, and it is therefore important to understand the exact mechanisms that link transport to O_3 and how these mechanisms will change in a warming world.

2.1 Introduction

It is well-known that high concentrations of surface-level O_3 coincide with high temperatures (e.g., Bloomer et al., 2009; Schnell and Prather, 2017; Kerr and Waugh, 2018). This relationship is often quantified by the slope of the linear regression of O_3 versus temperature, herein referred to as "dO_3/dT." The observed dO_3/dT in the U.S. generally ranges from 0-6 ppbv K^{-1}, with higher values found (1) in the Northeastern compared with the Southeastern U.S. (e.g., Rasmussen et al., 2012; Brown-Steiner et al., 2015), (2) in urban regions (e.g., Sillman and Samson, 1995), and (3) during periods with higher anthropogenic NO_x emissions (e.g., Bloomer et al., 2009; Rasmussen et al., 2012; Rasmussen et al., 2013).

By virtue of the coincidence of O_3 and temperature, some have raised the possibility of a warming planet worsening O_3 pollution irrespective of changes in emissions or other human activities. This idea has been termed the "climate penalty," or variations thereof, and is most often quantified by dO_3/dT (Wu et al., 2008; Bloomer et al., 2009; Rasmussen et al., 2012; He et al., 2013a; Rasmussen et al., 2013; Pusede et al., 2015; Jing et al., 2017). However, a wide range of processes influences O_3 and dO_3/dT, and these processes may not respond uniformly to future changes in the climate. On account of this, it is important to understand the processes responsible for dO_3/dT, their relative roles in order to interpret the variability and historical trends of O_3 in light of emission reductions (e.g., He et al., 2013b; de Gouw et al., 2014; Simon et al., 2015), and how future changes in the climate system will affect dO_3/dT.

The processes comprising dO_3/dT can be cast in a general form as the sum of partial derivatives (Rasmussen et al., 2012):

$$\frac{dO_3}{dT} = \sum_i \frac{\partial O_3}{\partial F_i} \frac{\partial F_i}{\partial T}, \tag{2.1}$$

where T is temperature and F_i refers to a process that is temperature dependent or associated with temperature. One example of F_i is chemical reactions: an increase in temperature increases the rates and energies of gas collisions and thereby affects the production and lifetimes of O_3, its precursor species, and its sinks (Jacob et al., 1993; Sillman and Samson, 1995; Pusede et al., 2015). Another F_i is atmospheric humidity, which is dependent upon temperature and affects photochemistry and O_3 production. The emissions of O_3 precursors

such as isoprene, monoterpenes, and other biogenic VOC represent yet another F_i as their emission rates depend on ambient temperature (Sillman and Samson, 1995; Jacob and Winner, 2009; Pusede et al., 2015). Although often overlooked, anthropogenic NO_x emissions are also dependent on temperature, increasing on hot days due to the electricity demand for air conditioning (He et al., 2013a; Abel et al., 2017).

Both vertical and horizontal transport are other examples of F_i, although not direct dependencies in the same vein as kinetics or emissions. Horizontal transport is inextricably associated with temperature variability and impacts O_3 through antecedent meteorological conditions ranging from frontal passages on mesoscales to stagnating high pressure systems on synoptic scales (Leibensperger et al., 2008; Barnes and Fiore, 2013; Fiore et al., 2015). Ultimately, these meteorological conditions influence mixing and dispersion and can lead to the accumulation of O_3 and its precursors under conditions amenable for photochemistry. With respect to vertical transport, PBL dynamics affect the entrainment and dilution of polluted air (Sillman and Samson, 1995), and dry deposition, the dominant sink for ozone in most of the continental surface layer (Racherla and Adams, 2006; Kavassalis and Murphy, 2017), varies with temperature (Wesely, 1989).

While dO_3/dT can be easily elicited from observations, disentangling the individual processes comprising this total derivative (Equation 2.1) is empirically more difficult. Previous studies have examined the role of different processes linking O_3 with temperature, but there is no general consensus on the relative roles of the drivers of the O_3-temperature relationship. For

example, Jacob et al. (1993) used model simulations over the continental U.S. with and without fixed temperature and determined that while a part of the O_3-temperature relationship reflected the association of high temperature with stagnation, most of the temperature dependence could be attributed to chemistry, mainly to the storage of NO_x by PAN at low temperatures but also to the association of high temperatures with stagnation. Using emissions data from the 1990s and 2000s and observations from the DISCOVER-AQ campaign in 2011, He et al. (2013a) estimated that one-third of dO_3/dT is attributable to temperature-dependent, anthropogenic NO_x emissions in the Mid-Atlantic U.S. Pusede et al. (2015) synthesized observations and modeling studies from around the U.S. to suggest that trends in dO_3/dT imply chemistry, not meteorology, controls dO_3/dT, and further NO_x reductions in NO_x-limited regions will cause dO_3/dT will reach a minimum in the future. Jing et al. (2017) reported that NO_x emission reductions were less effective at reducing dO_3/dT in the Midwestern U.S. during the 2000s and 2010s compared with the 1990s. These contradictory results motivate this study to systematically examine the drivers of the O_3-temperature relationship.

In this paper we combine observations together with CTM simulations to quantify the processes that link temperature to O_3. Rather than isolating individual examples of F_i (Equation 2.1), we group processes dependent upon or associated with temperature into three categories: transport, chemistry, and anthropogenic NO emissions. Sensitivity simulations are performed to examine the roles of these different pathways on O_3 variability, extremes, and its relationship with temperature over the contiguous U.S. Our main

objective is to determine the relative role of the indirect transport-temperature-O_3 pathway compared to the direct temperature dependence of chemistry and anthropogenic NO emissions by examining the cumulative impact of different groups of processes before examining the role of individual processes.

Section 2.2 describes NASA's GMI CTM, observations, and our statistical approach to evaluating results. We first evaluate the performance of the CTM against observations and demonstrate that the CTM captures the main features of surface-level O_3, its extremes and variability, and its relationship with temperature over the contiguous U.S. (Section 2.3). Sections 2.4 and 2.5 show results across the Northeastern U.S. and contiguous U.S., respectively, and we discuss the role of anthropogenic NO emissions on O_3 in light of observed precursor emissions reductions (Section 2.4.1).

2.2 Data and Methodology

2.2.1 Observations

We use hourly O_3 and temperature observations from the Clean Air Status and Trends Network (CASTNet) for summers JJA 2008-2010 at 78 sites across the contiguous U.S. to calculate the observed O_3-temperature relationship at individual CASTNet sites (Figure 2.1). From these hourly data, we average observations taken over 1300-1400 hours local time to produce daily afternoon values, commensurate with CTM output (Section 2.2.2). The summers in our measuring period reflect a period during which NO_x emissions and O_3 have stabilized across the Eastern U.S. following drastic reductions in NO_x emissions due to regulatory measures (He et al., 2013b). Additional discussion

on CASTNet history, monitor siting, and site relocations can be found in Cooper et al. (2012).

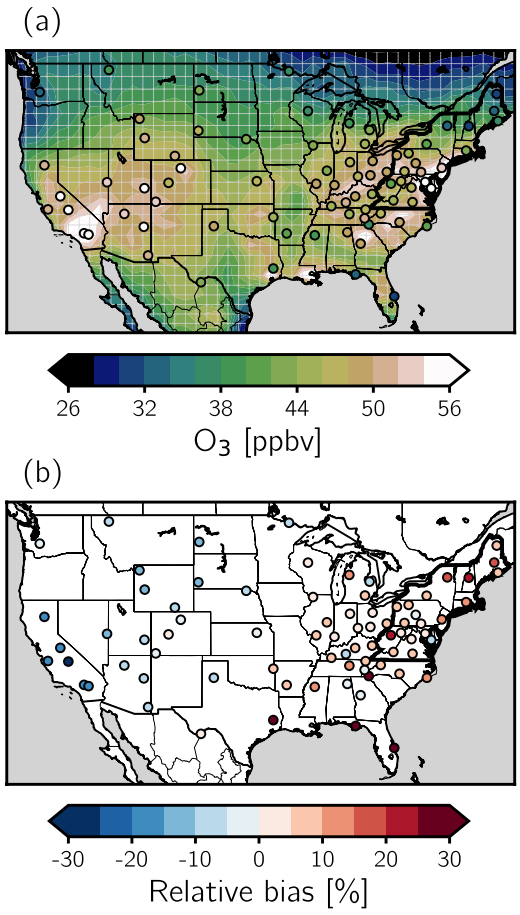

Figure 2.1: (a) Daily afternoon O_3 from observations (scatterpoints) and the +AnthroNO simulation (contours) averaged over the measuring period, summers 2008–2010. The resolution of the CTM, 1° latitude × 1.25° longitude, is represented by the parallels and meridians, respectively. (b) Scatterpoints indicate the O_3 relative bias of mean daily afternoon O_3 at individual CASTNet sites and their co-located CTM grid cell. Note the color scale saturates at −30% and 30% for better contrast. The Northeastern U.S. is outlined in black.

Anthropogenic NO_x emissions from stationary industrial sources (e.g.,

power plants, factories) are measured by the EPA CEMS We consider daily cumulative NO_x emissions recorded at these stationary sources, here shown in Figure 2.2.

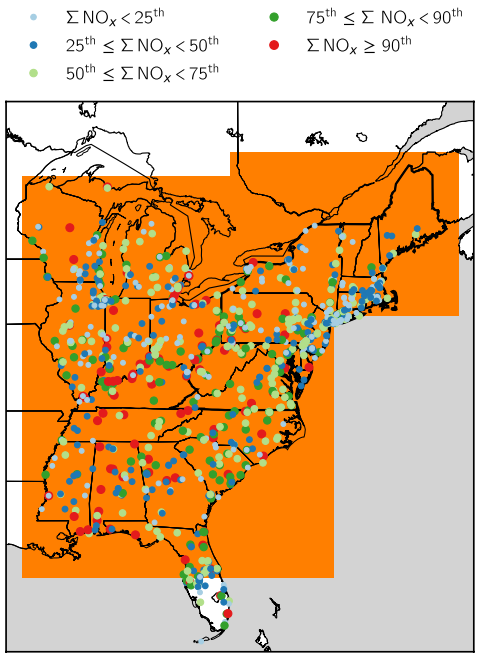

Figure 2.2: Stationary industrial facilities in the Eastern U.S. that report daily cumulative NO_x emissions to CEMS are classified in terms of the percentile rank of their cumulative NO_x emissions over summers 2008-2010. The region in which anthropogenic NO_x emissions are perturbed in the +AnthroNO simulation is shown in orange and generally encompasses the 26 states east of the Mississippi River and the District of Columbia. The Northeastern U.S. is outlined in black.

2.2.2 Model Description and Simulations

Our primary tool for disentangling the drivers of the O_3-temperature relationship is simulations of the global GMI CTM. Meteorological fields from

the MERRA-2 (Gelaro et al., 2017) are provided to the CTM every 3 hours (Goldberg et al., 2017). Our simulations have a spatial resolution of 1° latitude × 1.25° longitude (Figure 2.1). The 72 level hybrid vertical coordinate is terrain-following for the first 31 levels, changing to true pressure at 164 hPa. Seven model levels lie below 900 hPa (∼ 1 km); and, in this study, we use output from the lowest model level, which has a thickness of ∼ 130 m. The model's stratosphere-troposphere chemical mechanism contains roughly 120 gas phase species and simulates over 400 reactions, including heterogeneous chemical reactions (Strahan et al., 2007; Duncan et al., 2007; Strahan et al., 2013).

Emissions of CO, NO, and non-methane VOC vary on monthly or interannual bases and are derived from the Emissions Database for Global Atmospheric Research (EDGAR) 3.2 inventory (Olivier et al., 2005). The EDGAR inventory is overwritten with regional inventories (e.g., NEI, CAC, EMEP, etc.) when applicable, and annual scaling factors are applied from the GEOS-Chem CTM. Isoprene emissions depend on climatological leaf area index, temperature, and photosynthetically active radiation and are calculated online via the Model of Emissions of Gases and Aerosols from Nature (MEGAN; Guenther et al., 1995; Guenther et al., 2012). Soil NO_x emissions, dependent upon temperature and precipitation, are also calculated online (Yienger and Levy, 1995). NO_x resulting from lightning could vary with temperature and impact surface-level O_3 concentrations. Within the GMI CTM, lightning is calculated with a two-step procedure involving (1) a determination of lightning flash frequency and lightning NO_x production rate for each model grid cell and (2)

the repartitioning of lightning NO_x emissions in the vertical column (Allen et al., 2010). However, it has been shown that the impact of lightning on surface-level O_3 is small in the contiguous U.S. (Murray, 2016).

Hourly surface O_3 was archived at only specific sites in the GMI CTM simulations; however, O_3 averaged between 1300-1400 hours local time is archived daily for every grid cell on the globe, thus allowing us to conduct a more comprehensive analysis than could be conducted with hourly output alone. Output averaged over 1300-1400 hours local time is referred to as "overpass2" in https://modelingguru.nasa.gov/docs/DOC-2313 as it coincides with the overpass time of the Afternoon Constellation ("A-Train") of Earth-observing satellites. The early afternoon, the time of satellite overpass, typically represents peak daily O_3 concentrations (Fiore, 2002). We refer to both model output and observations from this time as "afternoon" throughout this manuscript.

We compare modeled and observed O_3 at overpass time to the same quantities from hourly output averaged over 1100-1600 hours local time after Strode et al. (2015), and we find that both temporal averaging approaches yield comparable model-observation agreement and variability. For the summer of 2010, O_3 averaged over 1100-1600 hours local time at sites with hourly output in the Northeastern U.S. is generally within ~ 5 ppbv of O_3 at overpass time averaged over grid cells in the region (Figure 2.3). We find no appreciable spatial pattern in the bias (not shown).

To calculate the O_3-temperature relationship in the model we use the same reanalysis product that drives the CTM, MERRA-2, and abbreviate it

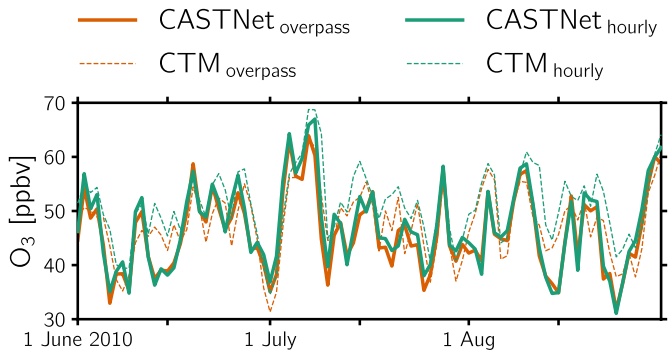

Figure 2.3: Summer 2010 Northeast-averaged O_3 from CASTNet and the GMI CTM using two approaches: "overpass" represents O_3 averaged over all CTM grid cells and CASTNet sites in the region at the time of afternoon satellite overpass (mean 1300-1400 hours local time), and "hourly" represents afternoon (mean 1100-1600 hours local time) CTM output averaged over CTM sites with hourly output and CASTNet sites in the region, similar to Strode et al. (2015).

as "T" in figures, tables, and equations. Since the MERRA-2 data have a higher resolution than that of the CTM, we degrade the MERRA-2 data from their native resolution (0.5° latitude × 0.625° longitude) to match the coarser resolution of the CTM using cubic splines for direct comparison. The MERRA-2 reanalysis has been shown to be in good agreement with observations in the mid-latitudes and an improvement over MERRA (Bosilovich, 2015).

We conduct three GMI CTM sensitivity simulations spanning summers 2008-2010 that isolate the influences of the three main groups of processes controlling $d\mathrm{O}_3/d\mathrm{T}$: transport, chemistry, and anthropogenic NO emissions (Section 2.1). Our approach to fix temperature as it pertains to certain processes within the CTM is similar to Jacob et al. (1993) and Porter and Heald (2019).

Transport: In this sensitivity simulation, the daily temperature dependence of chemical kinetics, fields related to solar radiation fluxes, and natural and anthropogenic emissions is removed ($\partial F_i/\partial \mathrm{T} = 0$) such that the variability of

Table 2.1: Summary of sensitivity simulations. We denote fields or processes with temperature variability reduced to monthly mean values by ✗ and fields or process with daily temperature variability by ✓.

	$\frac{\partial F_i}{\partial T} \neq 0$					
Simulation	**Transport**[a]	**Loss**[b]	**Reaction Rates**	**Solar Radiation Fluxes**[c]	**Biogenic VOC Soil NO_x**	**Anthropogenic NO Emissions**
Transport	✓	✓	✗	✗	✗	✗
+Chemistry	✓	✓	✓	✓	✓	✗
+AnthroNO	✓	✓	✓	✓	✓	✓

[a] wind components, vertical mixing, convective mass flux, PBL height, pressure, water vapor
[b] precipitation, wet and dry deposition
[c] clouds, aerosols, surface albedo

these fields at each CTM grid cell is reduced to a monthly mean diurnal curves, and emissions vary only from month to month (Table 2.1). As a result, the only processes that have daily variability and an association with temperature on sub-daily or daily timescales are transport by wind components, convective mass flux, planetary boundary layer height (PBLH), pressure, vertical mixing, water vapor, precipitation, and deposition (Table 2.1). We include variations in deposition in this simulation as it is the principal sink for O_3 over the contiguous U.S. (Racherla and Adams, 2006; Kavassalis and Murphy, 2017).

+**Chemistry**: Our second sensitivity simulation includes the same processes in the Transport simulation but also includes the daily variability of temperature-dependent fields related to chemistry, which had had their variability fixed to monthly mean values or diurnal cycles in the Transport simulation. This simulation is denoted as "+Chemistry" for brevity, but the processes included in this simulation encompass more than just kinetics alone: all variables or processes that affect reaction rates and photolysis are allowed to vary (temperature, surface albedo, clouds, and other fields related to solar radiation fluxes; Table 2.1). Additionally, this simulation includes the temperature dependence of biogenic VOC (Table 2.1), and we note the potential for an additional sensitivity simulation focused solely on the impact of these biogenic emissions on the O_3-temperature relationship. The +Chemistry simulation is identical to the simulation used in Douglass et al., 2017 but at higher resolution. Additional details can be found under "HindcastMR2" at `https://gmi.gsfc.nasa.gov/merra2hindcast/`.

+**AnthroNO**: The third and final sensitivity simulation focuses on the role

of temperature-dependent, anthropogenic NO emissions (Table 2.1). The first two sensitivity simulations (Transport and +Chemistry) have only monthly mean NO emissions from anthropogenic sources. As discussed in Section 2.1, there are daily, temperature-dependent variations in anthropogenic NO emissions. In the +AnthroNO simulation we add daily variability to these emissions with the observed relationship between industrial NO_x emissions and temperature. It is important to note that although we examine the relationship between observed industrial NO_x emissions and temperature, the CTM's emissions inventory contains only NO emissions (as NO_x is primarily emitted as NO).

We consider the impact of anthropogenic NO emissions by perturbing the CTM's NO emissions. Daily variations are added in such a way that the monthly averages of the daily-varying NO emissions in the +AnthroNO ($\mathrm{NO}_{\mathrm{CTM}}(t)$) are equal to the monthly mean NO emissions ($\overline{\mathrm{NO}_{\mathrm{CTM}}}$) in the Transport and +Chemistry simulations; specifically,

$$\mathrm{NO}_{\mathrm{CTM}}(t) = \overline{\mathrm{NO}_{\mathrm{CTM}}}[1 + \zeta \cdot \mathrm{T}(t)], \tag{2.2}$$

where ζ is the sensitivity of industrial NO_x emissions to temperature. To calculate ζ, we use CEMS data from the Eastern U.S. and define the sensitivity as

$$\zeta = \frac{\partial \widehat{\mathrm{NO}}_{x,\,\mathrm{CEMS}}(t)}{\partial \mathrm{T}(t)}, \tag{2.3}$$

where $\widehat{\mathrm{NO}}_{x,\,\mathrm{CEMS}}(t)$ are daily industrial NO_x emissions normalized by their monthly mean values. We calculate ζ for 26 states in the Eastern U.S. and find

that ζ ranges from $2.6 \pm 1.8\%$ K^{-1} (Tennessee) to $15.0 \pm 6.1\%$ K^{-1} (Connecticut) during the 2000s. Averaged over the entire Eastern U.S. $\zeta = 5.6 \pm 1.2\%$ K^{-1}. Our CEMS NO_x-temperature sensitivity is slightly higher than other values reported in the literature: He et al. (2013a) determined $\zeta = 2.5 - 4.0\%$ K^{-1} for five states in the Mid-Atlantic U.S., and Abel et al. (2017) found $\zeta = 3.6 \pm 0.49\%$ K^{-1} in the Eastern U.S. However, we note that our sensitivity was calculated using different methods, geographic regions, and time periods than these other studies.

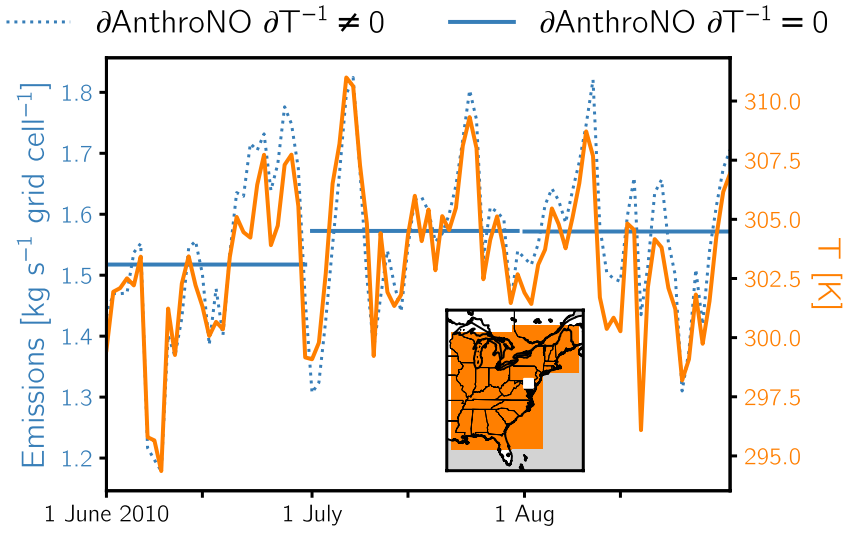

Figure 2.4: NO emissions from the emissions inventory of the +Chemistry simulation (solid blue) are shown alongside temperature-dependent NO emissions from the +AnthroNO simulation (dashed blue) and temperature (T) for the CTM grid cell shown in white in the inset map. Temperature-dependent NO emissions are applied to all grid cells in the shaded region of the inset map in the +AnthroNO simulation.

As industrial NO_x emissions contribute $\sim$ 60% to total ambient NO_x concentrations (He et al., 2013b), we perturb this percent of the NO in the emissions inventory. In our +AnthroNO simulation we apply our regionally-averaged sensitivity (i.e., 5.6% K^{-1}) to the shaded region in the inset map in Figure 2.4. Figure 2.4 illustrates how this sensitivity simulation's emissions inventory is temperature dependent compared with the emissions inventory for the +Chemistry simulation.

2.2.3 Metrics

We examine several different measures of the O_3-temperature relationship in both observations and our sensitivity simulations.

We use the Pearson product-moment correlation coefficient (r) to assess the temporal correlation between simulations and observations. Quantifying the significance of r requires us to calculate a critical value for r, r_c, below which the null hypothesis that there is no correlation between variables cannot be rejected. The magnitude of r_c is based on the sample size, and we derive an effective sample size (n') following Wilks (2011) for the Northeast-averaged O_3 due to the autocorrelation present in the time series. We find $n' \approx 64$ and, using $\alpha = 0.05$ for a two-tailed test, $r_c = 0.25$. Thus, for $r < r_c$ the correlation between variables is insignificant; however, in order to differentiate between greater degrees of linear relationships between our variables we refer to $0.25 < r < 0.5$ as moderately correlated and $r \geq 0.5$ as strongly correlated throughout the manuscript.

We define dO_3/dT as the slope of the Ordinary Least Squares (OLS) linear

regression of daily afternoon O_3 against daily afternoon temperature data from all summer days (= 92 days summer^{-1} $\times$3 summers) in our measuring period. In this study we use dO_3/dT to (1) evaluate the performance of the GMI CTM by examining the sensitivity of modeled O_3 to changes in temperature against the observed sensitivity and (2) quantify the relative differences in the sensitivity of O_3 to temperature between our simulations. Determining dO_3/dT with OLS is the most common approach in the literature (e.g. Bloomer et al., 2009; Rasmussen et al., 2012; Barnes and Fiore, 2013; Strode et al., 2015; Romer et al., 2018; Meehl et al., 2018) and allows us to compare our results with previous studies.

Differences between simulations are also examined in terms of the impact they have on days with extreme temperatures and O_3 concentrations. Similar to recent studies (e.g., Schnell and Prather, 2017; Sun et al., 2017; Kerr and Waugh, 2018), we define extremes in terms of exceedances above percentile thresholds. We adopt the 10^{th} and 90^{th} percentiles (P_{10} and P_{90}, respectively) as the thresholds for extreme O_3 and temperature events on both sides of the distributions, and we calculate the average O_3 concentration on days falling above (below) P_{90} (P_{10}). Specifically, we examine the enhancement (reduction) of O_3 on event days, and we define this as the difference between the average concentration on days exceeding (less than) the extreme threshold and days with median O_3 concentrations ($O_{3,\,P_{50}}$) or temperatures ($O_3(T_{P_{50}})$). Although using the 90^{th} percentile as a metric does not directly translate to exceedances of air quality standards (e.g., NAAQS in the U.S.), this approach ameliorates potential issues that model bias (Section 2.3) has on classifying days as above

or below an absolute threshold.

Our analysis is presented both in terms of a site-by-site or grid cell-by-grid cell basis and using regionally-averaged quantities. When we provide regionally averaged results, we first average O_3 and temperature over a given region and thereafter calculate r, dO_3/dT, or other metrics using these regionally-averaged quantities. Whether these metrics are calculated from regionally-averaged quantities or if they are calculated locally (at each grid cell) and then averaged over a region leads to similar values.

2.3 Model Evaluation

Before examining the results of our sensitivity simulations, we evaluate the CTM's representation of surface-level O_3 and its relationship with temperature with model-observation evaluation metrics detailed in Yu et al. (2006). For this evaluation we use the +AnthroNO simulation as this simulation includes all temperature dependencies considered in this study (Table 2.1) and, of our three simulations, should most closely mirror reality.

Observations show that the highest mean O_3 concentrations in the U.S. are found in Southern California and downwind regions, the Ohio River Valley, and Mid-Atlantic states, while the lowest concentrations occur in the Pacific Northwest and Northern New England (Figure 2.1a). The CTM generally captures this spatial variability. Although the bias and relative bias averaged over all CASTNet sites in the contiguous U.S. are low (0.20 ppbv and 1.97%, respectively; Figures 2.1b, 2.5a), there is a clear longitudinal pattern to the biases with a high model bias in the Eastern U.S. and a low model bias in

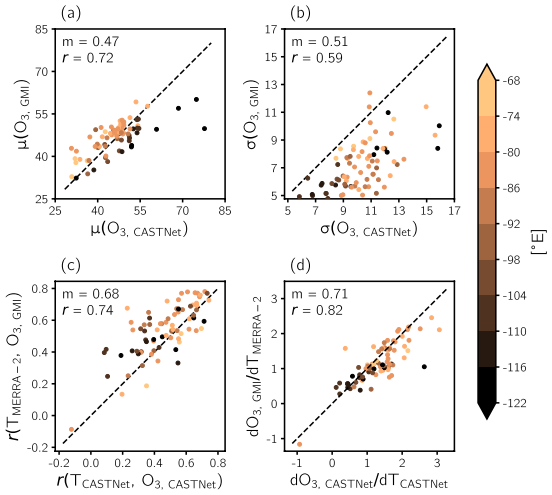

Figure 2.5: GMI CTM simulated metrics from the +AnthroNO simulation versus observed metrics from CASTNet: (a) mean O_3, (b) O_3 standard deviation, (c) the Pearson product-moment correlation coefficients (r) of O_3 and temperature, and (d) the slope of the OLS linear regression of O_3 versus temperature (dO$_3$/dT). Metrics are calculated with daily afternoon values for summers 2008-2010, and each scatter point corresponds to a CASTNet site in the contiguous U.S. and its coincident CTM grid cell with colors depicting the longitude of the site. The slope of the OLS linear regression (m) and r of the CTM versus CASTNet metrics are shown, along with the 1:1 line.

the West (Figure 2.1b). The bias at individual CASTNet sites and their co-located CTM grid cells ranges from -27.92 ppbv to 12.12 ppbv (Figure 2.5a), and the bias in the Northeast (outlined region in Figure 2.1a) is 3.15 ppbv. The modeled high bias in the Eastern U.S. is consistent with previous studies using other CTMs (e.g. Fiore et al., 2009; Rasmussen et al., 2012; Rieder et al., 2015; Brown-Steiner et al., 2015). These studies generally report a bias greater than 10 ppbv during the summer months and sometimes exceeding 30 ppbv with the exact magnitude of the bias dependent on the specific CTM used and the specific spatial domain considered. Also, even at coarser resolutions,

these CTMs are still capable of capturing synoptic-scale events (Fiore, 2003; Wu et al., 2008).

We note a tendency for the CTM to underestimate O_3 variability (Figure 2.5b), generally underestimating maximum concentrations and overestimating minimum concentrations by ~ 5 ppbv. Model resolution, dilution effects, and other theories have been proposed to explain this problem, which is common across CTMs (Yu et al., 2016). We acknowledge that this issue could affect our analysis of extreme O_3 events on both ends of the distribution, and our results pertaining thereto should be interpreted with this in mind.

To evaluate the ability of the GMI CTM to capture the observed timing of O_3 events, we compute r between daily afternoon O_3 at each CASTNet site and co-located CTM grid cell. For nearly all paired sites and grid cells $r(O_{3,\,\text{CASTNet}},\, O_{3,\,\text{GMI}}) \geq 0.5$; i.e., using our classification discussed in Section 2.2.3, the model and observations are strongly postively correlated at nearly all locations. Only six of 78 CASTNet sites and their co-located CTM grid cells have moderate correlations ($0.25 < r(O_{3,\,\text{CASTNet}},\, O_{3,\,\text{GMI}}) < 0.5$) with no detectable spatial pattern (not shown).

We next examine whether the model captures the observed O_3-temperature relationship across the U.S. Observed O_3 and temperature exhibit strong positive correlation in a broad swath extending westward from the Northeast to the Great Plains and in California with $r(T,\, O_3)$ exceeding 0.75 in some regions (Figure 2.6a). The observed correlation generally decreases with decreasing latitude, reaching a near-zero minimum in the Lower Mississippi River Valley (Figure 2.6a). Camalier et al. (2007) showed that temperature

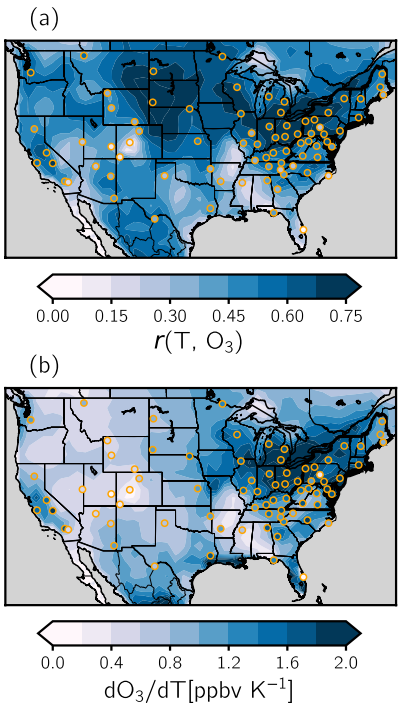

Figure 2.6: (a) $r(\mathrm{T}, \mathrm{O_3})$ and (b) $d\mathrm{O_3}/d\mathrm{T}$ calculated between daily afternoon temperature and $\mathrm{O_3}$ for summers 2008-2010. Contours represent CTM output from the +AnthroNO simulations, and orange outlined scatterpoints represent results from observations.

is no longer the leading meteorological variable explaining $\mathrm{O_3}$ variability south of $\sim 35°\mathrm{N}$, and humidity and transport become important in these regions. The cause of spatial variations in $r(\mathrm{T}, \mathrm{O_3})$ is beyond the scope of this study, but our findings are consistent with other studies. Tawfik and Steiner (2013) and Kavassalis and Murphy (2017) explained the latitudinal gradient of $r(\mathrm{T}, \mathrm{O_3})$ through land-atmosphere coupling involving soil moisture and dry deposition, while Barnes and Fiore (2013) linked variations in $r(\mathrm{T}, \mathrm{O_3})$ to the eddy-driven jet.

The CTM generally reproduces the spatial pattern of daily afternoon $r(\mathrm{T}, \mathrm{O_3})$ present in observations, with strong positive correlations in the Northeast, Great Lakes, and Great Plains and near-zero correlations in the Southeast and Intermountainous West (Figures 2.5c, 2.6a). At some sites, particularly those in the Western U.S., the CTM has a tendency to slightly overestimate the magnitude of the correlation (Figure 2.5c).

Next we compare $d\mathrm{O_3}/d\mathrm{T}$ from CASTNet with the CTM (Figures 2.5d, 2.6b). As with $r(\mathrm{T}, \mathrm{O_3})$, the CTM captures the high values of $d\mathrm{O_3}/d\mathrm{T}$ in the Northeast and Midwest and the lower, near-zero values in the South and West. There appears to be a systematic underestimate in the magnitude of $d\mathrm{O_3}/d\mathrm{T}$ by the CTM, with increasing differences in the Eastern U.S. (Figures 2.5d, 2.6b). Both Rasmussen et al. (2012) and Strode et al. (2015) conducted similar analyses but during the 1990s and early 2000s, and we note similarities with respect to the spatial variability of $d\mathrm{O_3}/d\mathrm{T}$. Since the 1990s and early 2000s, our analysis for 2008-2010 shows that the magnitude of $d\mathrm{O_3}/d\mathrm{T}$ has declined throughout the domain, especially in the Southeastern U.S. (Figure 2.6b). Thus, our nationwide map of $d\mathrm{O_3}/d\mathrm{T}$ provides an update to these previous studies that focused on time periods preceding the passage of the $\mathrm{NO_x}$ State Implementation Plan (SIP) Call. Other studies report that $d\mathrm{O_3}/d\mathrm{T}$ will continue to decline and reach a minimum in the U.S. due to $\mathrm{NO_x}$ reductions resulting from regulatory measures (Pusede et al., 2015).

The range in the $\mathrm{O_3}$-temperature relationship across the contiguous U.S. (Figure 2.6) is also illustrated in Figure 2.7, which shows time series of temperature and $\mathrm{O_3}$ for four locations with varying degrees of the strength in the

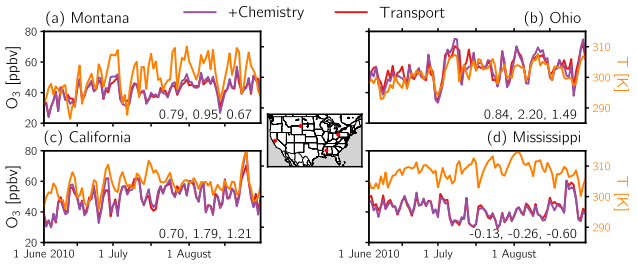

Figure 2.7: O_3 from the Transport and +Chemistry simulations and co-located temperature for summer 2010 for grid cells in regions with varying strengths of the O_3-temperature relationship. The exact location of grid cells are shown in the inset map. Text in the subplots' lower right corners indicate $r(\mathrm{T}, \mathrm{O}_{3,\,+\mathrm{Chemistry}})$, $d\mathrm{O}_{3,\,+\mathrm{Chemistry}}/d\mathrm{T}$, and $d\mathrm{O}_{3,\,\mathrm{Transport}}/d\mathrm{T}$.

relationship. In Montana, Ohio, and California (Figure 2.7a-c), $r(\mathrm{T}, \mathrm{O}_3) > 0.7$, yet $d\mathrm{O}_3/d\mathrm{T}$ is nearly 50% less in Montana than in Ohio and is intermediate in California. Figure 2.7d demonstrates the anticorrelation of O_3 and temperature common in the Southeastern U.S. and the subsequent negative values of $d\mathrm{O}_3/d\mathrm{T}$. The differences between the Transport and +Chemistry simulations at these locations will be further explored in Section 2.5.

Overall, our evaluation of the GMI CTM shows that despite biases that are consistent with other CTMs, the GMI CTM satisfactorily reproduces the synoptic distribution and temporal variability of O_3 and the large-scale covariance of O_3 with temperature, affirming its use as a tool to diagnose the drivers of $d\mathrm{O}_3/d\mathrm{T}$ and O_3 variability.

Although simulations at $\sim 1^\circ$ resolution are common in global modeling studies, we test the robustness of our analysis across horizontal resolutions using the Goddard Earth Observing System (GEOS) general circulation model (GCM) in "replay" mode (see Orbe et al., 2017). Within the GEOS GCM framework, metrics related to the O_3-temperature relationship were analyzed

at three different resolutions (2° latitude × 2.5° longitude, 1° × 1.25°, and 0.5° × 0.625°). Increasing model resolution led to improvement in model-observation agreement for O_3 variability, with the slope of the variability of O_3 at each paired CASTNet sites versus their co-located GEOS GCM grid cell increasing from 0.24 in the 2° × 2.5° simulation to 0.39 in the 0.5° × 0.625° simulation. However, there is no systematic change in the model-observation agreement for mean O_3, $r(\mathrm{T}, \mathrm{O_3})$, or $d\mathrm{O_3}/d\mathrm{T}$, with essentially the same slopes for all resolutions. CTMs or GCMs capable of simulations at higher spatial resolutions may reveal mesoscale features not resolved in our current simulations, the resolution of the GMI CTM used in this study is adequate for answering our questions regarding the large-scale drivers of the O_3-temperature relationship.

2.4 The Northeastern U.S.

As other studies have shown a strong positive correlation between O_3 and temperature in the Northeastern U.S. (i.e., Rasmussen et al., 2012; Schnell and Prather, 2017; Kerr and Waugh, 2018), we first examine the drivers of the O_3-temperature relationship using regionally-averaged quantities in this region (outlined region in Figure 2.1). As shown in Figure 2.8a and c, variations in regionally-averaged O_3 are accompanied by similar variations in temperature in the Northeast. This results in a strong positive correlation coefficient ($r(\mathrm{T}, \mathrm{O_3}) = 0.67$) and a high $d\mathrm{O_3}/d\mathrm{T}$ of 1.72 ppbv K^{-1}, both calculated using regionally-averaged quantities. These results hold beyond the summer shown in Figure 2.8 (Kerr and Waugh, 2018).

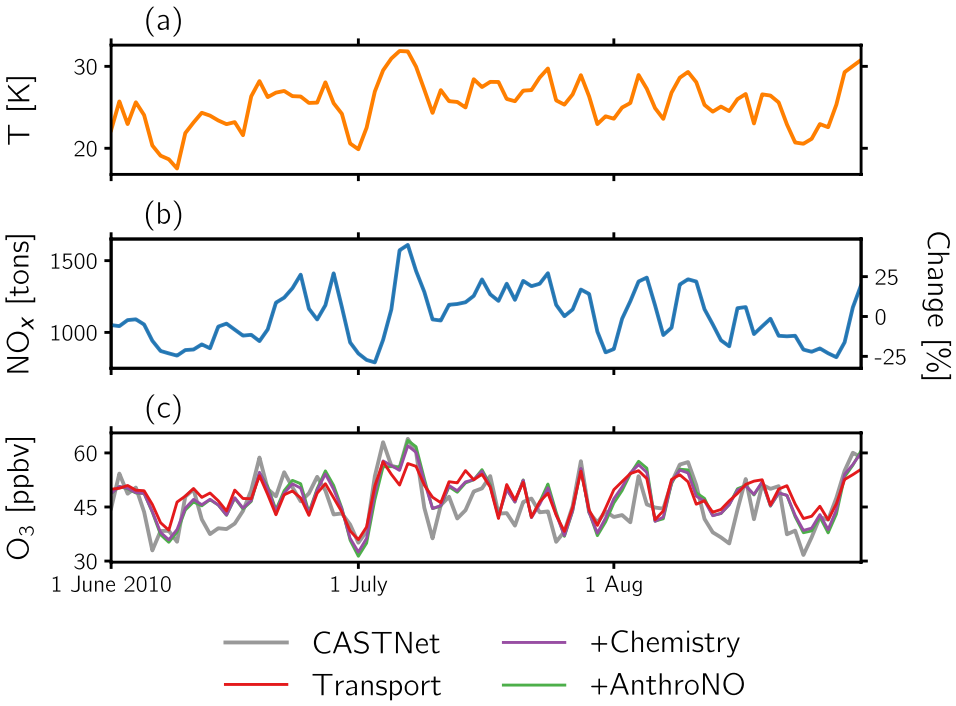

Figure 2.8: (a) Afternoon MERRA-2 2-meter temperature averaged over grid cells co-located with observational sites in the Northeast; (b) Northeast-summed anthropogenic NO_x emissions measured CEMS (Figure 2.2); (c) afternoon observed O_3 averaged over observational sites in the Northeast and O_3 from three CTM sensitivity simulations averaged over all grid cells in the Northeast. (a and c) represent daily afternoon values, while (b) represents daily cumulative values for summer 2010. The states included in the Northeast are outlined in Figure 2.1.

As stated in Section 2.1, anthropogenic NO_x emissions are one possible driver of O_3 variability. There are substantial daily variations in these emissions (Figure 2.8b). For instance, NO_x emissions are $\sim$ 25% below their mean value in early July, and as temperatures in the Northeast increase (Figure 2.8a), the emissions increase, peaking around 50% of their mean value (Figure 2.8b). Thus, this represents a change of $\sim$ 75% occurring over a period of only five days. The daily variability of NO_x emissions is strongly positively

correlated with temperature ($r(\mathrm{NO}_x, \mathrm{T}) = 0.72$), and the daily variability of NO_x is moderately positively correlated with O_3 ($r(\mathrm{NO}_x, \mathrm{O}_3) = 0.44$).

All sensitivity simulations capture the general timing of O_3 events present in observations resulting in strong positive correlations among each other (Northeast-averaged $r > 0.92$ for all combinations of the three simulations; Figure 2.8c). However, we note that the CTM misses some of the low O_3 events (Figure 2.8c). Similar behavior has been shown for other CTMs, such as GEOS-Chem (Travis et al., 2016).

The processes associated with temperature that are included in the Transport simulation achieve nearly 90% of the total daily variation present in the +AnthroNO simulation ($r^2 = 0.86$). The changes in the correlation coefficient calculated between CASTNet and different simulations of the CTM are small: $r(\mathrm{O}_{3,\mathrm{CASTNet}}, \mathrm{O}_{3,\ \mathrm{Transport}})$ increases from 0.67 to 0.77 when temperature-dependent chemistry and biogenic VOC is included in the +Chemistry simulation, but r slightly decreases in the +AnthroNO simulation ($r(\mathrm{O}_{3,\mathrm{CASTNet}}, \mathrm{O}_{3,+\mathrm{AnthroNO}}) = 0.76$). While these values reflect only results from summer 2010, examining all summers in our three year measuring period leads to similar conclusions, and r calculated between CASTNet and different simulations does not change by more than 0.06 when comparing results from summer 2010 to the entire measuring period. These small differences in the correlations between CASTNet and the different CTM simulations are not statistically significant at $\alpha = 0.01$.

Next, we turn to $d\mathrm{O}_3/d\mathrm{T}$ and how our sensitivity simulations change the

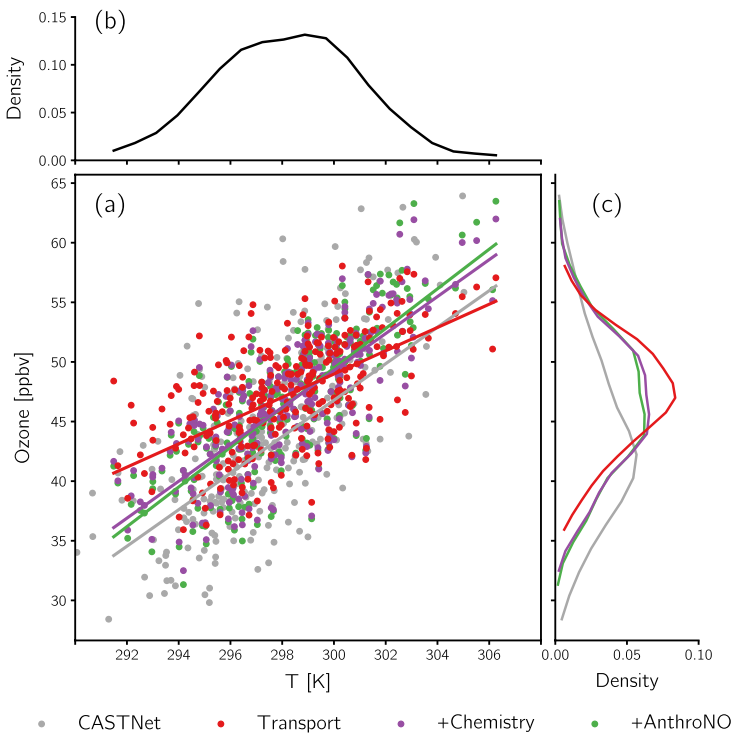

Figure 2.9: (a) Scatterpoints show Northeast-averaged daily afternoon O_3 from observations and CTM sensitivity simulations versus temperature. Lines are the OLS linear regressions fit through the data. (b) Kernel density estimate (KDE) of temperature and (c) KDEs of observed and simulated O_3.

magnitude of dO_3/dT (Figure 2.9). Our simulations generally agree with observations; and, as temperature dependencies are added, dO_3/dT is brought into closer agreement with observations. Figure 2.9b-c indicates a unimodal distribution for both temperature and O_3. Considering the association of transport with temperature alone yields $dO_3/dT = 0.98$ ppbv K^{-1} (Table 2.2). When temperature-dependent chemistry is included in the +Chemistry simulation, dO_3/dT increases to 1.55 ppbv K^{-1}. The inclusion of anthropogenic NO emissions (+AnthroNO simulation) further increases dO_3/dT to 1.66 ppbv K^{-1}. Therefore, transport- and chemistry-related processes are the primary

drivers of dO_3/dT compared to anthropogenic NO emissions.

The most obvious difference between simulations is the magnitude of O_3 extremes (Figure 2.8c). This is particularly evident during the multiday O_3 event occurring in early July. At the beginning (1 July), Northeast-averaged O_3 concentrations are at their minimum value for the summer with a ~ 5 ppbv spread between simulations and the +AnthroNO simulation having the lowest concentration. As the temperature rises (Figure 2.8a) and O_3 accumulates in the Northeastern U.S., all simulations miss the initial first peak recorded by CASTNet but capture the second peak on 7 July again with a ~ 5 ppbv spread between simulations and the +AnthroNO simulation closest to observed values (Figure 2.8c).

The results from this example event hold for most other extreme O_3 events in our measuring period, and these extreme O_3 events largely coincide with extreme temperatures, while mean O_3 concentrations remain nearly unchanged between simulations (μ in Table 2.2). If we systematically examine the enhancement of O_3 for high O_3 events ($O_{3,\,P_{90}} - O_{3,\,P_{50}}$ in Table 2.2), we find only a small spread (< 1 ppbv) between simulations. We note similar results for the other tail of the distribution ($O_{3,\,P_{10}} - O_{3,\,P_{50}}$ in Table 2.2). This small spread demonstrates that the Transport simulation with its invariant chemistry and emissions can still produce O_3 events of comparable magnitude to observed events.

The inclusion of temperature dependencies preferentially affects days with extreme temperatures, so it is no surprise that the largest difference between simulations occurs on hot days ($O_3(T_{P_{90}}) - O_3(T_{P_{50}})$ in Table 2.2) and cold

Table 2.2: Summary of results in the Northeastern U.S. (outlined region in Figure 2.1) determined with regionally-averaged quantities.

	μ [ppbv]	σ [ppbv]	$O_{3,\,P_{90}} - O_{3,\,P_{50}}$ [ppbv]	$O_{3,\,P_{10}} - O_{3,\,P_{50}}$ [ppbv]	$O_3(T_{P_{90}}) - O_3(T_{P_{50}})$ [ppbv]	$O_3(T_{P_{10}}) - O_3(T_{P_{50}})$ [ppbv]	dO_3/dT [ppbv K^{-1}]
Transport	47.26	4.52	5.27	-6.14	5.25	-3.86	0.98
+Chemistry	46.55	5.54	7.02	-7.44	8.75	-6.23	1.55
+AnthroNO	46.55	5.83	7.09	-7.81	9.49	-6.60	1.66
CASTNet	44.09	7.16	11.03	-7.85	10.44	-6.81	1.72

days ($O_3(T_{P_{10}}) - O_3(T_{P_{50}})$ in Table 2.2) when all temperature dependencies are considered in the +AnthroNO simulation. Additionally, as temperature dependencies are added from the Transport to +AnthroNO simulations, there are successive increases in O_3 variability (σ in Table 2.2).

If we transform dO_3/dT from different CTM simulations, given in Table 2.2, to their percentage contribution to the full dO_3/dT from the +AnthroNO simulation, we find that the Transport simulation contributes 58.7%, the +Chemistry simulation 34.5%, and the +AnthroNO simulation 6.8% to the full dO_3/dT. This finding is consistent across other metrics in Table 2.2: for example, the Transport simulation contributes 55.4%, the +Chemistry simulation 36.8%, and the +AnthroNO simulation 7.8% to the total enhancement of O_3 on hot days. Thus, the association of transport with temperature contributes $\sim$ 60% of the variability and extremes, while temperature-dependent chemistry and anthropogenic NO emissions contribute only $\sim$ 30% and $\sim$ 10%, respectively.

2.4.1 The Role of Anthropogenic NO Emissions

Our analysis in the Northeastern U.S. suggests that the inclusion of temperature-dependent, anthropogenic NO emissions are not a dominant driver of day-to-day variations in dO_3/dT or O_3 variability.

To further investigate our +AnthroNO simulation, which focuses on daily variations in anthropogenic NO emissions, we turn to another modeling study that examined the interannual effects of anthropogenic emissions reductions

through two GMI CTM simulations (Strode et al., 2015). This pair of simulations, which spans the measuring period 2000-2010, investigated long-term emission reductions in the Eastern U.S. and their effect on surface-level O_3. The first ("Standard," here abbreviated Std) is similar to our +Chemistry simulation but is driven by the MERRA reanalysis (Rienecker et al., 2011) and uses a previous version of the CTM's chemical mechanism. The second simulation used in Strode et al. (2015) is the same as Std, but anthropogenic and biomass burning emissions are held at 2000 levels ("Emissions Fixed," here abbreviated EmFix). As the chemical mechanism and meteorology driving this pair of simulations are identical, we attribute any changes between them solely to long-term reductions in emissions and not to other sources of variability, such as a changing climate. Additional details on model configuration and specifications can be found in Strode et al. (2015).

We quantify how changes within the CTM's emissions inventory alter NO_x and O_3 for (1) our +Chemistry and +AnthroNO simulations and (2) for the Std and EmFix simulations in Strode et al. (2015) and find that the changes in O_3 and NO_x are consistent whether emissions are altered on daily timescales (this study) or on interannual timescales (Strode et al., 2015). In other words, the change in O_3 that we find on hot versus cold days between our +AnthroNO and +Chemistry simulations is similar to the change over the course of a couple years of emissions reductions. Specifically, the effect of a 1 ppbv change in modeled NO_x on O_3 ($\frac{\Delta O_3}{\Delta NO_x}$) is $\sim$ 7.8 ppbv in our study and $\sim$ 9.0 ppbv in Strode et al. (2015) (Figure 2.10).

The real-world results of reductions in emissions bear a similar small

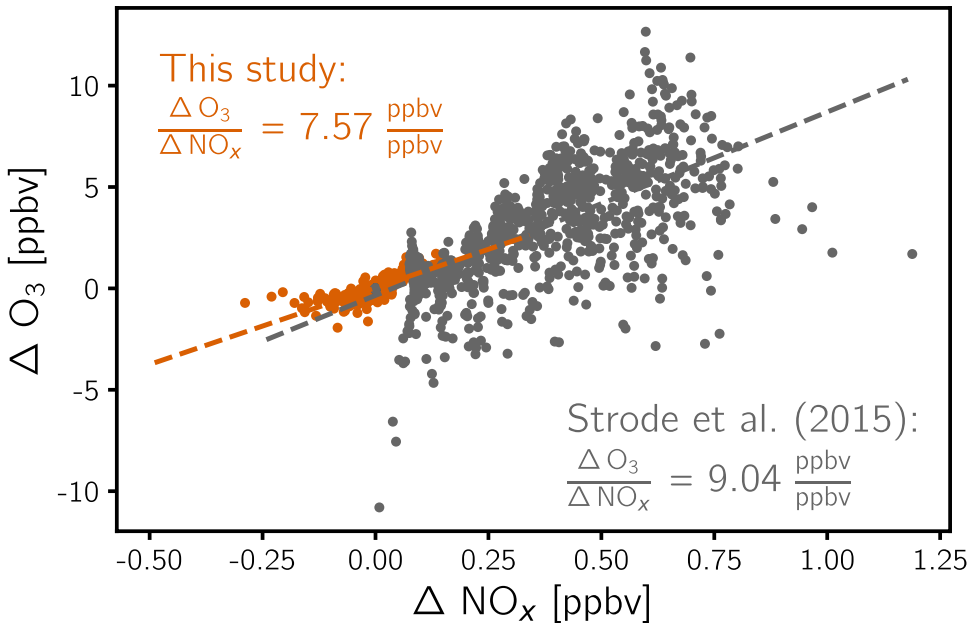

Figure 2.10: Northeast-averaged absolute changes of daily afternoon O_3 versus absolute changes of NO_x. For this study the change (i.e., Δ) corresponds to the difference between the +AnthroNO and +Chemistry simulations for summers 2008-2010. For Strode et al. (2015), Δ refers to the change between daily afternoon EmFix and Std simulations for summers 2000-2010. $\Delta O_3 \, \Delta NO_x^{-1}$ is calculated using OLS linear regression.

change in O_3 (Figure 2.11). Despite average summertime CEMS NO_x reductions of $>$ 50% in the Northeastern U.S. and similar trends of NO in the CTM's emissions inventory (Figure 2.11a), the summertime mean observed and modeled O_3 concentrations have decreased by substantially less, $\sim$ 10% (Figure 2.11b). Large changes in emissions resulting in much smaller changes in O_3 was earlier suggested by Jacob et al. (1993) who proposed a 50% reduction in NO_x emissions would only decrease O_3 levels by $\sim$ 15% in the Eastern U.S. This is broadly consistent with the $\sim$ 10% role we found temperature-dependent, anthropogenic NO emissions to have (Table 2.2).

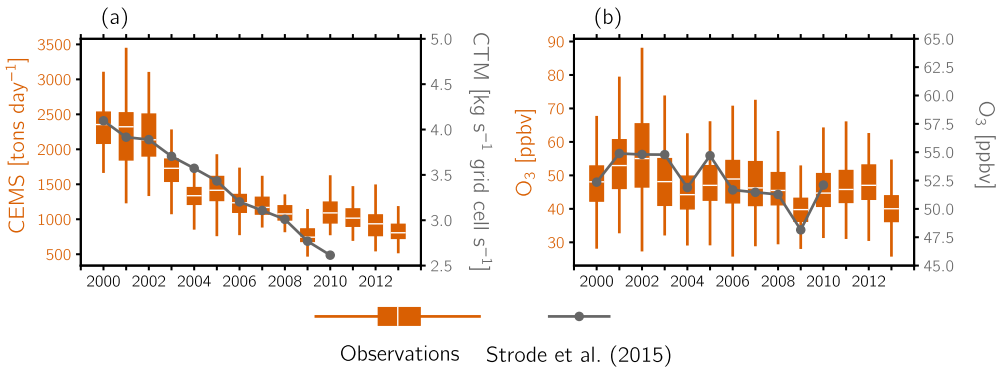

Figure 2.11: Summer (a) Northeast-summed daily anthropogenic NO_x emissions from CEMS (boxplots) and Northeast-averaged NO from the emissions inventory of the Std simulation of the CTM (timeseries) and (b) Northeast-averaged observed O_3 from CASTNet (boxplots) and modeled O_3 from Std simulation (time series). Center white lines in boxplots correspond to median summer values, and whiskers extend to 1.5 $\times$ IQR.

The small effect of the anthropogenic NO emissions is also consistent with He et al. (2013a) who suggested that approximately one-third of the increase of O_3 on hot days is due to anthropogenic NO emissions. Although the contribution we found from these emissions is slightly smaller than their estimation, our analysis has the advantage of using a modeling framework that takes into account non-linearity and daily variations among fields, whereas the analysis of He et al. (2013a) was based solely on time-averaged, linear relationships derived from observations. While our findings reflect the role of anthropogenic NO emissions in the Eastern U.S., the magnitude of the role could change in different regions or even in subsets of the Eastern U.S. depending on whether the region or subset is NO_x-limited or NO_x-saturated.

2.5 Contiguous U.S.

We have shown the importance of temperature on processes related to transport and chemistry in the Northeast, and we now examine if this holds across the contiguous U.S. Given that the temperature-dependent, anthropogenic NO emissions in the GMI CTM play only a small role in the Northeastern U.S. and generally contribute $< 10\%$ to the variability of O_3 and its relationship with temperature, we now focus only on the difference between the Transport and +Chemistry simulations. While our previous analysis used regionally-averaged quantities (Section 2.4), we next compare changes in several metrics between the Transport and +Chemistry simulations locally (at each grid cell).

As discussed in Section 2.3, the highest O_3 concentrations are generally found in industrial, populated regions (i.e., California, Ohio River Valley, and the Mid-Atlantic) and high elevation regions (i.e., Utah, Colorado, Arizona, New Mexico). Regions with moderate to strong positive $r(\mathrm{T},\ \mathrm{O_3})$ and a high $d\mathrm{O_3}/d\mathrm{T}$ largely coincide with the highest O_3 concentrations in the contiguous U.S. (Figures 2.1a, 2.6). However, there are some regions of the U.S., such as parts of the Great Plains and Upper Midwest, which have moderate mean O_3 concentrations (~ 40 ppbv) but moderate to strong positive $r(\mathrm{T},\ \mathrm{O_3})$ and a moderate $d\mathrm{O_3}/d\mathrm{T}$ (compare Figure 2.1 with Figure 2.6).

In Section 2.4 we quantified the roles of transport and chemistry on $d\mathrm{O_3}/d\mathrm{T}$ in the Northeastern U.S. and showed that the Transport simulation yielded the majority of the magnitude of the full $d\mathrm{O_3}/d\mathrm{T}$. A comparison of $d\mathrm{O_3}/d\mathrm{T}$ between the Transport and +Chemistry simulations across the contiguous U.S. reveals that regions with the highest $d\mathrm{O_3}/d\mathrm{T}$, such as the Northeast,

Midwest, Great Plains, and California (Figure 2.6b), see only small reductions (generally $< 25\%$) in dO_3/dT as temperature dependencies in the +Chemistry simulation are removed (Figures 2.7a-c, 2.12a-b). This indicates that transport-related processes are the dominant cause of the O_3-temperature relationship throughout much of the Northern U.S. (Figure 2.12c). This zonal band is roughly coincident with the southern climatological cyclone track and the mean eddy-driven jet latitude (Leibensperger et al., 2008; Barnes and Fiore, 2013). Mid-latitude cyclones provide a means to ventilate pollutants from the boundary layer, and the frequency of cyclone passages is associated with other variables, which have known effects on surface-level O_3 such as temperature and wind speed and direction. Although additional work is needed to understand the causal relationship between the passage of cyclones and anticyclones and their effect on O_3, these synoptic-scale systems could explain differences between the Northern and Southern U.S. (Figures 2.12-2.15).

Small values (i.e., $< 50\%$) in Figure 2.12c suggest that a majority of the magnitude of dO_3/dT results from the addition of temperature-dependent chemistry in the +Chemistry simulation. We see that these small values primarily occur in the southern half of the domain and particularly in the Southeastern U.S. The large purported role of chemistry-related processes in this region stems, in part, from the fact that there are insignificant correlations ($r < r_c$) between temperature and O_3 (Figure 2.6a, 2.7d), denoted in Figure 2.12c by orange contours. Including temperature-dependent chemistry in the +Chemistry simulation does not affect the O_3-temperature relationship in the same manner as in regions with strong positive correlations. We speculate that

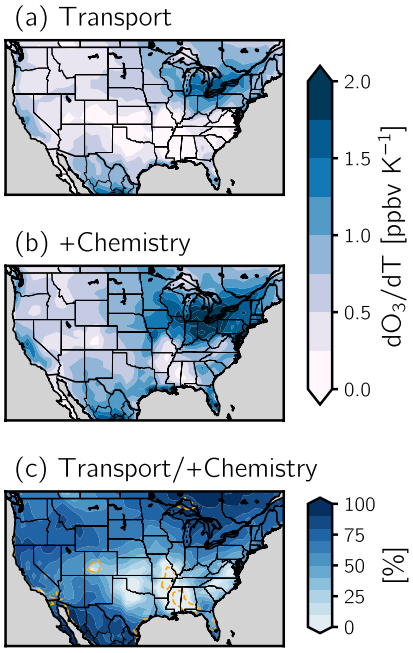

Figure 2.12: dO_3/dT in the (a) Transport and (b) +Chemistry simulations. (c) The quotient of each simulation's dO_3/dT multiplied by 100; a value of 100% implies that the $O_{3,\,P_{90}}$ magnitude did not change between simulations. Orange contours enclose regions where $r(T,\,O_3) < r_c(T,\,O_3)$.

this behavior in the Southeastern U.S. could arise, in part, from the dynamics of the Bermuda High: westward extensions of the high could advect warmer temperatures into the region while simultaneously bringing clean, maritime air onto the continent (Shen et al., 2015). This might explain why O_3 decreases with increasing temperature (Figure 2.6b) and the small role of transport-related processes in the Southeast (Figure 2.12c).

Disregarding the regions where $r(T,\,O_3) < r_c(T,\,O_3)$, there are regions such as Virginia and North Carolina where $r(T,\,O_3)$ is moderately positive,

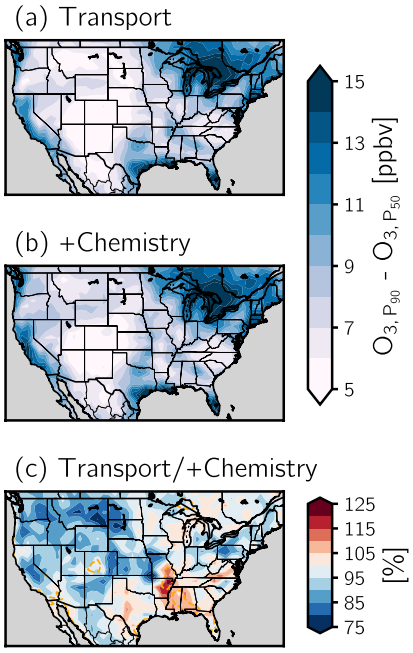

Figure 2.13: O_3 enhancements for high O_3 events ($O_{3,\,P_{90}} - O_{3,P_{50}}$) in the (a) Transport and (b) +Chemistry simulations. (c) The ratio of the enhancements from each simulation converted to percents, where the ratio is given by $(O_{3,\,P_{90}} - O_{3,P_{50}})_{\text{Transport}}/(O_{3,\,P_{90}} - O_{3,P_{50}})_{\text{+Chemistry}}$. Orange contours enclose regions where $r(\text{T}, O_3) < r_c(\text{T}, O_3)$.

yet the magnitude of $dO_3/d\text{T}$ more than doubles as temperature-dependent chemistry is included (Figure 2.12a-b). This region coincides with higher isoprene emissions compared with the Northeast (not shown). The large role of chemistry in this Mid-Atlantic region could be the result of processes relevant to this region: the aforementioned isoprene (or other biogenic) emissions, the infrequent passage of cyclones south of $\sim 35^\circ$N (Rasmussen et al., 2012), or the influence of mesoscale processes not captured by the GMI CTM (e.g.,

land-sea breezes in coastal regions, recirculation). Further investigation is needed to understand how these processes might alter O_3 in this region.

In the Northeast, we found that, on average, the magnitude of $O_{3,\,P_{90}}$ changes by only < 2 ppbv between the +Chemistry and Transport simulations. As we expand our analysis to the contiguous U.S., we find that the Northeast, parts of California, and Gulf Coast states have the largest increase of O_3 for $O_{3,\,P_{90}}$, generally > 10 ppbv with much more modest increases (~ 5 ppbv) in other regions (Figure 2.13a-b). Unlike the analysis of dO_3/dT in Figure 2.12 where differences between simulations were largely a product of O_3-temperature correlations, the differences in the analysis of the increase of O_3 for $O_{3,\,P_{90}}$ displays far greater spatial heterogeneity (Figure 2.13c). For instance, the Northeast, Midwest, and Great Plains are all regions with similar strengths of correlation between temperature and O_3, yet these regions do not respond uniformly as temperature-dependent chemistry is included. This is particularly evident for case studies shown in Figure 2.7a-b for Montana and Ohio. The O_3-temperature relationship is similar for both locations ($r(T,\,O_3) = 0.84$ in Ohio and $r(T,\,O_3) = 0.79$ in Montana), yet the Transport simulation provides nearly all the variability for the case of Montana (Figure 2.7a). Considering the association of temperature with transport alone in the Midwestern U.S. yields $O_{3,\,P_{90}}$ of slightly larger magnitude, albeit only a $\sim 5\%$ increase (Figure 2.13c). In the Southeastern U.S., a region where $r(T,\,O_3) \approx 0$, the enhancement of O_3 for $O_{3,\,P_{90}}$ implies that $O_{3,\,P_{90}}$ has a greater magnitude when the temperature-dependent processes included in our +Chemistry simulation are held at their monthly mean values (Figure 2.13c).

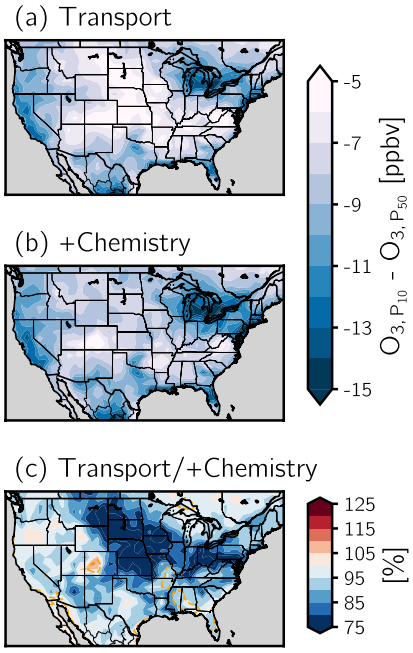

Figure 2.14: Same as Figure 2.13 but showing the reduction of O_3 for low O_3 events ($O_{3,\,P_{10}}$) where the decrease is defined as the difference in each simulation's $O_{3,\,P_{10}}$ and median O_3 ($O_{3,\,P_{50}}$)

We conduct a similar analysis to Figures 2.13 but for the reduction of O_3 for low O_3 events ($O_{3,\,P_{10}}$; Figure 2.14). Comparing these two figures leads to qualitatively similar outcomes inasmuch as the Northeast and Mid-Atlantic states see the largest reductions in O_3 for $O_{3,\,P_{10}}$ (Figure 2.14a-b). However, we note a general asymmetry between the change of O_3 for $O_{3,\,P_{90}}$ and $O_{3,\,P_{10}}$ (compare Figures 2.13 and 2.14) implying temperature-dependent chemistry makes a smaller difference for the upper tail of the O_3 distribution.

Similar to our analysis in Figure 2.13a-b showing the change of O_3 for O_3

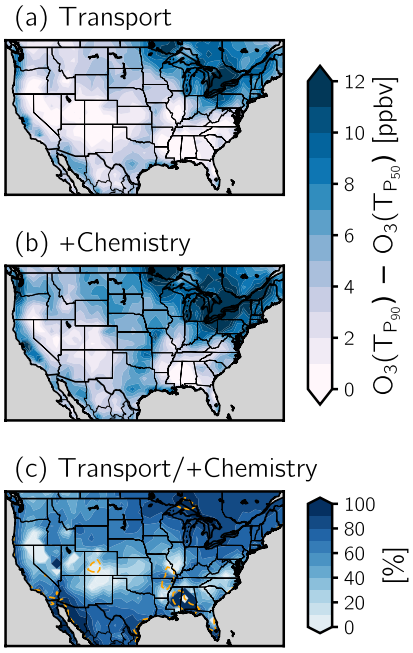

Figure 2.15: Same as Figure 2.13 but showing O_3 enhancements on hot days: $O_3(T_{P_{90}}) - O_3(T_{P_{50}})$.

events, we now turn to the change of O_3 for days with extreme temperatures. The Northeast stands out as the region with the largest O_3 enhancement on hot days (Figure 2.15a-b) and largest O_3 reduction on cold days (Figure 2.16a-b). In the Northeast, we found large changes between the Transport and +Chemistry simulations when we examined the increase of O_3 on hot days, implying that $\sim$ 60% of this increase came about by considering only the association of temperature with transport-related processes. This holds throughout the northern portion of the domain, and we see that the processes included in our Transport simulation generally provide the majority of the total increase of

O_3 for on hot days. The influence of transport's association with temperature diminishes with decreasing latitude reaching a minimum in the vicinity of regions where $r(\mathrm{T}, \mathrm{O_3}) < r_c(\mathrm{T}, \mathrm{O_3})$ (i.e., Northern California and Southern Oregon, the Four Corners region, and Virginia and North Carolina). Here we note some of the largest changes between simulations, suggesting that the Transport simulation provides as little as 20% of the increase of O_3 on hot days (Figure 2.15c). Regions in which temperature and O_3 are insignificantly correlated ($r < r_c$) display sharp gradients between very large and very small ratios stemming from the quotient of two near-zero numbers. Again, we note an asymmetry in the effects of temperature dependencies on hot versus cold days (compare Figures 2.15 and 2.16).

In regions where $r(\mathrm{T}, \mathrm{O_3}) < r_c(\mathrm{T}, \mathrm{O_3})$ such as the Southeastern U.S., transport still explains a majority of the variability of O_3. To illustrate this, we turn to a case study in Mississippi (Figure 2.7d). The difference between simulations throughout this region is often in the opposite direction of differences found elsewhere (i.e., the +Chemistry simulation reduces O_3 variability and extremes). These results are a manifestation of the lack of relationship between O_3 and temperature. As we have shown, the Northern U.S. and (to a lesser extent) California are generally defined by moderate to strong positive correlations along with a high $d\mathrm{O_3}/d\mathrm{T}$ (Figures 2.6, 2.7a-c) and the dominant role of transport (Figures 2.12-2.16). Thus, regardless of the strength of the relationship between O_3 and temperature, our comparison of the Transport and +Chemistry simulations in areas with moderate to strong $r(\mathrm{T}, \mathrm{O_3})$ versus insignificant r demonstrates that transport is the main driver of O_3 variability

(Figures 2.7, 2.12-2.16).

2.6 Discussion

In our sensitivity simulations we have grouped together several different processes and calculated the cumulative impact of these processes on the O_3-temperature relationship (e.g., the difference between the Transport and +Chemistry simulations includes the cumulative impact of the temperature dependence of kinetics, soil NO_x and biogenic VOC emissions, and fields related to solar radiation fluxes). While we have not performed simulations to further isolate the relative role of different processes, several other studies have done such calculations or provide insights into the importance of these processes (e.g., Jacob et al., 1993; Romer et al., 2018; Coates et al., 2016; Porter and Heald, 2019).

In particular, Porter and Heald (2019) recently conducted similar sensitivity simulations to ours, fixing temperature within the chemical mechanism as it pertained to different processes. Consistent with our results, they found that the majority of the O_3-temperature relationship was attributed to meteorological phenomena. In addition, they showed that the temperature dependence of the lifetime of PAN was the major chemistry contributor (accounting, on average, for 20% of the total O_3-temperature correlation in the U.S.), with smaller roles for the temperature dependence of soil NO_x emissions (10%) and the emissions of biogenic VOC (3%). The dominant role of the PAN with respect to chemistry-related influences on the O_3-temperature relationship is consistent with earlier studies (e.g., Jacob et al., 1993).

Other factors contributing to the O_3-temperature relationship are variations in clouds and albedo, leading to variations in solar radiation fluxes that, in turn, affect reaction and photolysis rates. These factors are included in the +Chemistry simulation but not the Transport simulation. The exact role of temperature-related variations in solar radiation fluxes has not been examined, but in an observational study of summertime drivers of O_3 variability in Europe, Otero et al. (2016) showed that solar radiation was among the least frequently chosen drivers using a multiple linear regression approach. Moreover, Kavassalis and Murphy (2017) demonstrated that O_3 was not significantly correlated with solar radiation at most CASTNet sites. It thus seems unlikely that variations in these fluxes would lead be a major driver of O_3-temperature variability in the +Chemistry simulation.

The O_3-temperature relationship in the Transport simulation is also the cumulative impact of many different processes (Table 2.1). Decoupling these processes is more difficult than for chemistry-related processes. Unlike photochemistry or emission pathways, the transport-temperature-O_3 pathway represents an indirect association; for example, a stagnating high pressure system is not directly dependent on temperature but generally coincides with high ambient temperatures. Furthermore, there is a coupling between the different transport-related processes, and they are generally not simply related to temperature or another meteorological field. One except is dry deposition: Porter and Heald (2019) performed a sensitivity simulation to isolate the impact of dry deposition and found that it makes only a minor contribution (6%) of the total O_3-temperature correlation in the U.S. It is an open question which

of the others processes dominates the transport-temperature-O_3 connection.

Previous studies have examined the roles of air mass type and origin, residence time, and mixing on O_3 (e.g., Samson and Ragland, 1977; Comrie, 1994; Davis et al., 2010), while more recent studies (e.g., Barnes and Fiore, 2013; Shen et al., 2015; Knowland et al., 2017; Porter and Heald, 2019) point to the important role of the jet stream and synoptic-scale transient eddy activity for O_3 variability and the covariance of O_3 with temperature. However, the exact mechanisms by which mid- to upper-troposphere transport influences surface-level O_3 variability and extremes are still unknown. Changes in the frequency of mid-latitude cyclones, which ventilate pollutants from the boundary layer and decrease surface ozone (e.g., Leibensperger et al., 2008), are one possibility. Transport associated with the Bermuda High may also play an important role, especially for the Southeastern U.S. (e.g., Shen et al., 2015).

A further process included in both the +Chemistry and Transport simulations is the temperature dependence of humidity. The relationship between O_3 and humidity is spatially varied across the contiguous U.S. with positive correlations between O_3 and relative humidity in the Northeastern U.S. and negative correlations in the Southeastern U.S. (Tawfik and Steiner, 2013). The exact impact of humidity varies based on the chemical background state: water vapor molecules can act as an O_3 sink via the production of OH; however, OH can potentially promote the formation of O_3 in polluted regions (Porter and Heald, 2019). Moreover, land-atmospheric interactions, which themselves are temperature-dependent, could also contribute to the temperature dependence of humidity (Kavassalis and Murphy, 2017). Given that the

temperature-water vapor-O_3 pathway was specifically isolated in Jacob et al. (1993) and this pathway was found to be insignificant due to the cancelling effects water vapor had on photochemistry, it is unlikely that this particular temperature dependence would have an appreciable impact.

2.7 Conclusions

We have found that the GMI CTM reproduces the large-scale distribution of O_3 and the O_3-temperature relationship. In both observations and the CTM the O_3-temperature relationship varies spatially. O_3 and temperature are strongly positively correlated throughout much of the Northern U.S. with the highest correlations found in the Great Plains, Upper Midwest, Northeast, and California, but the relationship between O_3 and temperature is insignificant in the Southeastern U.S. (Figure 2.6a). The slope of the linear regression of O_3 versus temperature, dO_3/dT, has similar spatial variability to $r(T, O_3)$, but there are some differences: the highest values of dO_3/dT are located in the Midwest and Northeast, while the magnitude of the slope diminishes to near-zero values in the Southeast and Intermountainous West.

In regions where O_3 and temperature have moderate to strong positive correlations, our analysis reveals the dominant role of transport on O_3. The processes included in our Transport simulation explain a majority ($\sim$ 60%) of O_3 variability and its coincidence with temperature and yield values of dO_3/dT that are comparable in magnitude to observed quantities. On the other hand, temperature-dependent chemistry contributes $\sim$ 30% to, for example, the full variability of O_3 or its relationship with temperature.

Even in regions with insignificant correlations between O_3 and temperature (e.g., Southeastern U.S.), transport is still an important contributor to O_3 variability, although the variability resulting from transport is not associated with similar variations in temperature. Overall, regardless of the exact relationship between O_3 and temperature, the processes included in our Transport simulation play an important role in controlling O_3 variability.

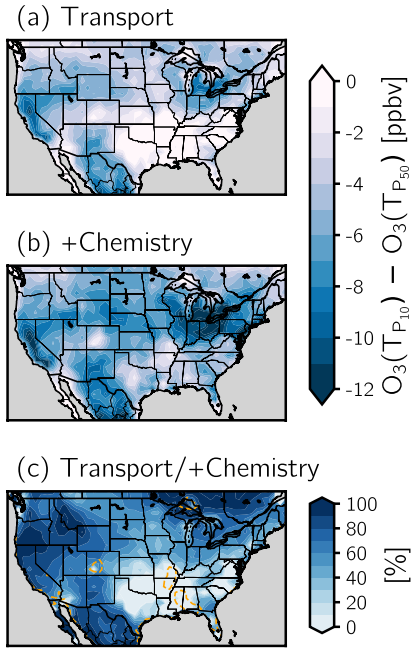

Figure 2.16: Same as Figure 2.15 but for the reduction of O_3 for low temperature events ($T_{P_{10}}$).

In the Northeastern U.S. we found that anthropogenic NO emissions play a small role ($\sim$ 10%) with respect to O_3 events and the O_3-temperature relationship. While climate and air quality models include the impact of temperature

on biogenic emissions and chemical processes, they do not include the impact of temperature on human behavior and anthropogenic emissions. Abel et al. (2017) have commented on this and called for an integration of the temperature dependence of anthropogenic NO into a modeling platform. Our present work does this and reveals that although the daily variability of anthropogenic NO emissions is large in terms of its percent change (Figure 2.8b), the day-to-day changes are small in terms of the impact they have ambient NO_x and O_3 concentrations, and their net effect on daily timescales is similar in magnitude to the changes that could be expected from long-term NO_x reductions over the course of one or two years.

The results from this study are potentially important for the use of dO_3/dT as a measure of how climate change may alter O_3 (or emission controls aimed at reducing O_3). The transport-temperature-O_3 pathway represents an indirect association, and it is possible that this indirect association may change under a changing climate. However, as discussed in Section 2.6, it is unclear which aspect(s) of transport is responsible for O_3 variability and the O_3-temperature relationship in the current climate. Understanding synoptic-scale transport dynamics that control historical O_3 variability and extremes is a prerequisite for inferring how future changes in large-scale transport could affect surface-level O_3. Our future work will focus on quantifying synoptic-scale transport features and their effect on surface-level pollutants.

References

Abel, David, Tracey Holloway, Ryan M. Kladar, Paul Meier, Doug Ahl, Monica Harkey, et al. (2017). "Response of power plant emissions to ambient temperature in the Eastern United States". In: *Environ. Sci. Technol.* 51.10, pp. 5838–5846. DOI: 10.1021/acs.est.6b06201.

Allen, Dale, Kenneth Pickering, Bryan Duncan, and Megan Damon (2010). "Impact of lightning NO emissions on North American photochemistry as determined using the Global Modeling Initiative (GMI) model". In: *J. Geophys. Res. Atmos.* 115.D22. DOI: 10.1029/2010jd014062.

Barnes, Elizabeth A. and Arlene M. Fiore (2013). "Surface ozone variability and the jet position: Implications for projecting future air quality". In: *Geophys. Res. Lett.* 40.11, pp. 2839–2844. DOI: 10.1002/grl.50411.

Bloomer, Bryan J., Jeffrey W. Stehr, Charles A. Piety, Ross J. Salawitch, and Russell R. Dickerson (2009). "Observed relationships of ozone air pollution with temperature and emissions". In: *Geophys. Res. Lett.* 36.9. DOI: 10.1029/2009GL037308.

Bosilovich, Michael (2015). *MERRA-2: Initial evaluation of the climate*. Tech. rep. Volume 43, p. 145.

Brown-Steiner, B., P.G. Hess, and M.Y. Lin (2015). "On the capabilities and limitations of GCCM simulations of summertime regional air quality: A diagnostic analysis of ozone and temperature simulations in the US using CESM CAM-Chem". In: *Atmos. Environ.* 101, pp. 134–148. DOI: 10.1016/j.atmosenv.2014.11.001.

Camalier, Louise, William Cox, and Pat Dolwick (2007). "The effects of meteorology on ozone in urban areas and their use in assessing ozone trends". In: 41.33, pp. 7127–7137. DOI: 10.1016/j.atmosenv.2007.04.061.

Coates, Jane, Kathleen A. Mar, Narendra Ojha, and Tim M. Butler (2016). "The influence of temperature on ozone production under varying NO_x conditions - a modelling study". In: *Atmos. Chem. Phys.* 16.18, pp. 11601–11615. DOI: 10.5194/acp-16-11601-2016.

Comrie, Andrew C. (1994). "Tracking ozone: Air-mass trajectories and pollutant source regions influencing ozone in Pennsylvania forests". In: *Ann. Am. Assoc. Geogr.* 84.4, pp. 635–651. DOI: 10.1111/j.1467-8306.1994.tb01880.x.

Cooper, Owen R., Ru-Shan Gao, David Tarasick, Thierry Leblanc, and Colm Sweeney (2012). "Long-term ozone trends at rural ozone monitoring sites across the United States, 1990-2010". In: *J. Geophys. Res. Atmos.* 117.D22. DOI: 10.1029/2012JD018261.

Davis, Robert E., Caroline P. Normile, Luke Sitka, David M. Hondula, David B. Knight, Stephen P. Gawtry, et al. (2010). "A comparison of trajectory and air mass approaches to examine ozone variability". In: *Atmos. Environ.* 44.1, pp. 64–74. DOI: 10.1016/j.atmosenv.2009.09.038.

De Gouw, J. A., D. D. Parrish, G. J. Frost, and M. Trainer (2014). "Reduced emissions of CO_2, NO_x, and SO_2 from U.S. power plants owing to switch from coal to natural gas with combined cycle technology". In: *Earths Future* 2.2, pp. 75–82. DOI: 10.1002/2013EF000196.

Douglass, Anne R., Susan E. Strahan, Luke D. Oman, and Richard S. Stolarski (2017). "Multi-decadal records of stratospheric composition and their relationship to stratospheric circulation change". In: *Atmos. Chem. Phys.* 17.19, pp. 12081–12096. DOI: 10.5194/acp-17-12081-2017.

Duncan, B. N., S. E. Strahan, Y. Yoshida, S. D. Steenrod, and N. Livesey (2007). "Model study of the cross-tropopause transport of biomass burning pollution". In: *Atmos. Chem. Phys.* 7.14, pp. 3713–3736.

Fiore, A. M., F. J. Dentener, O. Wild, C. Cuvelier, M. G. Schultz, P. Hess, et al. (2009). "Multimodel estimates of intercontinental source-receptor relationships for ozone pollution". In: *J. Geophys. Res.* 114.D4. DOI: 10.1029/2008JD010816.

Fiore, Arlene M. (2002). "Background ozone over the United States in summer: Origin, trend, and contribution to pollution episodes". In: *J. Geophys. Res.* 107.D15. DOI: 10.1029/2001JD000982.

Fiore, Arlene M. (2003). "Application of empirical orthogonal functions to evaluate ozone simulations with regional and global models". In: *J. Geophys. Res.* 108.D14. DOI: 10.1029/2002JD003151.

Fiore, Arlene M., Vaishali Naik, and Eric M. Leibensperger (2015). "Air quality and climate connections". In: 65.6, pp. 645–685. DOI: 10.1080/10962247.2015.1040526.

Gelaro, Ronald, Will McCarty, Max J. Suárez, Ricardo Todling, Andrea Molod, Lawrence Takacs, et al. (2017). "The Modern-Era Retrospective Analysis

for Research and Applications, Version 2 (MERRA-2)". In: *J. Clim.* 30.14, pp. 5419–5454. DOI: 10.1175/JCLI-D-16-0758.1.

Goldberg, Daniel L., Lok N. Lamsal, Christopher P. Loughner, William H. Swartz, Zifeng Lu, and David G. Streets (2017). "A high-resolution and observationally constrained OMI NO_2 satellite retrieval". In: *Atmos. Chem. Phys.* 17.18, pp. 11403–11421.

Guenther, A. B., X. Jiang, C. L. Heald, T. Sakulyanontvittaya, T. Duhl, L. K. Emmons, et al. (2012). "The Model of Emissions of Gases and Aerosols from Nature version 2.1 (MEGAN2.1): An extended and updated framework for modeling biogenic emissions". In: *Geosci. Model Dev.* 5.6, pp. 1471–1492. DOI: 10.5194/gmd-5-1471-2012.

Guenther, Alex, C. Nicholas Hewitt, David Erickson, Ray Fall, Chris Geron, Tom Graedel, et al. (1995). "A global model of natural volatile organic compound emissions". In: *J. Geophys. Res.* 100.D5, p. 8873. DOI: 10.1029/94JD02950.

He, Hao, Linda Hembeck, Kyle M. Hosley, Timothy P. Canty, Ross J. Salawitch, and Russell R. Dickerson (2013a). "High ozone concentrations on hot days: The role of electric power demand and NO_x emissions: Ozone and power demand on hot days". In: 40.19, pp. 5291–5294. DOI: 10.1002/grl.50967.

He, H., J. W. Stehr, J. C. Hains, D. J. Krask, B. G. Doddridge, K. Y. Vinnikov, et al. (2013b). "Trends in emissions and concentrations of air pollutants in the lower troposphere in the Baltimore/Washington airshed from 1997 to 2011". In: *Atmos. Chem. Phys.* 13.15, pp. 7859–7874. DOI: 10.5194/acp-13-7859-2013.

Jacob, Daniel J., Jennifer A. Logan, Geraldine M. Gardner, Rose M. Yevich, Clarisa M. Spivakovsky, and Steven C. Wofsy (1993). "Factors regulating ozone over the United States and its export to the global atmosphere". In: *J. Geophys. Res.* 98.D8, pp. 14817–14826.

Jacob, Daniel J. and Darrell A. Winner (2009). "Effect of climate change on air quality". In: 43.1, pp. 51–63. DOI: 10.1016/j.atmosenv.2008.09.051.

Jing, Ping, Zifeng Lu, and Allison L. Steiner (2017). "The ozone-climate penalty in the Midwestern U.S." In: *Atmos. Environ.* 170, pp. 130–142. DOI: 10.1016/j.atmosenv.2017.09.038.

Kavassalis, Sarah C. and Jennifer G. Murphy (2017). "Understanding ozone-meteorology correlations: A role for dry deposition". In: 44.6, pp. 2922–2931. DOI: 10.1002/2016GL071791.

Kerr, Gaige Hunter and Darryn W Waugh (2018). "Connections between summer air pollution and stagnation". In: *Environ. Res. Lett.* 13.8, p. 084001. DOI: 10.1088/1748-9326/aad2e2.

Kerr, Gaige Hunter, Darryn W. Waugh, Sarah A. Strode, Stephen D. Steenrod, Luke D. Oman, and Susan E. Strahan (2019). "Disentangling the Drivers of the Summertime Ozone-Temperature Relationship Over the United States". In: *J. Geophys. Res. Atmos.* 124.19, pp. 10503–10524. DOI: 10.1029/2019jd030572.

Knowland, K. Emma, Ruth M. Doherty, Kevin I. Hodges, and Lesley E. Ott (2017). "The influence of mid-latitude cyclones on European background surface ozone". In: *Atmos. Chem. Phys.* 17.20, pp. 12421–12447. DOI: 10.5194/acp-17-12421-2017.

Leibensperger, Eric M., Loretta J. Mickley, and Daniel J. Jacob (2008). "Sensitivity of US air quality to mid-latitude cyclone frequency and implications of 1980-2006 climate change". In: *Atmos. Chem. Phys.* 8.23, pp. 7075–7086.

Meehl, Gerald A, Claudia Tebaldi, Simone Tilmes, Jean-Francois Lamarque, Susan Bates, Angeline Pendergrass, et al. (2018). "Future heat waves and surface ozone". In: *Environ. Res. Lett.* 13.6, p. 064004. DOI: 10.1088/1748-9326/aabcdc.

Murray, Lee T. (2016). "Lightning NO_x and Impacts on Air Quality". In: *Curr. Pollut. Rep.* 2.2, pp. 115–133. DOI: 10.1007/s40726-016-0031-7.

Olivier, Jos G. J., John A. Van Aardenne, Frank J. Dentener, Valerio Pagliari, Laurens N. Ganzeveld, and Jeroen A. H. W. Peters (2005). "Recent trends in global greenhouse gas emissions: regional trends 1970–2000 and spatial distribution of key sources in 2000". In: *Environmental Sciences* 2.2-3, pp. 81–99. DOI: 10.1080/15693430500400345.

Orbe, Clara, Luke D. Oman, Susan E. Strahan, Darryn W. Waugh, Steven Pawson, Lawrence L. Takacs, and Andrea M. Molod (2017). "Large-Scale Atmospheric Transport in GEOS Replay Simulations". In: *J. Adv. Model. Earth Syst.* 9.7, pp. 2545–2560. DOI: 10.1002/2017ms001053.

Otero, N, J Sillmann, J L Schnell, H W Rust, and T Butler (2016). "Synoptic and meteorological drivers of extreme ozone concentrations over Europe". In: *Environ. Res. Lett.* 11.2, p. 024005. DOI: 10.1andothers088/1748-9326/11/2/024005.

Porter, William C. and Colette L. Heald (2019). "The mechanisms and meteorological drivers of the ozone-temperature relationship". In: *Atmos. Chem. Phys.* Pp. 1–26. DOI: 10.5194/acp-2019-140.

Pusede, Sally E., Allison L. Steiner, and Ronald C. Cohen (2015). "Temperature and recent trends in the chemistry of continental surface ozone". In: 115.10, pp. 3898–3918. DOI: 10.1021/cr5006815.

Racherla, Pavan Nandan and Peter J. Adams (2006). "Sensitivity of global tropospheric ozone and fine particulate matter concentrations to climate change". In: *J. Geophys. Res.* 111.D24. DOI: 10.1029/2005JD006939. (Visited on 05/25/2016).

Rasmussen, D. J., Jianlin Hu, Abdullah Mahmud, and Michael J. Kleeman (2013). "The ozone-climate penalty: Past, present, and future". In: *Environ. Sci. Technol.* 47.24, pp. 14258–14266. DOI: 10.1021/es403446m.

Rasmussen, D.J., A.M. Fiore, V. Naik, L.W. Horowitz, S.J. McGinnis, and M.G. Schultz (2012). "Surface ozone-temperature relationships in the eastern US: A monthly climatology for evaluating chemistry-climate models". In: *Atmos. Environ.* 47, pp. 142–153. DOI: 10.1016/j.atmosenv.2011.11.021.

Rieder, Harald E., Arlene M. Fiore, Larry W. Horowitz, and Vaishali Naik (2015). "Projecting policy-relevant metrics for high summertime ozone pollution events over the eastern United States due to climate and emission changes during the 21st century". In: *J. Geophys. Res. Atmos.* 120.2, pp. 784–800. DOI: 10.1002/2014JD022303.

Rienecker, Michele M., Max J. Suarez, Ronald Gelaro, Ricardo Todling, Julio Bacmeister, Emily Liu, et al. (2011). "MERRA: NASA's Modern-Era Retrospective Analysis for Research and Applications". In: *J. Clim.* 24.14, pp. 3624–3648. DOI: 10.1175/JCLI-D-11-00015.1.

Romer, Paul S., Kaitlin C. Duffey, Paul J. Wooldridge, Eric Edgerton, Karsten Baumann, Philip A. Feiner, et al. (2018). "Effects of temperature-dependent NO_x emissions on continental ozone production". In: 18.4, pp. 2601–2614. DOI: 10.5194/acp-18-2601-2018.

Samson, Perry J. and Kenneth W. Ragland (1977). "Ozone and visibility reduction in the Midwest: Evidence for large-scale transport". In: *J. Appl. Meteorol.* 16, pp. 1101–1106. DOI: https://doi.org/10.1175/1520-0450(1977)016<1101:AFWSIA>2.0.CO;2.

Schnell, Jordan L. and Michael J. Prather (2017). "Co-occurrence of extremes in surface ozone, particulate matter, and temperature over eastern North America". In: *Proc. Natl. Acad. Sci. U. S. A.* 114.11, pp. 2854–2859. DOI: 10.1073/pnas.1614453114.

Shen, L., L. J. Mickley, and A. P. K. Tai (2015). "Influence of synoptic patterns on surface ozone variability over the eastern United States from 1980 to

2012". In: *Atmos. Chem. Phys.* 15.19, pp. 10925–10938. DOI: 10.5194/acp-15-10925-2015.

Sillman, Sanford and Perry J. Samson (1995). "Impact on temperature on oxidant photochemistry in urban, polluted rural and remote environments". In: *J. Geophys. Res.* 100.D6, pp. 11497–11508.

Simon, Heather, Adam Reff, Benjamin Wells, Jia Xing, and Neil Frank (2015). "Ozone trends across the United States over a period of decreasing NO_x and VOC emissions". In: *Environ. Sci. Technol.* 49.1, pp. 186–195. DOI: 10.1021/es504514z.

Strahan, S. E., A. R. Douglass, and P. A. Newman (2013). "The contributions of chemistry and transport to low arctic ozone in March 2011 derived from Aura MLS observations". In: *J. Geophys. Res. Atmos.* 118.3, pp. 1563–1576. DOI: 10.1002/jgrd.50181.

Strahan, S. E., B. N. Duncan, and P. Hoor (2007). "Observationally derived transport diagnostics for the lowermost stratosphere and their application to the GMI chemistry and transport model". In: *Atmos. Chem. Phys.* 7.9, pp. 2435–2445. (Visited on 10/09/2017).

Strode, Sarah A., Jose M. Rodriguez, Jennifer A. Logan, Owen R. Cooper, Jacquelyn C. Witte, Lok N. Lamsal, et al. (2015). "Trends and variability in surface ozone over the United States". In: *J. Geophys. Res. Atmos.* 120.17, pp. 9020–9042. DOI: 10.1002/2014JD022784.

Sun, Wenxiu, Peter Hess, and Chengji Liu (2017). "The impact of meteorological persistence on the distribution and extremes of ozone". In: *Geophys. Res. Lett.* Pp. 1545–1553. DOI: 10.1002/2016GL071731.

Tawfik, Ahmed B. and Allison L. Steiner (2013). "A proposed physical mechanism for ozone-meteorology correlations using land-atmosphere coupling regimes". In: 72, pp. 50–59. DOI: 10.1016/j.atmosenv.2013.03.002.

Travis, Katherine R., Daniel J. Jacob, Jenny A. Fisher, Patrick S. Kim, Eloise A. Marais, Lei Zhu, et al. (2016). "Why do models overestimate surface ozone in the Southeast United States?" In: *Atmos. Chem. Phys.* 16.21, pp. 13561–13577. DOI: 10.5194/acp-16-13561-2016.

Wesely, M.L. (1989). "Parameterization of surface resistances to gaseous dry deposition in regional-scale numerical models". In: *Atmos. Environ.* 23.6, pp. 1293–1304. DOI: 10.1016/0004-6981(89)90153-4.

Wilks, Daniel S. (2011). *Statistical methods in the atmospheric sciences*. eng. 3rd. Vol. 100. International Geophysics Series. Oxford, UK: Academic Press. ISBN: 9780123850225.

Wu, Shiliang, Loretta J. Mickley, Eric M. Leibensperger, Daniel J. Jacob, David Rind, and David G. Streets (2008). "Effects of 2000–2050 global change on ozone air quality in the United States". In: *J. Geophys. Res.* 113.D6. DOI: 10.1029/2007JD008917.

Yienger, J. J. and H. Levy (1995). "Empirical model of global soil-biogenic NO_x emissions". In: *J. Geophys. Res.* 100.D6, p. 11447. DOI: 10.1029/95JD00370.

Yu, Karen, Daniel J. Jacob, Jenny A. Fisher, Patrick S. Kim, Eloise A. Marais, Christopher C. Miller, et al. (2016). "Sensitivity to grid resolution in the ability of a chemical transport model to simulate observed oxidant chemistry under high-isoprene conditions". In: *Atmos. Chem. Phys.* 16.7, pp. 4369–4378. DOI: 10.5194/acp-16-4369-2016.

Yu, Shaocai, Brian Eder, Robin Dennis, Shao-Hang Chu, and Stephen E. Schwartz (2006). "New unbiased symmetric metrics for evaluation of air quality models". In: *Atmos. Sci. Lett.* 7.1, pp. 26–34. DOI: 10.1002/asl.125.

Chapter 3

Connections between Summer Air Pollution and Stagnation

This chapter is published by *Environmental Research Letters* (Kerr and Waugh, 2018).

The body of literature on ambient air pollution suggests that atmospheric stagnation events trigger high levels of air pollution. In this paper we use fifteen years (2000-2014) of summertime *in-situ* air quality measurements together with meteorological reanalysis data to examine the temporal correlation of pollutants with the Air Stagnation Index (ASI) on daily timescales. We find that while the direction of the relationship between the ASI and summertime $PM_{2.5}$ and O_3 ranges from near-zero to positive throughout regions comprising the contiguous United States (U.S.), the strength of the relationship is very weak (e.g., in the Northeast the correlation coefficient between the ASI and $PM_{2.5}$ is 0.09). Moreover, similar to our analysis of the correlation of day-to-day variations of the ASI and pollutants, the percentage of co-occurring extreme pollution and stagnation events is small (e.g., days with a high coverage of stagnation only co-occur with extreme pollution events about one-third

of the time in the Northeast). The Southern U.S. is an exception to our overall findings as the strength of the relationship between the ASI and pollution is stronger and the percentage of co-occurring events is higher compared with other regions. The results of this study suggest a reevaluation of the ASI as an index to assess meteorological and climatic impacts to air quality.

3.1 Introduction

There is a widely-accepted paradigm that air stagnation events are a major cause of elevated surface concentrations of air pollutants such as O_3 and $PM_{2.5}$ (e.g., review articles Jacob and Winner, 2009; Fiore et al., 2012; Fiore et al., 2015). Recently there has been an increased focus on possible increases in the frequency of stagnation events due to climate change (Leung and Gustafson, 2005; Horton et al., 2012; Horton et al., 2014). The study of stagnation as a possible cause of extreme surface-level $PM_{2.5}$ and O_3 concentrations is scientifically and societally relevant due to their public health risks. These two pollutants lead to a myriad of adverse health impacts, particularly affecting human respiratory function (Ebi and McGregor, 2008).

Stagnation is characterized by the trapping of air within the planetary boundary layer due to lack of ventilation or the presence of an inversion under clear sky conditions, often occurring in the presence of slow-moving high pressure systems (Wang and Angell, 1999; Jacob and Winner, 2009). These conditions lead to elevated pollutant concentrations on daily to interannual timescales (e.g., Logan, 1989; Vukovich, 1995; Wang and Angell, 1999; Vautard et al., 2005; Leibensperger et al., 2008; Tai et al., 2010; He et al., 2013b; Dawson

et al., 2014; Oswald et al., 2015; Hou and Wu, 2016; Schnell and Prather, 2017; Sun et al., 2017); however, the change in pollutant concentrations due to stagnant conditions is small and the connections between stagnation and pollution are weak in some of these studies. Thus, there remains uncertainty in the exact impact of stagnation on air pollution.

We examine the daily variability of, and occurrence of, extreme events in $PM_{2.5}$, O_3, surface temperature and stagnation in the contiguous U.S. by performing a systematic study that quantifies the connection between pollutants and stagnation on daily timescales and with individual pollution events. Using the common ASI (described in Section 3.2), we diagnose stagnation events and show only a weak correspondence between the ASI and pollution with regard to day-to-day variations as well as the co-occurrence of events.

3.2 Data and Methods

3.2.1 Data

We use station-based measurements of $PM_{2.5}$ and O_3 from the U.S. Environmental Protection Agency (EPA) Air Quality System (AQS). For $PM_{2.5}$ we analyze the maximum value for each 24-hour period at each station, while for O_3 we analyze the maximum daily 8-hour average concentrations at each station.

We focus on Northern Hemisphere summer, June-July-August (JJA), as high O_3 concentrations (Vukovich, 1995; Dawson et al., 2007b; Jacob and Winner, 2009; Rieder et al., 2013), high $PM_{2.5}$ concentrations (Dawson et al., 2007a; Hand et al., 2012), or both high O_3 and $PM_{2.5}$ concentrations (Schnell

and Prather, 2017) have been shown to occur during this season. We use all available AQS measurements from summers between 2000 and 2014, including rural, suburban, and urban stations (Figure 3.1). O_3 measurements are typically taken every day at a particular station whereas observations of $PM_{2.5}$ concentrations display more heterogeneity in time. A majority of $PM_{2.5}$ stations sample every 3 days, although some stations sample at a daily frequency while others sample every 6 days (Tai et al., 2010; Saunders and Waugh, 2015; Liu et al., 2017).

We assess meteorology with the Modern Era Retrospective-Analysis for Research and Applications (MERRA) (Rienecker et al., 2011). The MERRA data have resolution 0.5° latitude $\times$ 0.67° longitude, and we use daily mean values of 2-meter temperature (T_{2m}), 10 meter wind ($\tilde{U}_{10m}$), 500 hPa wind ($\tilde{U}_{500hPa}$), and total surface precipitation flux (pr). Each field is sampled only at MERRA grid cells containing AQS stations on days with $PM_{2.5}$ and O_3 observations. If there are > 1 AQS stations within the bounds of a particular MERRA grid cell, this cell is counted proportionally to the number of AQS stations contained within when we calculate regionally-averaged T_{2m} and the percentage of stagnant grid cells in a region.

3.2.2 Methods

The daily variations of $PM_{2.5}$, O_3, T_{2m}, and the ASI are examined; the first two derived from AQS and latter two from MERRA. The ASI is described in detail in Horton et al. (2012) and Horton et al. (2014), and the use of the ASI for air quality applications is ubiquitous in the literature (e.g., Leung and Gustafson,

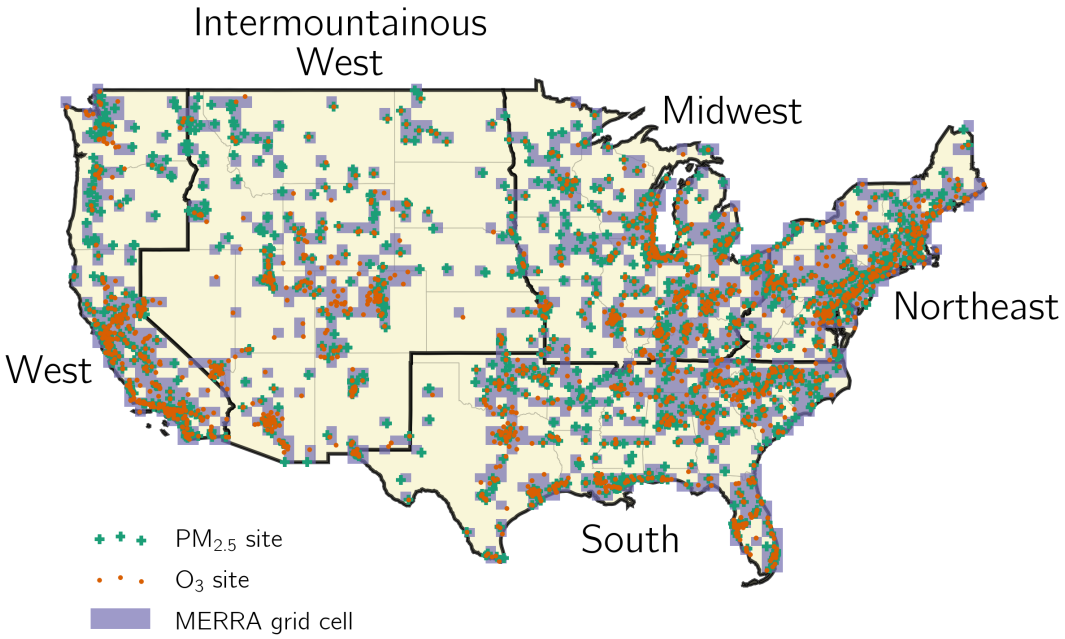

Figure 3.1: Scatterpoints indicate the locations of AQS stations with $PM_{2.5}$ or O_3 observations during the measuring period 2000-2014. When regionally-averaged meteorological quantities or the percentage of stagnant grid cells is shown in subsequent figures, MERRA reanalysis data has been sampled at grid cells nearest to AQS stations on days with pollutant observations and averaged over each of the five regions.

2005; Horton et al., 2012; Dawson et al., 2014; Oswald et al., 2015; Strode et al., 2015; Hou and Wu, 2016; Schnell and Prather, 2017; Sun et al., 2017). The ASI is a binary index based on absolute thresholds. Here we consider a MERRA grid cell as stagnant when daily mean $\tilde{U}_{500\text{hPa}} < 13$ m s^{-1}, daily mean $\tilde{U}_{10\text{m}} < 3.2$ m s^{-1}, and total daily pr < 1 mm.

The definition of the ASI used in this study and described in Horton et al. (2012) and Horton et al. (2014) slightly differs from the definition used by the National Centers for Environmental Information (NCEI, formerly the National Climatic Data Center), detailed in Wang and Angell (1999) and Korshover

and Angell (1982). To this end, we compared the spatial distribution of stagnant days determined after Horton et al. (2012) and Horton et al. (2014) with maps of the number of stagnant days in a given month from the NCEI website (https://www.ncdc.noaa.gov/societal-impacts/air-stagnation/), and we found similar results regardless of the precise definition of the ASI.

Concerns may be raised that our results are an artifact of our choice of the MERRA reanalysis to calculate the ASI. To counter this, we have compared the ASI derived from MERRA to that from the coarser NCEP reanalysis as well as using gauge-based precipitation from the Climate Prediction Center (CPC) Unified Precipitation Project. The results of this (not shown) indicate similar ASI distributions using MERRA, NCEP, and CPC datasets, and our broad conclusions do not change; however, specific results could change if other reanalyses are used.

These findings are reinforced by a sensitivity analysis through which we examined the sensitivity of the pollutant - ASI correlations to each of the three thresholds used to define the ASI (Figure 3.2). By varying the $\tilde{U}_{10m}$, $\tilde{U}_{500hPa}$, and pr thresholds by values ranging from 25 to 175% of the standard threshold we found only small changes in the correlations between $PM_{2.5}$ and O_3 with the ASI that did not change our overall results. Thus, we have confidence that our results are robust to both data and methods used and that the conclusions of our study are not sensitive to the precise definition of stagnant conditions.

We calculate daily regionally- or state-averaged values for all four quantities used in this study ($PM_{2.5}$, O_3, T_{2m}, and ASI) by computing the arithmetic mean using all available daily values for each region or state (Figure 3.1 and

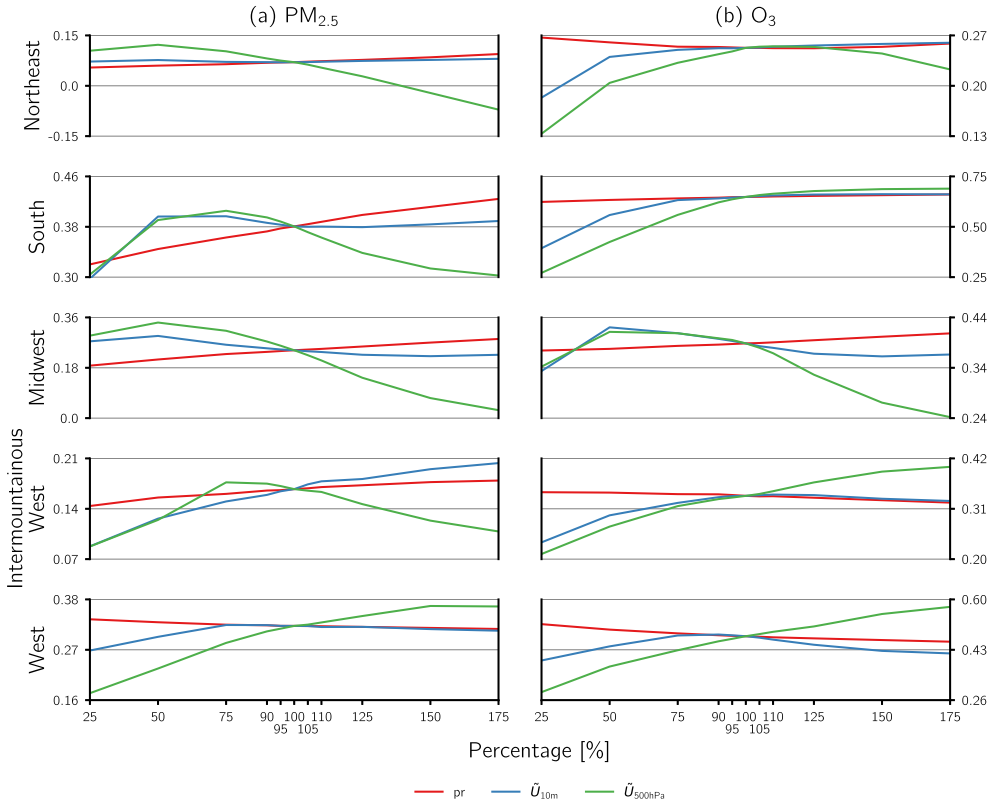

Figure 3.2: The sensitivity of pollutant - ASI correlations to the values of the three variables used to calculate the ASI (i.e. $\tilde{U}_{10\mathrm{m}}$, $\tilde{U}_{500\mathrm{hPa}}$, and pr). (**a**) the correlation of $PM_{2.5}$ with the ASI is found by relaxing or restricting each ASI variable by the discrete percentages specified on the independent axes. Values of the Pearson product-moment correlation coefficient (r), indicated on the dependent axes, represent the 2000-2015 summertime average. (**b**) same as (**a**) but for O_3.

Figure 3.3). Since the ASI is a binary field, we use a different approach to form spatially-averaged values: for a given day we calculate the percentage of AQS stations within a region that is classified as stagnant (ASI = true). Therefore, the regional ASI varies between 0 and 100%.

We use two approaches to quantify the relationship between the four different quantities. First, we calculate the Pearson product-moment correlation coefficient, r, between the daily time series of pairs of quantities. Second, we

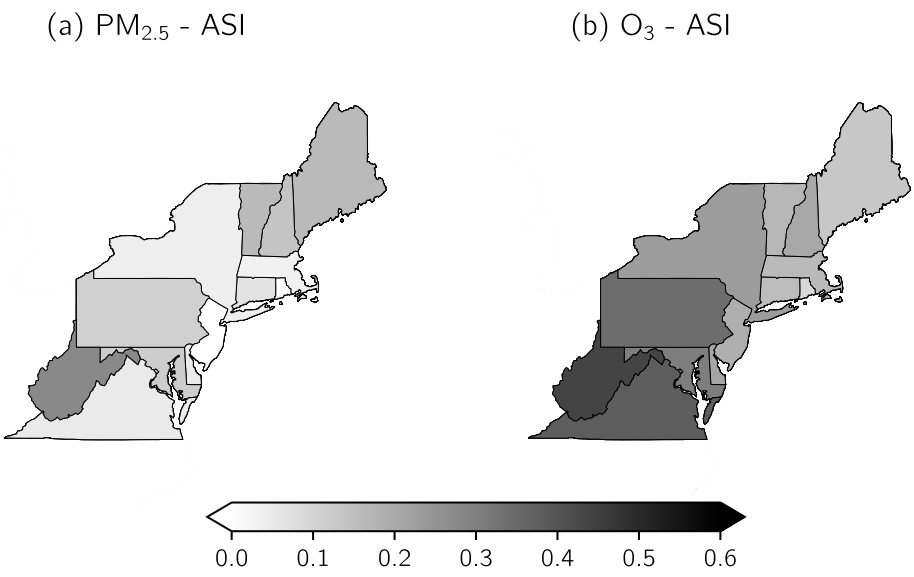

Figure 3.3: Average JJA correlation coefficients (r) between state-averaged $PM_{2.5}$ and the percentage of stagnation coverage within the state (**a**) and state-averaged O_3 and the percentage of stagnation coverage within the state (**b**) for states contained in the Northeast, defined in Figure 3.1.

consider days which are "events" in one quantity (i.e., days with high regional ASI) and calculate the distribution of the other quantities to see how often they are concurrently extreme events. We consider an event as a day in which regionally-averaged quantities equal or exceed their 80^{th} percentile (P_{80}) of daily JJA values for a particular summer. The use of a quantity's percentile as a threshold for events allows for a consistent number of events each summer (by definition, 19 events per summer) because focusing on exceedences over an absolute value would preferentially group $PM_{2.5}$ and O_3 events towards the beginning of the measuring period due to the decreasing trend in ambient pollutant concentrations between 2000 and 2014. This approach is similar to

that of Schnell and Prather (2017) and Sun et al. (2017), although the exact percentile we have chosen (P_{80}) differs. For both approaches we also consider how lag might affect the correspondence since temporal offsets between $PM_{2.5}$, O_3, and temperature events exist (Schnell and Prather, 2017).

3.3 Northeast United States

We first consider stagnation and pollution in the Northeast U.S. (Figure 3.1) and examine the variability of, and relationships among, Northeast-averaged pollutants, the percentage of stagnation coverage, and surface temperature. As an example, Figure 3.4a-c shows the daily variation of these quantities during the summer of 2011. All quantities display large daily variability, but Figure 3.4a-c shows that the variabilities of these quantities are not always correlated. In particular, days or periods with a high percentage of stagnation coverage do not generally correspond to days or periods with high pollutant concentrations (compare Figures 3.4a and 3.4b), and r between the ASI and $PM_{2.5}$ or O_3, as indicated in Figure 3.4d, are near zero. We note that there are some hints that the ASI might precede pollution in some cases, and the role of lag will be further explored in this section; but, overall, the correlation between $PM_{2.5}$ - ASI and O_3 - ASI is weak. In contrast, $PM_{2.5}$ and O_3 are highly correlated during the summer of 2011 and are generally accompanied by similar temperature variations (Figure 3.4b-c).

Although we primarily use regionally-averaged quantities in our present work, evaluating the spatial overlap of stagnant regions with the regions of highest pollutant concentrations leads to similar results. For example, in the

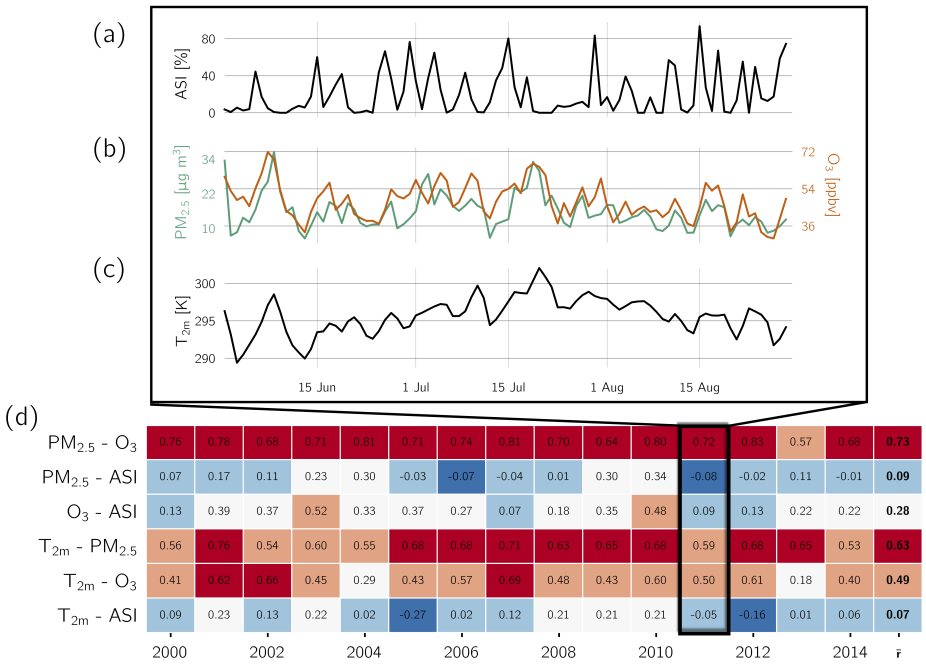

Figure 3.4: Daily percentage of stagnant stations in the Northeast is shown in (**a**), and regionally-averaged pollutant concentrations from stations in the Northeast are depicted and labeled with consistent colors in (**b**). Here $PM_{2.5}$ and O_3 represent daily regionally-averaged concentrations from all available monitoring stations in the Northeast. (**c**) shows average 2-meter temperatures averaged colocated with stations in the Northeast. Pearson product-moment correlation coefficients (r) between each pair of variables for each summer in the measuring period were calculated for the Northeast (**d**), and the multi-year average r values are noted in boldface in the table's final column.

case study shown in Figure 3.5, representing the highest Northeast-averaged pollutant concentrations during the summer of 2011, stagnant regions show little cohesive structure and are mostly confined to the Southern U.S., not the region with the highest $PM_{2.5}$ and O_3 concentrations (in this case, the Eastern Seaboard). On the other hand, we observe that the pollutants display much of the same spatial and temporal progression and the highest temperatures closely coincide with the region of maximum pollutant concentrations observed in the Northeast.

The results from summer 2011 hold for most years between 2000 and 2014. This is shown in Figure 3.4d, which shows r between each pair of variables for each summer and multi-year average correlation coefficients. Of the pairs examined, $PM_{2.5}$ and O_3 consistently have the strongest positive relationship followed by T_{2m} - $PM_{2.5}$ and T_{2m} - O_3. The correlation between the pollutants and ASI is weak and, for the case of $PM_{2.5}$ - ASI, near-zero indicating almost no degree of a linear relationship. The average correlation coefficient of O_3 - ASI is higher than $PM_{2.5}$ - ASI (i.e., 0.28 versus 0.09) and is strongly influenced by the high r values in 2003 and 2010 (for these two summers the relationship between the ASI and O_3 was approximately as strong as the relationship of O_3 and T_{2m}). The cause of this strong O_3 - ASI correlation for these two summers requires further examination; but, in general, the correlation is weak.

The correlation between T_{2m} and ASI in the Northeast is the weakest of all the pairs analyzed, and several years indicate that the correlation coefficients between surface temperature and the ASI are slightly negative. These results

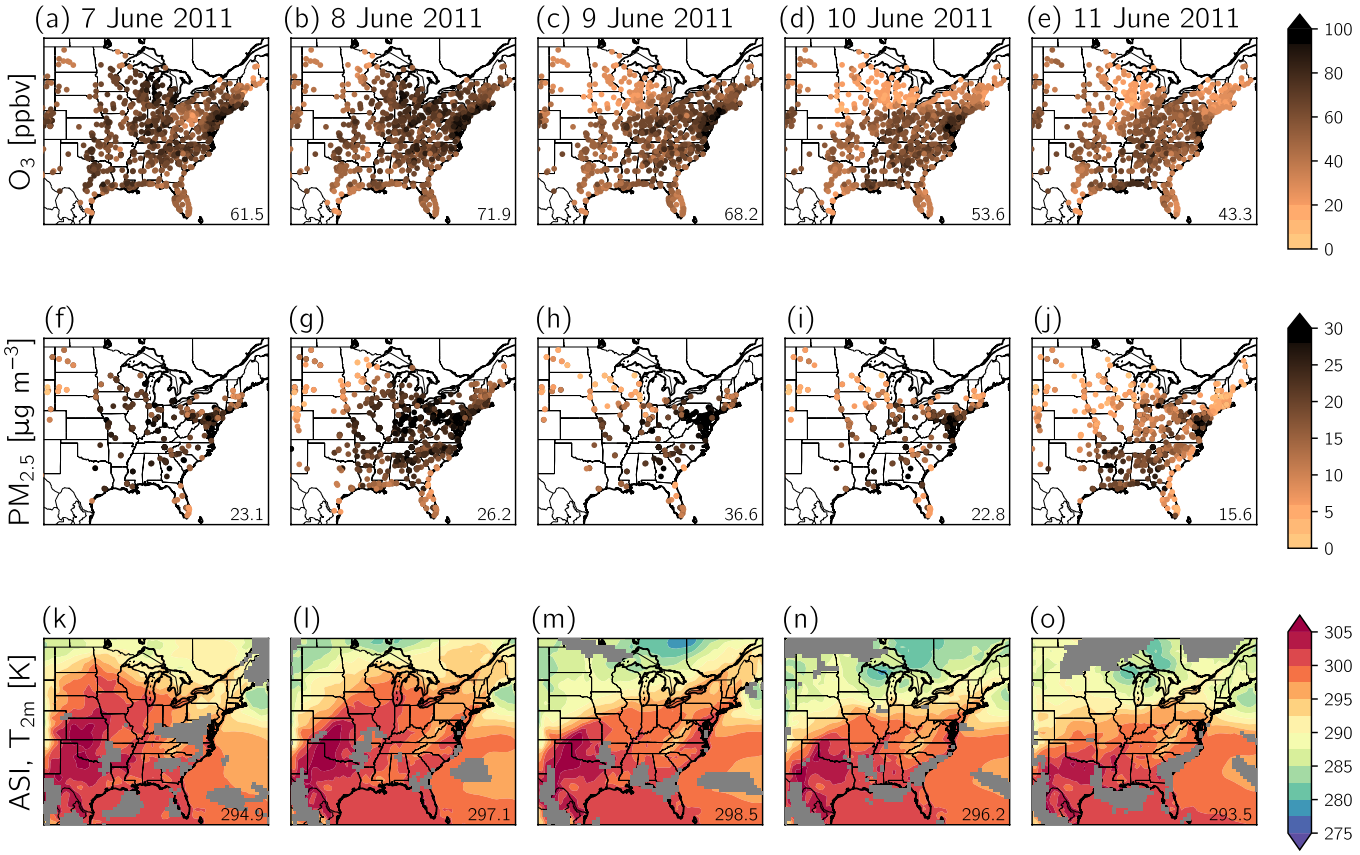

Figure 3.5: Progression of pollutants, surface temperature, and stagnation for a five day case study, 7-11 June 2011. (**a-e**) Scatterpoints indicate O_3 concentrations at AQS stations for each day of the event. Average O_3 concentrations for the Northeast, as defined in Figure 1 in the main text, are shown in the lower right corner. (**f-j**) Same as (**a-e**) but for $PM_{2.5}$ concentrations. (**k-o**) MERRA 2-meter temperatures are indicated with color-filled contours. The Northeast-averaged temperature is shown on the lower right corner and stagnated areas are shaded.

are inconsistent with the commonly-made statements linking stagnant conditions with high ambient temperatures (Tai et al., 2010; Austin et al., 2014; Fiore et al., 2015; Shen et al., 2016; Zhang et al., 2017).

Given the size of the Northeast region, pollutant concentrations and colocated meteorology could substantially differ from station to station; however, we find similar correlations for individual states comprising the Northeast region compared with the regionally-averaged Northeast correlation (Figure 3.3). For example, r between Northeast-averaged $PM_{2.5}$ and the regional percentage of stagnant cells is 0.09. Upon considering the correlation coefficients for the 14 individual states in the Northeast, we find that r varies from -0.01 to 0.28. Thus, although stationary (or quasi-stationary) anticyclones could migrate within a particular region and affect the relationship between pollutants and the ASI within, we find that our methodology is spatially-insensitive up to a region that is roughly the size of a typical anticyclone.

We also repeated the correlation analysis between the ASI and pollutants (Figure 3.4d) for AQS stations in rural, suburban, or urban environments, and the details of this analysis are shown in Table 3.1. Considering pollutant concentrations in different environments could lead to different relationships between the ASI and pollutants due to, for example, nitrogen oxides ($NO+NO_2$) (NO_x) titration, but we find that comparing only rural-, urban-, or suburban-averaged $PM_{2.5}$ (O_3) with the percentage of stagnant cells calculated for each environment leads to correlation coefficients ranging from 0.05 to 0.13 (0.24 to 0.31) compared to an correlation of 0.09 (0.28) using an average of all rural, urban, and suburban AQS stations.

We have shown that there are weak correlations between the daily time series of the spatial extent of the ASI and pollutants or temperature, but this does not necessarily mean that this lack of relationship applies for extreme events. We now examine whether pollution events show preferential co-occurrence with ASI events. As described in Section 3.2, an event is defined as a day in which pollutant concentrations, surface temperature, or the percentage of stagnant cells fall into the top 20^{th} percentile of days for a particular summer. Given the dates of pollutant and ASI events, we calculate the same-day percentile distributions of other variables (grey histograms in Figure 3.6) and the maximum percentile of the other variables on the day before the event and the day following the event (lag = ± 1 day; black outlined histograms). Our results are not sensitive to the use of P_{80} as the threshold for events, and we observe similar relative differences between the combinations of different quantities.

Table 3.1: Pearson correlation coefficients (r) calculated between $PM_{2.5}$ and ASI (normal emphasis) and O_3 and ASI (italics) for different environments and regions.

	Region[a]				
Environment	Northeast	South	Midwest	Intermountainous West	West
Rural	0.10, *0.24*	0.27, *0.62*	0.33, *0.44*	0.17, *0.32*	0.11, *0.55*
Suburban	0.13, *0.31*	0.35, *0.62*	0.22, *0.43*	0.10, *0.38*	0.31, *0.47*
Urban	0.05, *0.27*	0.36, *0.63*	0.28, *0.40*	0.16, *0.35*	0.35, *0.43*
All	0.09, *0.28*	0.38, *0.64*	0.27, *0.43*	0.16, *0.36*	0.32, *0.51*

[a] Defined in Figure 3.1.

We first consider the relationship between $PM_{2.5}$ and O_3 events. Given the high correlation in the daily time series of these quantities, a high co-occurence

of events is expected. This is indeed the case, and nearly two-thirds of $PM_{2.5}$ and O_3 events co-occur, while the frequency of co-occurring events increases to over 80% if we consider that $PM_{2.5}$ or O_3 could also precede or proceed each other by a day (Figure 3.6a-b). The picture is, however, different for co-occurrence between pollution and ASI events, and there is only a small percentage of co-occurring pollutant and ASI events (Figure 3.6d-e). Allowing for the ASI to lag pollutant events by ± 1 day leads to a higher frequency of co-occurring events (46% for both $PM_{2.5}$ and O_3, black outlined histograms in Figure 3.6d-e). Although this indicates that nearly half of pollution events tend to occur within a day of ASI events, over 50% of pollution events do occur under non-stagnant conditions, presenting a possible gap in the community's understanding of the drivers of these events.

The percentile distributions of temperature for pollutant events (Figure 3.6g-h) are negatively skewed and indicate that polluted days are likely to also be hot days in the Northeast. Comparing the percentage of same day or lagged co-occurring events in Figure 3.6g-h versus Figure 3.6d-e suggests that a metric as simple as surface temperature is a much better predictor than the ASI; for instance, 2.5 times as many same-day temperature and $PM_{2.5}$ events co-occur than same-day ASI and $PM_{2.5}$ events (55% versus 22%).

The lack of co-occurrence of ASI events with pollution and temperature events is highlighted in the third column of Figure 3.6, which shows the percentile distributions of pollutants and temperature for ASI events. Days with ASI events are characterized by relatively flat, uniform distributions of same-day $PM_{2.5}$, O_3, and T_{2m}: therefore, regional ASI events in the Northeast are

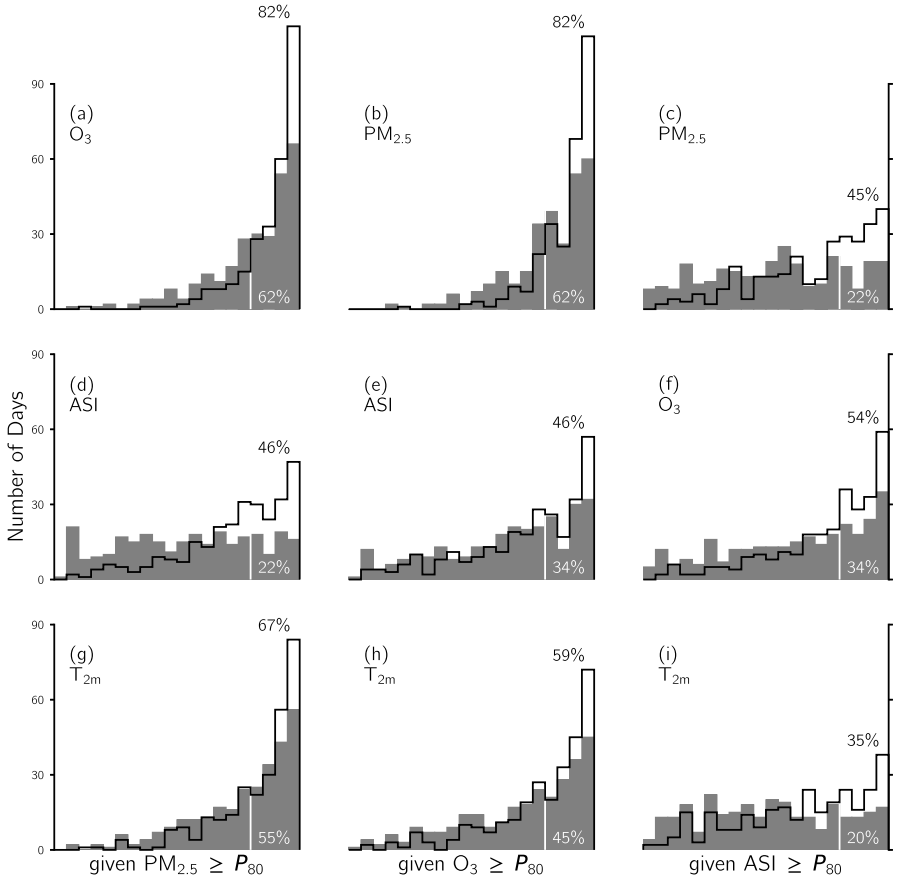

Figure 3.6: Percentile distributions of Northeast-averaged quantities are plotted in grey 5 percentile bins on days with $PM_{2.5}$ (**a, d, g**), O_3 (**b, e, h**), and ASI events (**c, f, i**). White vertical lines superimposed on the grey histograms indicate the 80^{th} percentile (P_{80}), and the corresponding white-colored text states the percentage of events occurring above this threshold and are therefore also pollution, temperature, or ASI events by definition. The same distributions but for the given quantity preceding or proceeding the other quantities by a day (lag = ± 1 day) is shown in black outlined histograms. Text above these outlined histograms is the percentage of lagged events that are also events in the other quantity.

generally neither polluted nor hot days; however, allowing for lag increases the percentage of co-occurrence for ASI events, although these lagged distributions are not as negatively skewed as the lagged temperature-pollutant distributions.

Sun et al. (2017) have recently shown the impact of meteorological persistence on O_3. Using different data and methods than us, they drew similar conclusions to our study: a single stagnation day is not a good predictor of high O_3, while the best single day predictor of high O_3 concentrations is high temperature (Sun et al., 2017). Their results also suggested that successive (multi-day) ASI events have the potential to enhance pollutant concentrations. We evaluate this possibility by calculating the average percentiles of Northeast-averaged $PM_{2.5}$ and O_3 for ASI events of different lengths (i.e., single-day ASI event, 2 successive ASI events, etc.). This analysis shows a small increase in the percentile of $PM_{2.5}$ and O_3 on the event's final day with increasing event length (Figure 3.7), but overall, even 3 or 4 consecutive days with ASI events fail to enhance $PM_{2.5}$ or O_3 to levels that would classify their average concentrations as events (i.e., $\geq P_{80}$). This is consistent with Sun et al. (2017) who showed that 4 consecutive ASI days could only increase the conditional probability of a high O_3 day to ~ 0.60.

3.4 Contiguous United States

The analysis in the previous section showed a weak correspondence between the ASI and pollution, both with respect to daily variability and the co-occurrence of extreme events, in the Northeast U.S. We next turn our focus

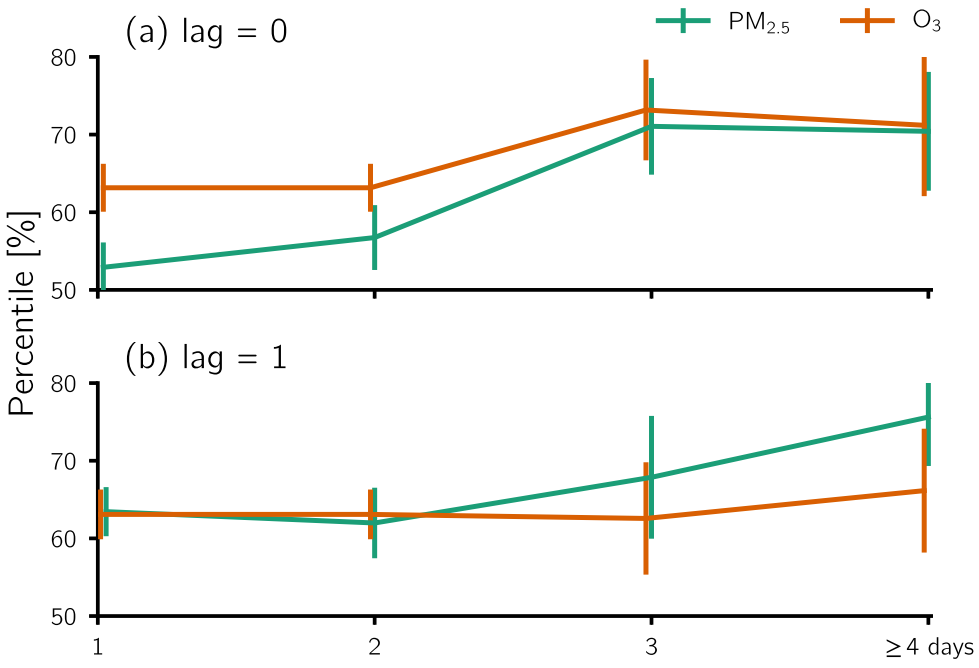

Figure 3.7: The role of lag and stagnation length on pollutant enhancement is quantified by identifying all stagnation events in the measuring period and grouping these events by their length, denoted here on the dependent axis. Subplots depict the average percentile of Northeast-averaged $PM_{2.5}$ and O_3 on the final day of the stagnation event (**a**) as well as the day following the ASI event's end (**b**). Error bars correspond to the standard error of the percentiles for each event length.

to the other regions shown in Figure 3.1 and highlight the correspondence of pollution and the ASI in these regions. We use the correlation coefficient (r) averaged over all summers (Figure 3.8a) and the percentage of co-occurring events (Figure 3.8b) to analyze the correspondence of pollution, surface temperature, and the ASI for each region.

The relationships between the variables in the Midwest are qualitatively similar to the Northeast. High $PM_{2.5}$ concentrations are often accompanied by high O_3 concentrations and high temperatures and vice versa, but same-day pollution and temperature events co-occur with ASI events with greater

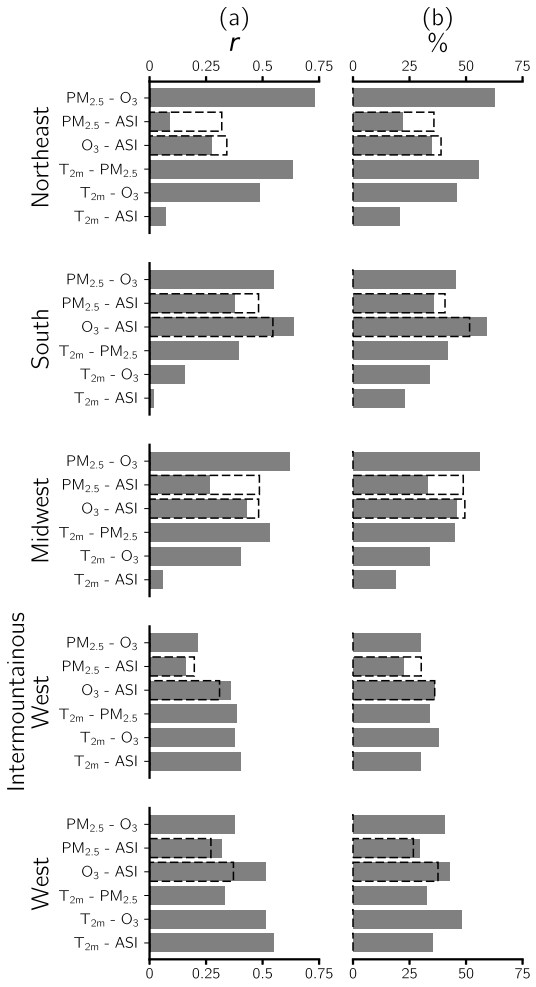

Figure 3.8: Spatially-averaged daily pollutant concentrations, surface temperatures, and the percentage of stagnant cells over each region defined in Figure 3.1. (**a**) 2000-2014 average correlation coefficients between the variables. The grey bars show correlations with no time lag, while dashed, outlined bars show the correlation coefficient for $PM_{2.5}$ - ASI and O_3 - ASI when ASI precedes the pollutants by 1 day. (**b**) The frequency of event co-occurrence for each region. Again, the dashed lines correspond to the frequency of event co-occurrence when the ASI precedes $PM_{2.5}$ or O_3 events by 1 day.

frequency in the Midwest compared to the Northeast (i.e., 32% for $PM_{2.5}$ - ASI, 45% for O_3 - ASI, and 18% for T_{2m} - ASI; Figure 3.9c, f, i); however, the ASI cannot explicitly explain a majority of pollution events, even when allowing for the ASI to precede pollution by 1 day (dashed outlined bars in Figure 3.8). Again, as in the Northeast, there is not a strong relationship between the ASI and temperature ($r = 0.05$, 18% of events co-occur).

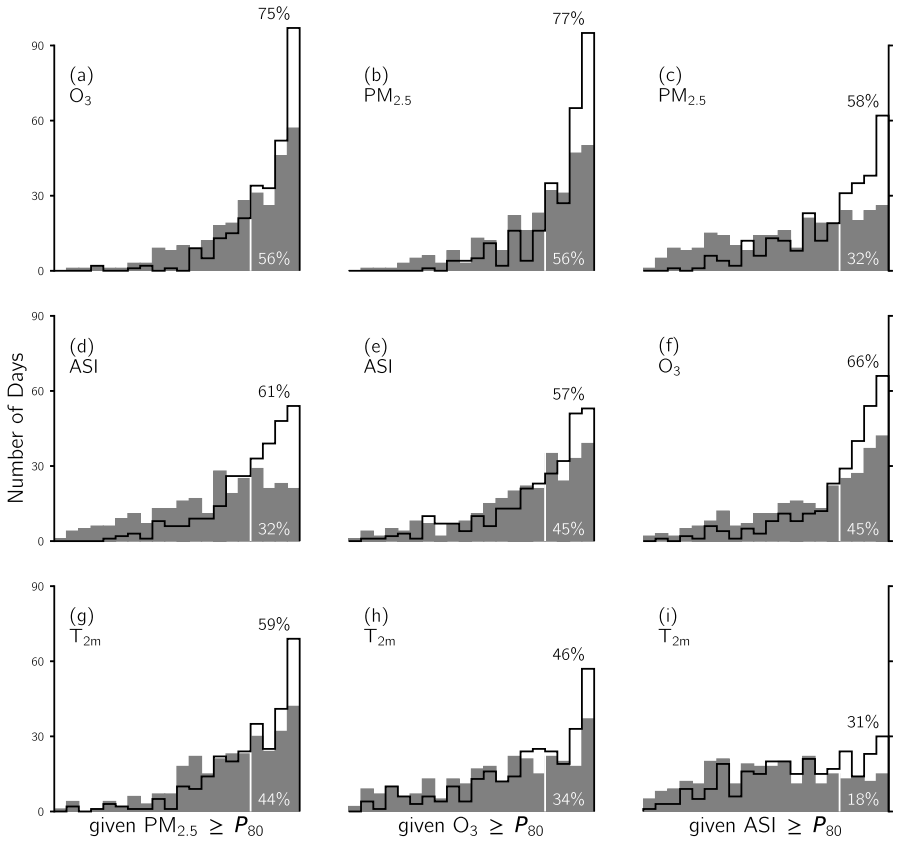

Figure 3.9: Same as Figure 3.6 but for the Midwest.

We repeat the analysis shown in Figure 3.6 for the other regions defined

in Figure 3.1 and present these findings in Figures 3.9 - 3.12. The South stands out as the region with the highest correlation and event co-occurrence between the ASI and pollution. Allowing for ± 1 day lag between the ASI and pollutants increases the event co-occurrence in the South; however, an interesting aspect of the lag analysis in this region is that allowing the ASI to lag O_3 events by $\pm$ 1 day (Figure 3.10e) increases the likelihood of co-occurring events (71%) whereas only allowing the ASI to *precede* O_3 by 1 day (Figure 3.8b) decreases the likelihood (52%). This implies stagnant conditions occurs the day *following* O_3 events in the South. This result is counter-intuitive, and further work is needed beyond this study to understand the timing of event onset. Unlike in the Northeast, $PM_{2.5}$ and O_3 events are less likely to co-occur in the South by $\sim$ 20% (Figure 3.6a-b versus Figure 3.10a-b). In the South stagnation events preferentially occur on days with more moderate to cooler temperatures (Figure 3.10i).

In the Intermountainous West and West the relationship between $PM_{2.5}$ and O_3 is weaker than in other regions and could reflect compositional differences of $PM_{2.5}$ in these regions (Hand et al., 2012) and the role of $PM_{2.5}$ composition on the chemical coupling between $PM_{2.5}$ and O_3 (Meng et al., 1997; Brown and Jin, 2013). Of all the regions examined, same-day temperature and ASI events occur with the greatest frequency in the Intermountainous West and West (35% and 42%, respectively) (Figure 3.8b). Correlations between the ASI and pollutants in the Intermountainous West and West are intermediate between the South and the Midwest/Northeast. However, allowing for the ASI to precede pollutants by 1 day in the Intermountainous West and West does

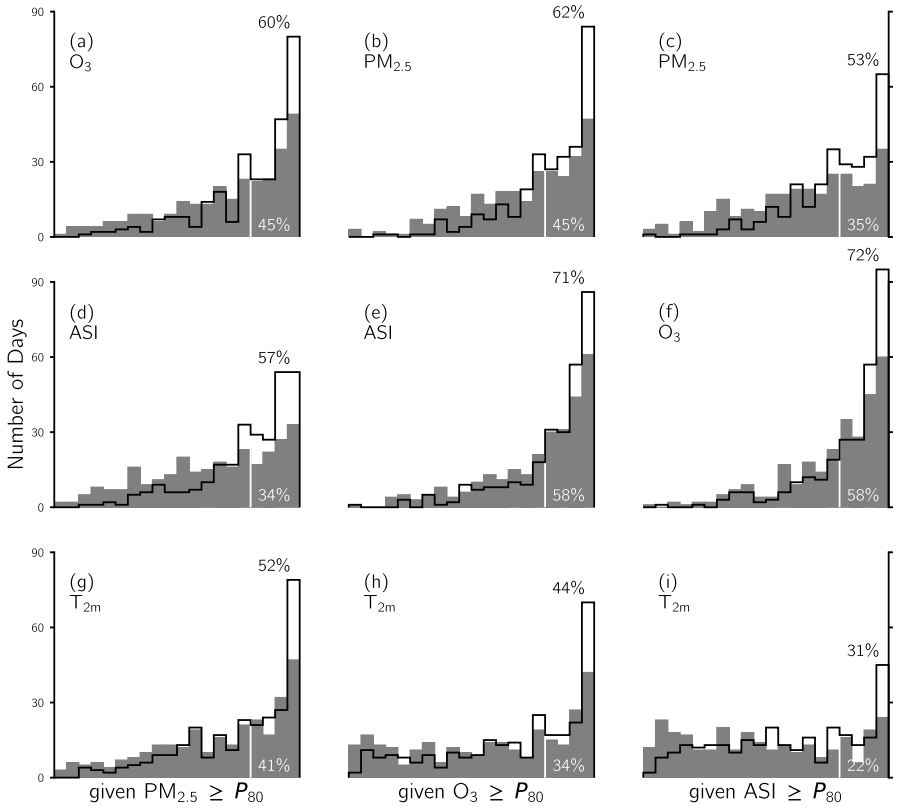

Figure 3.10: Same as Figure 3.6 but for the South.

not increase the likelihood of co-occurring events or strengthen correlation coefficients by the same margin as for other regions. Similar to the South, this 1 day lag decreases the coincidence of co-occurring ASI and pollutant events (29 to 27% for $PM_{2.5}$, 43 to 38% for O_3) and weakens correlation coefficients (0.31 to 0.27 for $PM_{2.5}$, 0.51 to 0.37 for O_3) in the West (Figure 3.8).

Understanding the regional heterogeneity of stagnation's correspondence with pollutants requires further examination, but the increased frequency of

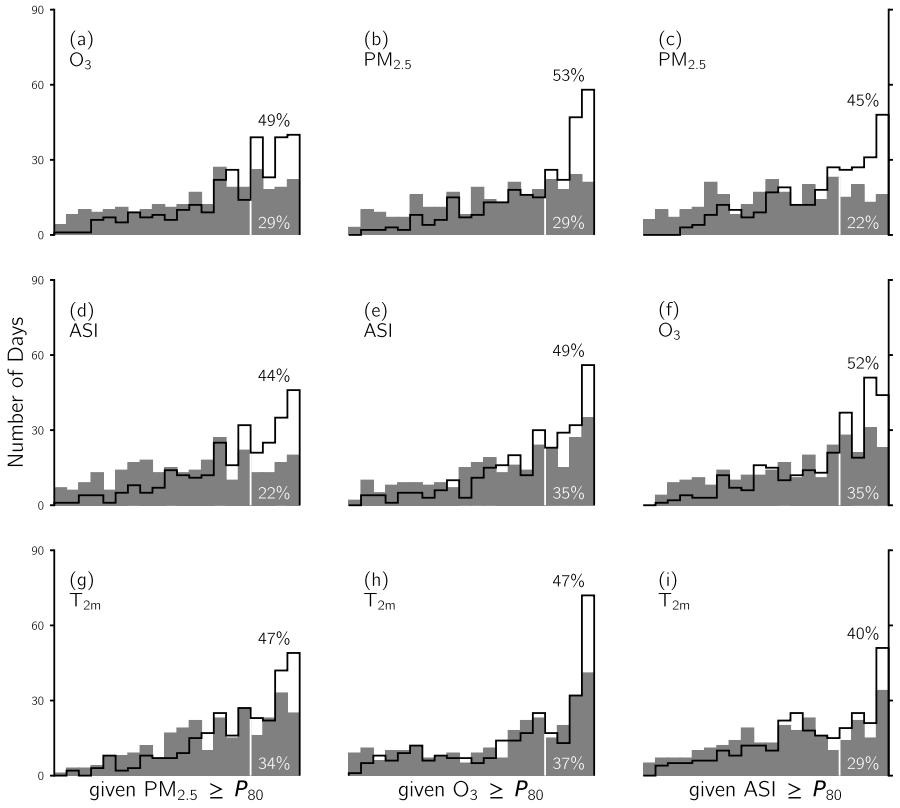

Figure 3.11: Same as Figure 3.6 but for the Intermountainous West.

concurrent stagnation and pollution events in the South and West (Figures 3.7, 3.10) could stem from the increased persistence of pollution events in these regions compared to the northern regions (e.g., Lehman et al., 2004) as lengthened pollution events could allow for a preferential coincidence with stagnant regions. Similarly, Zhang et al. (2018) found the highest coincidence of stagnation with O_3 occurred in the South, Southeast, and along the West Coast. Thus, the increased frequency of co-occurrence in these regions might

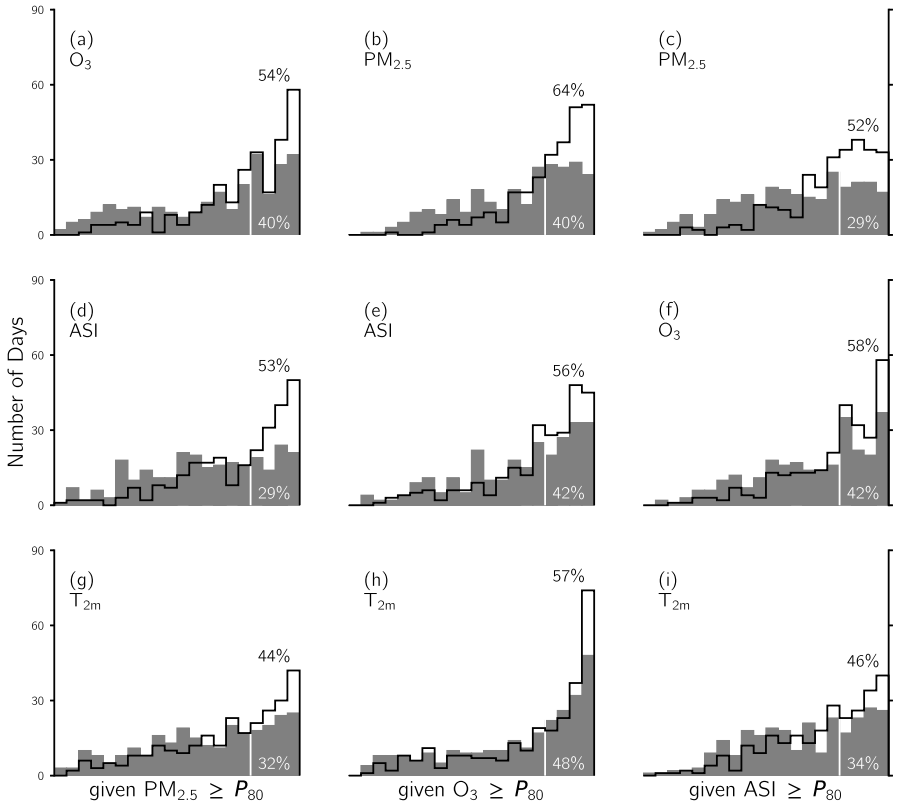

Figure 3.12: Same as Figure 3.6 but for the West.

also arise from the strong correlation between pollutants and $\tilde{U}_{10\mathrm{m}}$, one of the three variables used to calculate the ASI.

As done for the Northeast, we also considered the ASI - pollutant correlations from different environments and observed only small differences using only rural, urban, or suburban stations (Table 3.1). The correlation between rural $PM_{2.5}$ and the ASI in the West is a peculiar case: here, the rural correlation is $r = 0.11$ whereas the correlations for urban, suburban, or all locations

are ~ 0.30; we speculate that this could arise from the paucity of AQS stations in this region or if rural stations in this region are located at higher altitudes than the urban and suburban stations and therefore sample the lower free troposphere.

3.5 Reconciliation with Previous Studies

As discussed in the Introduction (Section 3.1), it is widely-accepted that atmospheric stagnation is one of main causes of extreme air pollution. However, we reveal that stagnant conditions, as characterized by the ASI, cannot explain a majority of pollutant events and are not well-correlated with pollutant concentrations. This appears to contradict some previous studies. For example, Tai et al. (2010) and Dawson et al. (2014) have shown high $PM_{2.5}$ during stagnant compared to non-stagnant days or periods. The apparent contradiction is because the increase in $PM_{2.5}$ between stagnant and non-stagnant days is much smaller than daily variability in these studies (for example, Tai et al. (2010) report an increase in $PM_{2.5}$ of 2.6 $\mu g\ m^{-3}$ on stagnant days across the contiguous U.S.). If we calculate the difference in $PM_{2.5}$ and O_3 concentrations between summertime stagnant and non-stagnant days (Figure 3.13), we also find a small increase (for instance, 2.34 $\mu g\ m^{-3}$ for $PM_{2.5}$ and 7.94 ppbv for O_3 in the Northeast). This is consistent with our correlation analysis: although the strength of the correlation between the ASI and $PM_{2.5}$ or O_3 is weak, there is, in general, a positive association, indicating increased $PM_{2.5}$ or O_3 with increased stagnation coverage. Thus, on average, days with a high percentage of stagnation coverage have higher pollutant concentrations than days with a

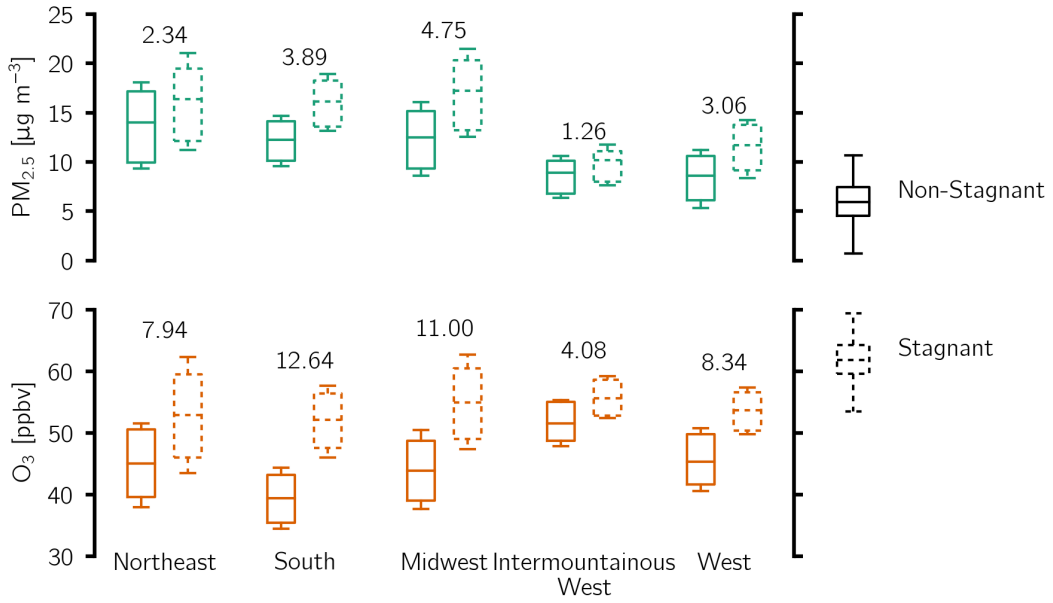

Figure 3.13: For the five regions defined in Figure 3.1, the regionally-averaged distributions of summer $PM_{2.5}$ (top) and O_3 (bottom) concentrations are determined for the top 20^{th} percentile of days with ASI coverage ("Stagnant") and the bottom 20^{th} percentile ("Non-Stagnant"). Text above the pairs of boxplots corresponds to the relative enhancement in mean pollutant concentrations between stagnant and non-stagnant days.

low percentage. However, the difference is small, and we have shown that there are many days when the percentage of stagnant cells and pollutants are not both high (or both low).

The fact that there is on average a small increase in pollutant concentrations on stagnant days (Figure 3.13) also reconciles our analysis with previous studies showing the interannual relationship between stagnation and pollution (Leibensperger et al., 2008; Schnell and Prather, 2017). Repeating our analysis for mean JJA values we also find moderate positive correlations between pollutants and the ASI in the Northeast (i.e., $r_{\text{ASI}-\text{PM}_{2.5}} = 0.42$ and

$r_{\mathrm{ASI}-\mathrm{O}_3} = 0.67$; Figure 3.14), but the difference in pollutants between years is small (i.e., interannual standard deviation of mean JJA values for $\mathrm{PM}_{2.5}$ (O_3) is only 1.89 $\mu\mathrm{g\ m}^{-3}$ (4.11 ppbv) in the Northeast).

Figure 3.14: Summer mean $\mathrm{PM}_{2.5}$ and O_3 concentrations (with trends removed) along with the summertime average percentage of stagnant grid cells in the Northeast. Correlation coefficients (r) between the quantities are: $r_{\mathrm{PM}_{2.5}-\mathrm{O}_3} = 0.74$, $r_{\mathrm{ASI}-\mathrm{PM}_{2.5}} = 0.42$, and $r_{\mathrm{ASI}-\mathrm{O}_3} = 0.67$.

In summary, there are differences in average $\mathrm{PM}_{2.5}$ or O_3 concentrations between stagnant and non-stagnant days or between summers with different frequencies of stagnation events, but these differences are very small and there is far from a one-to-one correspondence between stagnation and pollutants on daily timescales or for the co-occurrence of extreme events.

Our findings of a weak relationships between pollution and the ASI is consistent with Wang et al. (2018) and Huang et al. (2018) who showed that

the ASI was not well-correlated with $PM_{2.5}$ and O_3, respectively, in China. Furthermore, Oswald et al. (2015) determined that various statistical methods did not find stagnation to be the strongest predictor of surface-level O_3. Finally, while Schnell and Prather (2017) showed interannual correlations between $PM_{2.5}$, O_3, and the ASI, maps depicting the day-to-day spatial correspondence of pollutants and the ASI yielded similar findings to our results in Figure 3.5; that is, ASI coverage shows erratic overlap with pollutant extremes.

This study serves to document the correspondence between common criteria pollutants, temperature, and stagnation during the summer, and its purpose is not to propose an alternative metric beyond the ASI for understanding pollution. However, we offer the following commentary to address the weak correspondence between the ASI and pollutants: the meteorological variables which define the ASI may not be the best predictor variables for diagnosing polluted areas or periods. Camalier et al. (2007) examined the effects of meteorology on O_3 trends in urban areas and found that, for much of the Northeast and South, temperature, humidity, and transport direction were the best meteorological parameters to predict O_3; none of these variables are included in the ASI. Shen et al. (2015) uncovered that the largest fraction of the total variance in O_3 can be explained by the north-south movement of the mid-latitude jet. Since the jet is often confined to more northerly latitudes, the increased correspondence of stagnation with pollutants in the South (Figures 3.8, 3.10) could result from weaker mid-tropospheric wind speeds at 500 hPa. Regardless, the exact position of the the jet is not taken into account by the ASI, nor can the ASI characterize all of the known microscale patterns (e.g., Jacob

and Winner, 2009, and references therein), synoptic patterns (e.g., Barnes and Fiore, 2013; Shen et al., 2015; Otero et al., 2016), teleconnection patterns (e.g., Shen and Mickley, 2017), and distribution of anthropogenic precursor emissions (e.g., He et al., 2013a) which have been shown to influence surface-level pollution. Another possibility is that stagnant flow and limited ventilation simply are not the dominant factors causing pollution events. We plan further research to answer this question.

3.6 Conclusions

There are good mechanistic reasons to suspect that stagnation would (via pollutant trapping by weak winds and no scavenging by precipitation) lead to increased surface-level pollution. However, we fail to find a widespread correspondence. In most regions of the U.S. there is only a weak correspondence between stagnation and summertime $PM_{2.5}$ and O_3, both with regard to day-to-day variations as well as the co-occurrence of events. For example, in the Northeast, 78% (66%) of same-day $PM_{2.5}$ (O_3) events occur when the percentage of stagnant cells is such that it is not classified as a stagnation event. Similarly, days with a high coverage of stagnation only co-occur with pollution events about one-third of the time in the Northeast. This signal is relatively consistent across the contiguous U.S.; although the South is an exception as pollution and ASI events co-occur with greater likelihood and correlations are strongest compared with other regions, but even in the South same-day correlations do not exceed 0.38 for $PM_{2.5}$ - ASI and 0.64 for O_3 - ASI, and there are many pollution events not associated with stagnation events.

Our results also indicate a lack of consensus between stagnation and high temperature across the U.S. In the South, the region with the strongest correlation between stagnation and pollution, the correlation between stagnation and temperature is near-zero. Thus, we cannot make any definitive statements on the relationship between hot and stagnant days. In contrast to the general lack of relationship between stagnation and pollution concentrations or surface temperature, there is generally a strong correlation between temperature and $PM_{2.5}$ and O_3 concentrations ($r = 0.46$ and 0.38 averaged over the contiguous U.S., respectively). Jacob and Winner (2009) found that no significant correlations of $PM_{2.5}$ with temperature had been reported in the literature. While the $PM_{2.5}$ - temperature relationship is complicated and varies between summer and winter (e.g., Dawson et al., 2014), our findings uncover consistently positive correlations between $PM_{2.5}$ - temperature for the summer season and are an important update to Jacob and Winner (2009).

The findings from this study suggest that the community shy away from using the ASI as a metric to understand pollution events and instead test different pollution-related indices using meteorological predictors such as temperature or boundary layer height as correlations and event co-occurrence between pollution and these other indices could differ from the ones shown here. Furthermore, our results suggest caution is required when inferring changes in air pollution from projected changes of stagnation under climate change.

References

Austin, Elena, Antonella Zanobetti, Brent Coull, Joel Schwartz, Diane R. Gold, and Petros Koutrakis (2014). "Ozone trends and their relationship to characteristic weather patterns". In: *J. Expo. Sci. Environ. Epidemiol.*

Barnes, Elizabeth A. and Arlene M. Fiore (2013). "Surface ozone variability and the jet position: Implications for projecting future air quality". In: 40.11, pp. 2839–2844. DOI: 10.1002/grl.50411.

Brown, Nancy and Ling Jin (2013). *Improving the understanding $PM_{2.5}$ and ozone chemistry from air quality monitoring for more accurate prediction of power generation impacts*. Tech. rep. CEC-500-2014-015. Lawrence Berkeley National Laboratory.

Camalier, Louise, William Cox, and Pat Dolwick (2007). "The effects of meteorology on ozone in urban areas and their use in assessing ozone trends". In: 41.33, pp. 7127–7137. DOI: 10.1016/j.atmosenv.2007.04.061.

Dawson, J. P., P. J. Adams, and S. N. Pandis (2007a). "Sensitivity of $PM_{2.5}$ to climate in the Eastern US: A modeling case study". In: *Atmos. Chem. Phys.* 7.16, pp. 4295–4309. URL: http://www.atmos-chem-phys.net/7/4295/2007/ (visited on 12/31/2016).

Dawson, John P., Peter J. Adams, and Spyros N. Pandis (2007b). "Sensitivity of ozone to summertime climate in the eastern USA: A modeling case study". In: *Atmos. Environ.* 41.7, pp. 1494–1511. DOI: 10.1016/j.atmosenv.2006.10.033.

Dawson, John P., Bryan J. Bloomer, Darrell A. Winner, and Christopher P. Weaver (2014). "Understanding the meteorological drivers of US particulate matter concentrations in a changing climate". In: *Bull. Am. Meteorol. Soc.* 95.4, pp. 521–532.

Ebi, Kristie L. and Glenn McGregor (2008). "Climate change, tropospheric ozone and particulate matter, and health impacts". en. In: *Environ. Health Perspect.* 116.11, pp. 1449–1455. DOI: 10.1289/ehp.11463.

Fiore, Arlene M., Vaishali Naik, and Eric M. Leibensperger (2015). "Air Quality and Climate Connections". In: 65.6, pp. 645–685. DOI: 10.1080/10962247.2015.1040526.

Fiore, Arlene M., Vaishali Naik, Dominick V. Spracklen, Allison Steiner, Nadine Unger, Michael Prather, et al. (2012). "Global air quality and climate". In: *Chem. Soc. Rev.* 41.19, p. 6663. DOI: 10.1039/c2cs35095e.

Hand, J. L., B. A. Schichtel, M. Pitchford, W. C. Malm, and N. H. Frank (2012). "Seasonal composition of remote and urban fine particulate matter in the United States". In: *J. Geophys. Res. Atmos.* 117.D5, n/a–n/a. DOI: 10.1029/2011JD017122.

He, Hao, Linda Hembeck, Kyle M. Hosley, Timothy P. Canty, Ross J. Salawitch, and Russell R. Dickerson (2013a). "High ozone concentrations on hot days: The role of electric power demand and NO_x emissions: Ozone and power demand on hot days". In: 40.19, pp. 5291–5294. DOI: 10.1002/grl.50967.

He, H., J. W. Stehr, J. C. Hains, D. J. Krask, B. G. Doddridge, K. Y. Vinnikov, et al. (2013b). "Trends in emissions and concentrations of air pollutants in the lower troposphere in the Baltimore/Washington airshed from 1997 to 2011". In: 13.15, pp. 7859–7874. DOI: 10.5194/acp-13-7859-2013.

Horton, Daniel E, Harshvardhan, and Noah S Diffenbaugh (2012). "Response of air stagnation frequency to anthropogenically enhanced radiative forcing". In: *Environ. Res. Lett.* 7.4. DOI: 10.1088/1748-9326/7/4/044034.

Horton, Daniel E., Christopher B. Skinner, Deepti Singh, and Noah S. Diffenbaugh (2014). "Occurrence and persistence of future atmospheric stagnation events". In: *Nature Climate Change* 4.8, pp. 698–703. DOI: 10.1038/nclimate2272.

Hou, Pei and Shiliang Wu (2016). "Long-term changes in extreme air pollution meteorology and the implications for air quality". In: *Sci. Rep.* 6.1. DOI: 10.1038/srep23792.

Huang, Qianqian, Xuhui Cai, Jian Wang, Yu Song, and Tong Zhu (2018). "Climatological study of a new air stagnation index (ASI) for China and its relationship with air pollution". In: *Atmos. Chem. Phys.* Pp. 1–39. DOI: 10.5194/acp-2017-1145.

Jacob, Daniel J. and Darrell A. Winner (2009). "Effect of climate change on air quality". In: 43.1, pp. 51–63. DOI: 10.1016/j.atmosenv.2008.09.051.

Kerr, Gaige Hunter and Darryn W Waugh (2018). "Connections between summer air pollution and stagnation". In: 13.8, p. 084001. DOI: 10.1088/1748-9326/aad2e2.

Korshover, Julius and J. K. Angell (1982). "A review of air-stagnation cases in the eastern United States during 1981". In: *Mon. Weather Rev.* 110, pp. 1515–1518. DOI: http://dx.doi.org/10.1175/1520-0493(1982)110<1515:AROASC>2.0.CO;2.

Lehman, Jeff, Kristen Swinton, Steve Bortnick, Cody Hamilton, Ellen Baldridge, Brian Eder, and Bill Cox (2004). "Spatio-temporal characterization of tropospheric ozone across the eastern United States". In: *Atmos. Environ.* 38.26, pp. 4357–4369. DOI: 10.1016/j.atmosenv.2004.03.069.

Leibensperger, Eric M., Loretta J. Mickley, and Daniel J. Jacob (2008). "Sensitivity of US air quality to mid-latitude cyclone frequency and implications of 1980-2006 climate change". In: 8.23, pp. 7075–7086.

Leung, L. Ruby and William I. Gustafson (2005). "Potential regional climate change and implications to U.S. air quality". In: *Geophys. Res. Lett.* 32.L16711, p. 4. DOI: doi:10.1029/2005GL022911.

Liu, Ying, Naizhuo Zhao, Jennifer K. Vanos, and Guofeng Cao (2017). "Effects of synoptic weather on ground-level $PM_{2.5}$ concentrations in the United States". In: *Atmos. Environ.* 148, pp. 297–305. DOI: 10.1016/j.atmosenv.2016.10.052.

Logan, Jennifer A. (1989). "Ozone in rural areas of the United States". In: *J. Geophys. Res. Atmos.* 94.D6, pp. 8511–8532. DOI: 10.1029/JD094iD06p08511.

Meng, Z., D. Dabdub, and J. H. Seinfeld (1997). "Chemical coupling between atmospheric ozone and particulate matter". In: *Science* 277.5322, pp. 116–119.

Oswald, Evan M., Lesley-Ann Dupigny-Giroux, Eric M. Leibensperger, Rich Poirot, and Jeff Merrell (2015). "Climate controls on air quality in the Northeastern U.S.: An examination of summertime ozone statistics during 1993-2012". In: *Atmos. Environ.* 112, pp. 278–288. DOI: 10.1016/j.atmosenv.2015.04.019.

Otero, N, J Sillmann, J L Schnell, H W Rust, and T Butler (2016). "Synoptic and meteorological drivers of extreme ozone concentrations over Europe". In: 11.2, p. 024005. DOI: 10.1088/1748-9326/11/2/024005.

Rieder, H E, A M Fiore, L M Polvani, J-F Lamarque, and Y Fang (2013). "Changes in the frequency and return level of high ozone pollution events over the eastern United States following emission controls". In: *Environ. Res. Lett.* 8.1, p. 014012. DOI: 10.1088/1748-9326/8/1/014012.

Rienecker, Michele M., Max J. Suarez, Ronald Gelaro, Ricardo Todling, Julio Bacmeister, Emily Liu, et al. (2011). "MERRA: NASA's Modern-Era Retrospective Analysis for Research and Applications". In: 24.14, pp. 3624–3648. DOI: 10.1175/JCLI-D-11-00015.1.

Saunders, Rolando O. and Darryn W. Waugh (2015). "Variability and potential sources of summer $PM_{2.5}$ in the Northeastern United States". In: *Atmos. Environ.* 117, pp. 259–270. DOI: 10.1016/j.atmosenv.2015.07.007.

Schnell, Jordan L. and Michael J. Prather (2017). "Co-occurrence of extremes in surface ozone, particulate matter, and temperature over eastern North America". In: 114.11, pp. 2854–2859. DOI: 10.1073/pnas.1614453114.

Shen, L., L. J. Mickley, and A. P. K. Tai (2015). "Influence of synoptic patterns on surface ozone variability over the eastern United States from 1980 to 2012". In: 15.19, pp. 10925–10938. DOI: 10.5194/acp-15-10925-2015.

Shen, Lu and Loretta J. Mickley (2017). "Seasonal prediction of US summertime ozone using statistical analysis of large scale climate patterns". In: *Proc. Natl. Acad. Sci.* 114.10, pp. 2491–2496. DOI: 10.1073/pnas.1610708114.

Shen, Lu, Loretta J. Mickley, and Lee T. Murray (2016). "Strong influence of 2000–2050 climate change on particulate matter in the United States: Results from a new statistical model". In: *Atmos. Chem. Phys.* Pp. 1–26. DOI: 10.5194/acp-2016-954.

Strode, Sarah A., Jose M. Rodriguez, Jennifer A. Logan, Owen R. Cooper, Jacquelyn C. Witte, Lok N. Lamsal, et al. (2015). "Trends and variability in surface ozone over the United States". In: 120.17, pp. 9020–9042. DOI: 10.1002/2014JD022784.

Sun, Wenxiu, Peter Hess, and Chengji Liu (2017). "The impact of meteorological persistence on the distribution and extremes of ozone". In: DOI: 10.1002/2016GL071731.

Tai, Amos P.K., Loretta J. Mickley, and Daniel J. Jacob (2010). "Correlations between fine particulate matter ($PM_{2.5}$) and meteorological variables in the United States: Implications for the sensitivity of $PM_{2.5}$ to climate change". In: *Atmos. Environ.* 44.32, pp. 3976–3984. DOI: 10.1016/j.atmosenv.2010.06.060.

Vautard, R, C Honore, M Beekmann, and L Rouil (2005). "Simulation of ozone during the August 2003 heat wave and emission control scenarios". In: *Atmos. Environ.* 39.16, pp. 2957–2967. DOI: 10.1016/j.atmosenv.2005.01.039.

Vukovich, Fred M. (1995). "Regional-scale boundary layer ozone variations in the eastern United States and their association with meteorological variations". In: *Atmos. Environ.* 29.17, pp. 2259–2273.

Wang, Julian XL and James K. Angell (1999). "Air stagnation climatology for the United States". In: *NOAA/Air Resource Laboratory ATLAS* 1.

Wang, Xiaoyan, Robert E. Dickinson, Liangyuan Su, Chunl ue Zhou, and Kaicun Wang (2018). "$PM_{2.5}$ pollution in China and how it has been exacerbated by terrain and meteorological conditions". In: *Bull. Am. Meteorol. Soc.* 99.1, pp. 105–119. DOI: 10.1175/BAMS-D-16-0301.1.

Zhang, Henian, Yuhang Wang, Tae-Won Park, and Yi Deng (2017). "Quantifying the relationship between extreme air pollution events and extreme weather events". In: *Atmos. Res.* 188, pp. 64–79. DOI: 10.1016/j.atmosres.2016.11.010.

Zhang, Junxi, Yang Gao, Kun Luo, L. Ruby Leung, Yang Zhang, Kai Wang, and Jianren Fan (2018). "Impacts of compound extreme weather events on ozone in the present and future". In: *Atmos. Chem. Phys.* Pp. 1–32. DOI: 10.5194/acp-2018-231.

Chapter 4

Surface ozone-meteorology relationships: Spatial variations and the role of the jet stream

This chapter is submitted to the *Journal of Geophysical Research: Atmospheres* (Kerr et al., 2020).

We investigate the relationships among summertime O_3, temperature, and humidity on daily timescales across the Northern Hemisphere using observations and model simulations. Temperature and humidity are significantly positively correlated with O_3 across continental regions in the mid-latitudes ($\sim 35-60^{\circ}$N), but this is not the case at high latitudes, in the tropics and subtropics, and over the oceans. These O_3-meteorology relationships are due to an indirect association with transport rather than through the direct dependence of chemistry or emissions, and their spatial patterns are linked to the position and meridional movement of the jet stream. Within the latitudinal range of the jet, there is an increase (decrease) in O_3, temperature, and humidity over land with poleward (equatorward) movement of the jet, while over the oceans

poleward movement of the jet results in decreases of these fields and vice versa. Beyond the latitudes where the jet traverses, the meridional movement of the jet stream has variable or negligible effects on surface-level O_3, temperature, and humidity. The movement of the jet influences these fields primarily by altering the surface-level meridional flow, and the O_3-meteorology relationships are largely the product of the jet-induced changes in the surface-level transport by the mean meridional circulation. These results underscore the importance of considering the role of the jet stream and the mean meridional circulation for the O_3-meteorology relationships, especially in light of expected changes to these features under climate change.

4.1 Introduction

Ambient surface-level O_3 plays a prominent role in atmospheric chemistry (e.g., Fiore et al., 2015; Pusede et al., 2015) and the climate system (Tarasick et al., 2019), while posing significant threats to human health (Landrigan et al., 2018) and ecosystem productivity (Tai and Martin, 2017). Long-term trends in observed O_3 in the Northern Hemisphere mid-latitudes reveal sustained, year-round increases in baseline O_3 concentrations, generally attributed to increasing anthropogenic emissions (Parrish et al., 2012). These changes underpin the need for a better understanding of the drivers of O_3 variability. Meteorology strongly affects O_3 concentrations and chemistry through both variations in prevailing weather conditions on daily, seasonal, or interannual timescales as well as long-terms trends associated with climate change (e.g., Jacob and Winner, 2009; Fiore et al., 2015; Otero et al., 2016; Lefohn et al.,

2018). However, the meteorological phenomena that affect O_3 are not direct relationships in the same sense as emissions or kinetics and energetics. Previous studies have focused on characterizing the relationship between O_3 and temperature or humidity in historical data. Generally these studies found a positive O_3-temperature relationship (e.g., Rasmussen et al., 2012; Rasmussen et al., 2013; Pusede et al., 2015) and a variable O_3-humidity relationship with substantial latitudinal variability (e.g., Camalier et al., 2007; Tawfik and Steiner, 2013; Kavassalis and Murphy, 2017).

The majority of past studies on the O_3-meteorology relationships focused on populated, industrialized portions of the Northern Hemisphere mid-latitudes, potentially overlooking important variations of these relationships elsewhere. These studies have been conducted for different and often non-overlapping time periods during which changes of O_3 precursors could affect chemical background conditions (Kim et al., 2006; Derwent et al., 2010; Cooper et al., 2012; Simon et al., 2015; Lin et al., 2017). Finally, past studies have used different methodologies (e.g., O_3-relationships derived from hourly, daily, or seasonal data; see Brown-Steiner et al. (2015) for additional information). All these factors complicate direct comparisons from study to study; thus, it is difficult to piece together a comprehensive sense of how the O_3-meteorology relationships vary across the globe and what processes drive these relationships. Recent work by Kerr et al. (2019) and Porter and Heald (2019) suggests that greater than 50% of the covariance between O_3 and temperature in the United States (U.S.) and Europe on daily timescales stems from meteorological phenomena, not chemistry or emissions. It is an open question whether this

also holds for the O_3-humidity relationship.

There have been several meteorological, or transport-related, mechanisms proposed to link O_3 with temperature or humidity. However, little consensus exists as to which mechanism is the most important in linking temperature and humidity with O_3 and the regions or timescales over which it operates. Baroclinic cyclones can disperse built-up concentrations of pollution by entraining polluted air from the planetary boundary layer (PBL) into the free troposphere (Mickley, 2004; Leibensperger et al., 2008; Knowland et al., 2015; Knowland et al., 2017). Quasi-stationary anticyclones such as the Bermuda High can influence regional climate and O_3 (Zhu and Liang, 2013, e.g.,). Properties of the PBL, such as its height or temperature inversions and mixing within the PBL, have also been suggested as transport-related mechanisms that affect surface-level O_3 (Dawson et al., 2007; He et al., 2013; Reddy and Pfister, 2016; Barrett et al., 2019). Winds near the earth's surface or aloft can ventilate pollution away from its source region (Camalier et al., 2007; Hegarty et al., 2007; Tai et al., 2010; Sun et al., 2017). Interactions among the atmosphere, land surface, and biosphere have been proposed to explain the O_3-humidity relationship in North America (Tawfik and Steiner, 2013; Kavassalis and Murphy, 2017). The jet stream is a pronounced feature of the general circulation of atmosphere in both the Northern and Southern Hemisphere mid-latitudes and is characterized by a region of strong eastward wind aloft. Its existence arises from momentum and heat fluxes forced by transient eddies, and the jet extends throughout the depth of the troposphere (Woollings et al., 2010). The variability of surface-level summertime O_3 as well as its relationship with

temperature have been linked to the latitude of the jet stream over eastern North America (Barnes and Fiore, 2013; Shen et al., 2015). Similar connections between the jet position, persistence of the jet in a given position, and wintertime particulate matter with a diameter < 2.5 μm ($PM_{2.5}$) have also been demonstrated in Europe (Ordóñez et al., 2019).

The aim of this paper is to document the relationships of surface-level temperature and specific humidity (henceforth "humidity") with O_3 in the Northern Hemisphere during boreal summer and explore the processes responsible for spatial variations of these relationships. Through our model simulations, we demonstrate that transport-related processes, not chemistry or emissions, drive the covariance of O_3 with temperature and humidity. We build off of the previous regionally-focused work of Barnes and Fiore (2013), Shen et al. (2015), and Ordóñez et al. (2019) to show the connections between the position of the jet stream and surface-level temperature, humidity, and O_3 variability hold across the Northern Hemisphere. Finally, we develop and test hypotheses that tie the jet stream to the surface-level relationships among O_3, temperature, and humidity.

4.2 Data and Methodology

4.2.1 Model Simulations

The majority of our analysis of the O_3-meteorology relationships is performed using simulations of NASA's Global Modeling Initiative chemical transport model (GMI CTM) (Duncan et al., 2007; Strahan et al., 2007; Strahan et al., 2013). The GMI CTM is driven by meteorological fields from the Modern Era

Retrospective-Analysis for Research and Applications, Version 2 (MERRA-2) (Gelaro et al., 2017). GMI CTM simulations used in this study have 1° latitude x 1.25° longitude horizontal resolution ($\sim$ 100 km) with 72 vertical levels, extending from the surface to 0.01 hPa. The chemical mechanism of the CTM includes tropospheric and stratospheric chemistry with approximately 120 species and over 400 reactions. Information about the natural and anthropogenic emission inventories and model parameterizations (e.g., biogenic emissions, lightning NO_x, etc.) for the current model configuration is provided in Kerr et al. (2019).

The GMI CTM is a proven model to understand surface-level O_3 variability and its drivers (e.g., Duncan et al., 2008; Strode et al., 2015; Kerr et al., 2019). Kerr et al. (2019) evaluated the CTM with observations from *in-situ* networks in the U.S. and showed that the model skillfully simulated the observed summertime variability of O_3 during the afternoon despite a high model bias in the eastern U.S. and low model bias in the western U.S; these biases are common among CTMs (e.g., Brown-Steiner et al., 2015; Guo et al., 2018; Phalitnonkiat et al., 2018).

In this study we focus on the O_3-meteorology relationships in the Northern Hemisphere for a three-year period (2008 $-$ 2010) during boreal summer (1 June$-$31 August). We use O_3 from the model's surface level, which has a nominal thickness of $\sim$ 130 m. CTM output from the early afternoon (mean 1300 $-$ 1400 local time), coinciding with the overpass time of the Afternoon Constellation ("A-Train") of Earth observing satellites, was archived as gridded fields, whereas hourly output was archived only at select sites. We

consequently use modeled O_3 from this early afternoon period, noting that this time of day typically represents a time in which the PBL is well-mixed (Cooper et al., 2012) and daily O_3 concentrations reach their maximum (Schnell et al., 2014). Considering O_3 during this early afternoon period versus longer averaging periods leads to similar O_3 concentrations and variability (Kerr et al., 2019).

Two simulations are analyzed in this study. The first is a control simulation with daily (or sub-daily) variations in meteorological inputs, chemistry, and natural emissions. Anthropogenic emissions in this simulation vary from month to month. Unless otherwise indicated, all subsequent figures and analysis use this control simulation. In a second simulation referred to as "transport-only," we isolate the role of transport. Fields that affect chemistry (e.g., temperature, clouds and albedo-related variables, surface roughness, specific humidity, and ground wetness) are averaged such that their diurnal cycles are identical for all days within a month for a particular grid cell. Natural and anthropogenic emissions are fixed to monthly mean values. Only the diurnal variations of wind, precipitation, convective mass flux, pressure, and PBL height change from day to day in this simulation. This transport-only simulation is similar to the "Transport" simulation discussed in Kerr et al. (2019) with the exception that specific humidity is also averaged to a monthly mean diurnal cycle.

4.2.2 Observations

We use *in-situ* observations of O_3 across North America, Europe, and China to examine the observed variations of the O_3-meteorology relationships and assess the accuracy of the GMI CTM. We choose these regions because their *in-situ* networks, described below, measure and archive O_3 hourly. Since the model outputs O_3 averaged over 1300-1400 hours (local time), comparing this output with hourly O_3 observations averaged over the same time of the day represents the most direct comparison. The lack of *in-situ* networks with observations at a high temporal frequency in many other parts of the world hinders our ability to examine model performance over other regions.

Observations of O_3 from 233 Canadian sites are part of the National Air Pollution Surveillance Network (NAPS), collected and analyzed by Environment and Climate Change Canada (ECCC, 2017). In the U.S. we use observations from the Air Quality System (AQS) which contains O_3 observations collected by the U.S. Environmental Protection Agency and state, local, and tribal air pollution control agencies at 1483 sites (EPA, 2019). The European Monitoring and Evaluation Programme (EMEP) provides O_3 observations at 142 sites in the European Union (Hjellbrekke and Solberg, 2019).

For China we use observations from the Chinese Ministry of Ecology and Environment (MEE) for summers $2016-2017$ (Li et al., 2019). Observations are primarily from urban centers, and if a particular Chinese city has >1 monitor, a city-wide average was computed following Zhao and Wang (2017), resulting in data from 360 Chinese cities. The choice of this $2016-2017$ time period is because this Chinese observational network did not come online

until the mid-2010s. Accordingly, when we assess the performance of the GMI CTM and discuss the observed O_3-meteorology relationships in China, we use model simulations (Section 4.2.1) and reanalysis data (Section 4.2.3) for $2016-2017$ rather than the $2008-2010$ period used elsewhere in this study.

4.2.3 Meteorological Reanalysis

In addition to providing meteorological input to drive the GMI CTM, MERRA-2 is also used to determine the relationships between O_3 and meteorology. Several of the observational networks detailed in Section 4.2.2 lack co-located meteorological observations, and Varotsos et al. (2013) commented that lack of co-located O_3 and temperature (or other meteorological) observations necessitates the use of gridded products to examine the relationships between O_3 and meteorology.

MERRA-2 meteorological fields are not available at the satellite overpass times sampled by the GMI CTM simulations (Section 4.2.1). We calculate daily averages from the following MERRA-2 fields: hourly 10-m zonal (U_{10}) and meridional (V_{10}) wind, three-hourly 2-m specific humidity (q), three-hourly 500 hPa zonal wind (U_{500}), and hourly planetary boundary layer height (PBLH). Daily 2-m maximum temperature (T) is computed as the maximum of hourly values. Our use of daily maximum temperature follows Zhang and Wang (2016) and Meehl et al. (2018).

There are uncertainties associated with an assimilated product like MERRA-2, but Bosilovich et al. (2015) presented evidence that MERRA-2 provides a very good quality reanalysis data set. As the MERRA-2 data have higher

horizontal resolution than the GMI CTM (0.5° latitude $\times$0.625° longitude for MERRA-2 versus 1° latitude $\times$1.25° longitude for the CTM), we degrade the MERRA-2 data to the resolution of the CTM using xESMF, a universal regridding tool for geospatial data (Zhuang, 2018).

4.2.4 Methodology

4.2.4.1 Statistical analysis

We use the Pearson product-moment correlation coefficient and the slope of the ordinary least squares (OLS) regression (denoted $r(x, y)$ and dy/dx for variables x and y, respectively) to (1) quantify the O_3-meteorology relationships on daily timescales and (2) evaluate the ability of the GMI CTM to accurately simulate observed O_3 from the *in-situ* networks detailed in Section 4.2.2. The correlation coefficient is a parametric test that measures the degree of linear correlation between x and y, and the OLS regression describes the linear relationship between x (explanatory variable) and y (dependent variable).

The serial dependence (persistence) in our meteorological and chemical data reduces the effective sample size by an amount not known *a priori* and inhibits the use of traditional hypothesis testing methods such as t-tests to evaluate significance (Zwiers and von Storch, 1995; Wilks, 1997; Mudelsee, 2003). Therefore, we use moving block bootstrapping to quantify the significance of the correlation coefficient. While traditional bootstrapping resamples individual, independent values of the time series, moving block bootstrapping resamples continuous subsets of the time series with blocklength L and does

not destroy the ordering responsible for the persistence (Wilks, 2011). At each grid cell we synthetically construct a null distribution of 10000 bootstrapped realizations of the correlation coefficient (Mudelsee, 2014) and use $L = 10$ days. As a rule of thumb, blocklengths should generally exceed the decorrelation time. More rigorous methods for optimizing L exist, but we find that $L = 10$ is adequate for our application and our results are not sensitive to the exact value of L. To evaluate the significance, we estimate the 95% confidence interval using the percentile method of the bootstrapped values (i.e., the 95% confidence interval of our 10000 realizations is given by the 250th and 9750th sorted values). If this confidence interval does not contain zero, we declare the correlation coefficient significant.

4.2.4.2 Jet stream position

We define the latitude of the jet (ϕ_{jet}) as the latitude of maximum zonal winds at 500 hPa (U_{500}) on each day. This approach to determine ϕ_{jet} follows Barnes and Fiore (2013) but differs in two ways: (1) Barnes and Fiore (2013) determined using U_{500} averaged over the eastern North America zonal sector. We determine ϕ_{jet} locally (at each longitudinal grid cell) and between $20 - 70^{\circ}$N; (2) After finding the maximum U_{500} for each longitude, we employ a simple moving average that is essentially a convolution of daily ϕ_{jet} of a general rectangular pulse with width $\sim 10^{\circ}$. We also conducted similar analyses with unsmoothed data and by varying the width of the pulse and obtained similar results.

4.2.4.3 Cyclone detection and tracking

To assess the impact of extratropical cyclones on surface-level O_3, we use the MAP Climatology of Mid-latitude Storminess (MCMS) database to locate cyclones (Bauer and Genio, 2006; Bauer et al., 2016). Within MCMS, cyclones are detected as minima in the ERA-Interim sea level pressure (SLP) dataset (Dee et al., 2011) and are subject to additional filters to screen for spurious detections. Once detected, MCMS tracks cyclones with criteria that require gradual changes in SLP, no sudden changes in direction, and cyclones travel distances < 720 km over single six-hourly time steps. Additional details can be found in Bauer and Genio (2006) and Bauer et al. (2016).

4.3 Global O_3 distribution and evaluation

We begin with an analysis of the distribution and variability of modeled surface-level O_3 during summer (Figure 4.1a). Concentrations of O_3 are highest ($\sim 35-60$ ppbv) in a broad mid-latitude band over continental regions extending from $20-50$°N. The GMI CTM indicates that O_3 is not zonally-symmetric within this mid-latitude band and that the highest mean concentrations (> 50 ppbv) are in the Middle East and central and eastern Asia. Outside of the mid-latitudes, the CTM simulates lower O_3 concentrations (< 30 ppbv), and the lowest concentrations in the hemisphere (< 15 ppbv) are found in the remote tropical marine atmosphere. This spatial distribution of mean summertime surface O_3 is consistent with other models (e.g., Sadiq et al., 2017). We characterize the daily variability of O_3 by the standard deviation, and two levels (8 and 10 ppbv) are highlighted with the thin dashed and thick

contours in Figure 4.3a.

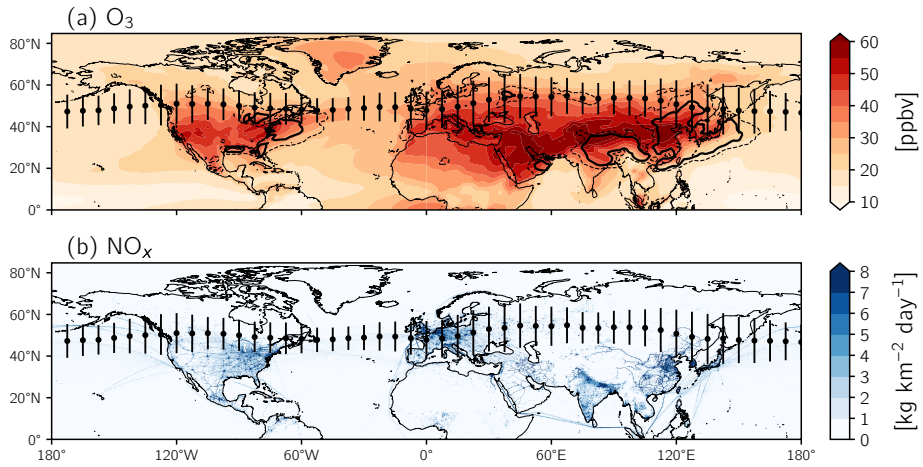

Figure 4.1: (a) Time-averaged O_3 from the surface-level of the GMI CTM (colored shading). Black contours indicate O_3 variability (standard deviation): thin dashed contour, 8 ppbv; thick contour, 10 ppbv. (b) Time-averaged anthropogenic NO_x emissions from EDGAR. Scatter points and vertical bars in (a-b) specify the mean position and variability of the jet stream, respectively.

To illustrate the possible influence of anthropogenic emissions on the spatial variability of mean O_3 concentrations, we show mean annual anthropogenic NO_x emission data from the Emissions Database for Global Atmospheric Research (EDGAR; Crippa et al., 2018) at their native resolution (0.1° latitude x 0.1° longitude) in Figure 4.1b. EDGAR is used in the GMI CTM, but is overwritten by regional inventories (see Kerr et al., 2019). Elevated O_3 concentrations generally coincide with industrialized regions that have high precursor emissions (Figure 4.1a). However, there are areas with high emissions and low O_3 or vice versa. For example, central Asia has low NO_x emissions (Figure 4.1b) but mean summertime O_3 in central Asia is generally $>$ 50 ppbv, suggesting there is more at play than these anthropogenic

emissions alone.

We evaluate whether the modeled O_3 distribution shown in Figure 4.1a is realistic using the correlation coefficient (r), calculated for CTM grid cells containing *in-situ* monitors (Section 4.2.2). The temporal correlation between modeled and observed O_3 exceeds $\sim$ 0.5 in the vast majority of grid cells (Figure 4.2). The strength of the correlation is slightly weaker in central China than other parts of China or Europe and North America (compare Figure 4.2c with 2a-b), but there are no other readily-detectable spatial patterns regarding the strength of the correlation.

The primary goal of our study is to document the O_3-meteorology relationships in terms of the strength of the temporal correlation of O_3 with temperature and humidity. Thus, the model's ability to reproduce the temporal variability of O_3 (Figure 4.2) is the relevant litmus test for model performance. As the strength of the temporal correlation is consistent from region to region and in light of recent work showing that the GMI CTM has skill in capturing the O_3-temperature relationships (Strode et al., 2015; Kerr et al., 2019), we believe the GMI CTM is a suitable tool to meet our goal. The agreement between the observed and modeled O_3-meteorology correlations will be explored in the following section (Section 4.4), and this analysis will also support our use of the GMI CTM to simulate the covariance between O_3 and temperature or humidity.

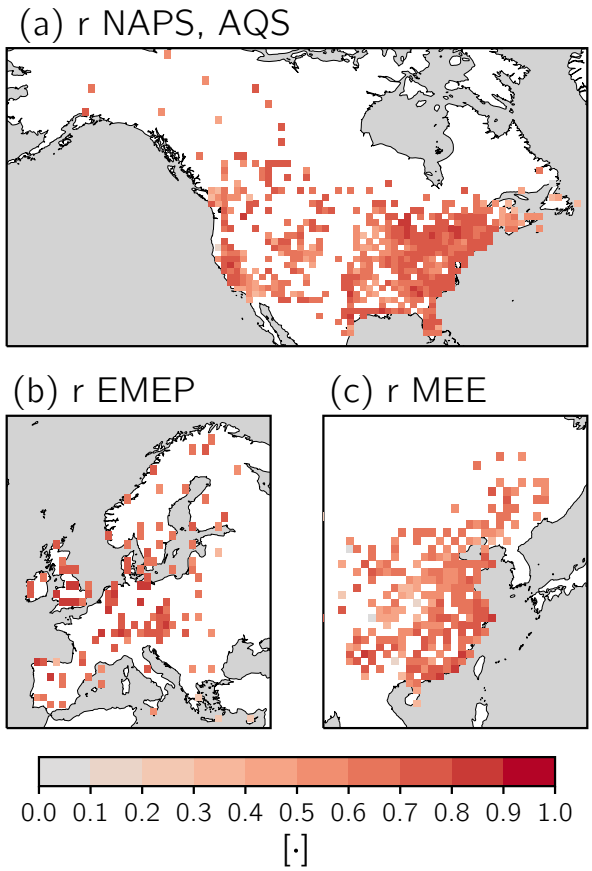

Figure 4.2: The correlation coefficient (r) calculated between modeled O_3 from the GMI CTM and observed O_3 for model grid cells containing *in-situ* monitor(s). The networks in (a) North America, (b) Europe, and (c) China from which monitor-based observations have been derived are indicted in the subplots' titles. If there is > 1 monitor in a grid cell, all O_3 observations are averaged to produce a grid cell average prior to computing r.

4.4 O_3-meteorology relationships

In this section we describe the relationships among O_3, temperature, and humidity on daily timescales in the Northern Hemisphere during summer. We primarily use the GMI CTM but also compare the modeled relationships to

observed values. As discussed in the Introduction (Section 4.1), other studies have focused mainly on subsets of the Northern Hemisphere mid-latitudes, while our examination of the relationships across the entire hemisphere allows us to have a more holistic sense of the synoptic-scale variations of these relationships.

In the mid-latitudes ($\sim 30 - 60^{\circ}$N), statistically-significant positive values of $r(T, O_3)$ are simulated by the CTM throughout continental regions of North America and Eurasia (Figure 4.3a), but over all oceans $r(T, O_3)$ is negative. Poleward of the mid-latitudes, the strength of $r(T, O_3)$ decreases nearly monotonically over land, reaching either weak values or significantly negative correlations (Figure 4.13a). The O_3-temperature relationship is varied equatorward of the mid-latitudes over land, but generally the strength of $r(T, O_3)$ decreases to statistically non-significant values or significantly negative values (Figure 4.3a). Previous work by Rasmussen et al. (2012) and Brown-Steiner et al. (2015) in the U.S. and Han et al. (2020) and Lu et al. (2019a) in China showed a similar latitudinal gradient of $r(T, O_3)$. Despite the general tendency of a positive-to-negative relationship between O_3 and temperature with decreasing latitude, there are regions at low latitudes with significant positive correlations between O_3 and temperature (Indo-Gangetic Plain, Sahel; Figure 4.3a).

Similar to $r(T, O_3)$, the strength of $r(q, O_3)$ transitions from significantly positive in the mid-latitudes to significantly negative at higher and lower latitudes, notwithstanding parts of the Middle East and southeast Asia (Figure 4.3b). These results are supported by modeling and observational studies in

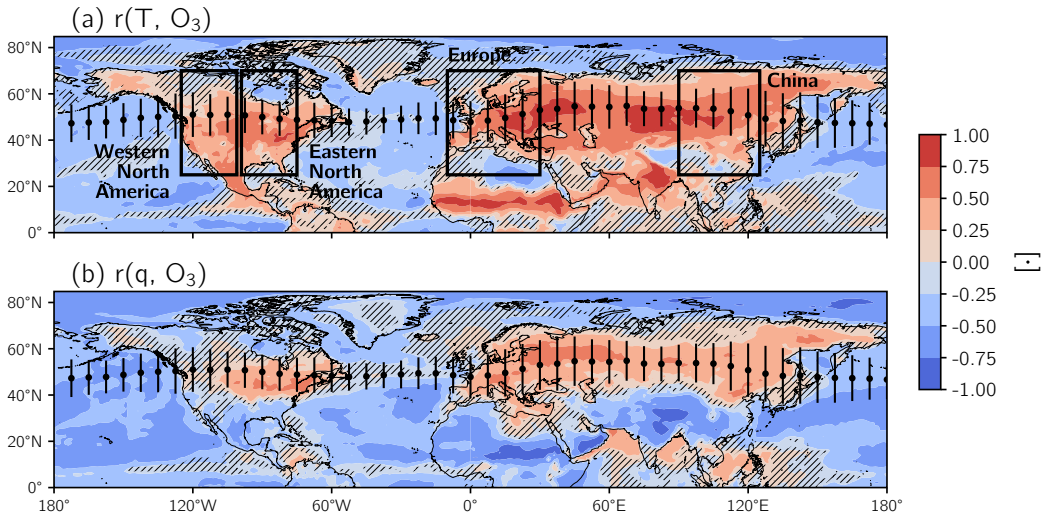

Figure 4.3: (a) The correlation coefficient calculated between O_3 from the GMI CTM and MERRA-2 temperature, $r(T, O_3)$. Hatching denotes regions where the correlation is not statistically significant, determined using moving block bootstrap resampling to estimate the 95% confidence interval. (b) Same as (a) but for the correlation coefficient calculated between between O_3 and MERRA-2 specific humidity, $r(q, O_3)$. Scatter points and vertical bars in (a-b) specify the mean position and variability of the jet stream, respectively. Black boxes in (a) outline the regions over which zonal averages were performed in Figure 4.5.

the U.S. and China, which indicate $r(q, O_3) > 0$ in the northern U.S. and China and $r(q, O_3) < 0$ in southern U.S. and China (e.g., Tawfik and Steiner, 2013; Kavassalis and Murphy, 2017; Li et al., 2019). Specific humidity and O_3 are also significantly anticorrelated over the oceans.

In continental regions of the mid-latitudes, the O_3-meteorology correlations suggest that temperature is a better predictor of O_3 than specific humidity, as $r(T, O_3) > r(q, O_3)$. Other studies support temperature as a leading covariate in the mid-latitudes (e.g., Camalier et al., 2007; Porter et al., 2015; Otero et al., 2016; Sun et al., 2017; Kerr and Waugh, 2018).

Many other studies report dO_3/dT (Rasmussen et al., 2012; Zhao et al., 2013; Brown-Steiner et al., 2015; Kerr et al., 2019; Porter and Heald, 2019), and we also present dO_3/dT and dO_3/dq in Figure 4.4 for comparisons with these other studies. The spatial variations of the slopes shown in Figure 4.4 are qualitatively similar to $r(T, O_3)$ and $r(q, O_3)$ shown in Figure 4.3, as is expected by construction.

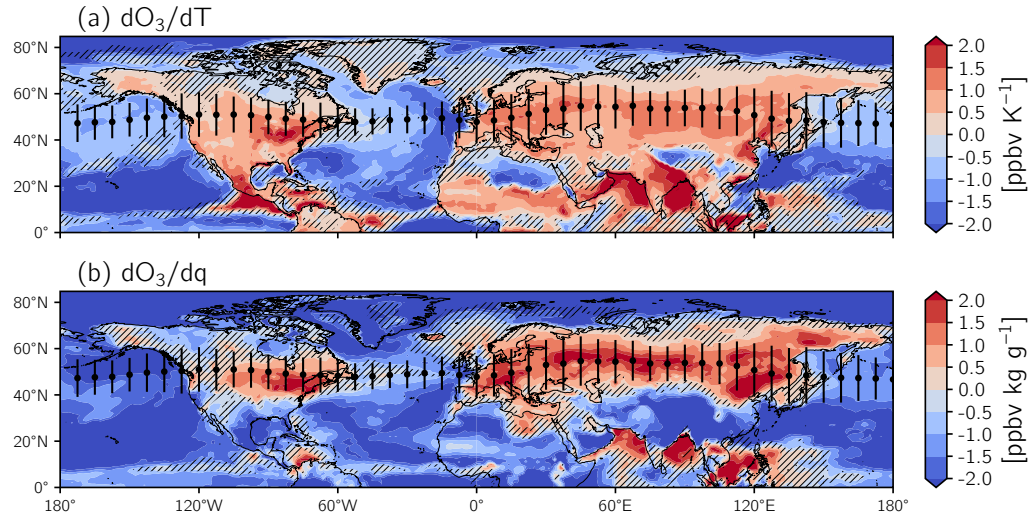

Figure 4.4: (a) The slope of the ordinary least squares (OLS) regression of O_3 versus temperature, dO_3/dT. Hatching denotes regions where the correlation between O_3 and temperature is not statistically significant, determined using moving block bootstrap resampling to estimate the 95% confidence interval. (b) Same as (a) but for O_3 versus specific humidity, dO_3/dq, with hatching showing statistically non-significant correlation between O_3 and specific humidity. Scatter points and vertical bars are identical in (a-b) and show the mean latitude of the eddy-driven jet and its variability.

To test whether the modeled O_3-meteorology relationships are realistic, we calculate $r(T, O_3)$ and $r(q, O_3)$ from the *in-situ* networks described in Section 4.2.2. The strength of the zonally-averaged values of observed and modeled

$r(T, O_3)$ and $r(q, O_3)$ generally reaches a maximum around 50°N across four distinct regions (Figure 4.5). In Europe and the eastern U.S., the CTM slightly overestimates the strength of $r(T, O_3)$ and $r(q, O_3)$ by $\sim 0.1 - 0.3$, similar to other studies (e.g., Brown-Steiner et al., 2015; Kerr et al., 2019). Observations are sparse outside of the mid-latitudes. A small number of AQS monitors in Alaska and NAPS monitors in northern Canada support the transition of $r(T, O_3)$ and $r(q, O_3)$ from positive to negative at high latitudes that is suggested by the model (Figure 4.5).

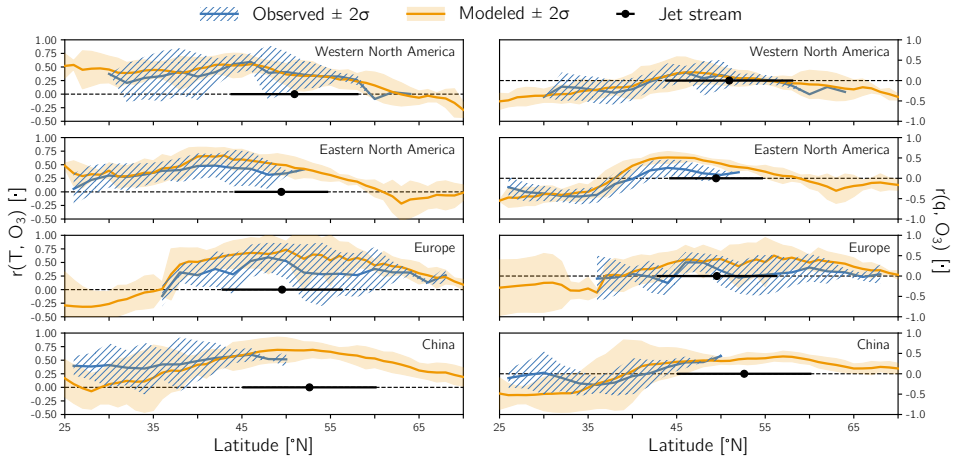

Figure 4.5: A comparison of the O_3-meteorology relationships between the GMI CTM and observational networks. The left panel shows $r(T, O_3)$ and the right panel shows $r(q, O_3)$ zonally-averaged over four regions: Western North America ($125° - 100°$W), Eastern North America ($100° - 65°$W), Europe ($10°$W$-30°$E), and East Asia ($90 - 125°$E). These regions are also outlined in Figure 4.3a. Zonally-averaged modeled relationships consider only grid cells over land, and the observed relationships are binned by latitude to compute the zonal average. The dashed grey lines delineate positive from negative values of the O_3-meteorology relationships, and the scatter points and vertical bars corresponding to the jet and its variability are the same as in Figure 4.1 but averaged over each region.

In summary, the observation- and model-based analysis of the relationships among surface-level O_3 and temperature or humidity reveals substantial

variability across the Northern Hemisphere during summer. Within a mid-latitude band ($\sim 30 - 60^{\circ}$N) over land, O_3 is significantly correlated with temperature and humidity (Figures 4.3-4.5). Over the oceans and outside of the mid-latitudes, the strength of the O_3-relationships are either near-zero or significantly negative (Figures 4.3-4.5). These results suggest positive O_3-meteorology relationships are the exception, not the norm, over the entire hemispheric domain.

4.5 Factors causing the O_3-meteorology relationships

The O_3-meteorology relationships in Figure 4.3 are far from uniform, and their spatial structure begs the question: what factors drive these relationships? In Section 4.1, we discussed several direct and indirect drivers that have been linked to O_3 variability, such as emissions, chemistry, and transport. Recent work has shown that transport-related processes are key contributors to the O_3-temperature relationship in the U.S. and Europe (Kerr et al., 2019; Porter and Heald, 2019), and we expand on these previous findings and examine the covariance of O_3 with temperature and humidity over the Northern Hemisphere. We do this using the transport-only GMI CTM simulation in which the daily variability of chemistry and emissions are fixed (Section 4.2.1).

The difference in the magnitudes of $r(T, O_3)$ and $r(q, O_3)$ calculated between the control and transport-only simulations (Figure 4.6) demonstrates that considering only daily variations in transport-related processes yields O_3-meteorology relationships of similar magnitude as in the control simulation (Figure 4.3). Over all the oceans and a majority of the continental regions

in the Northern Hemisphere, the strength of $r(T, O_3)$ and $r(q, O_3)$ increases or decreases < 0.1 (Figure 4.6). The hatching in Figure 4.6 demonstrates that the significance of the O_3-meteorology relationships is largely retained when only daily variations in transport-related processes are considered. This further supports the role of transport as the key driver of the O_3-meteorology relationships.

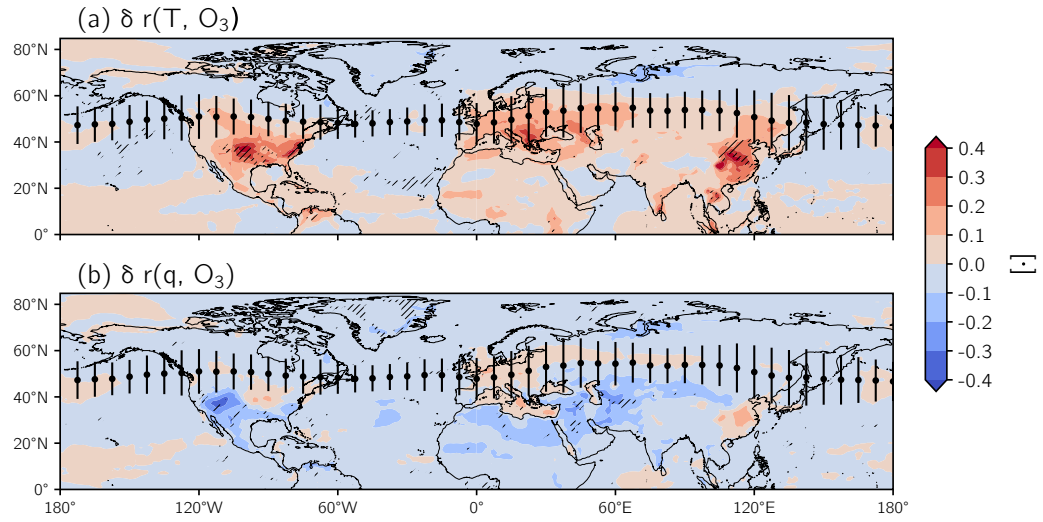

Figure 4.6: The difference in (a) $r(T, O_3)$ and (b) $r(q, O_3)$ calculated between the control and transport-only CTM simulations. Hatching indicates regions with significant $r(T, O_3)$ or $r(q, O_3)$ in the control simulation that became statistically non-significant in the transport-only simulation. Scatter points and vertical bars in (a-b) specify the mean position and variability of the jet stream, respectively.

There are a few continental regions with significant O_3-meteorology correlations in the control simulation where r decreases or increases by up to ~ 0.5 and becomes statistically non-significant (e.g., southern U.S. and southeast Asia for $r(T, O_3)$ and the southwestern U.S. for $r(q, O_3)$ in Figure 4.6). In these regions, the daily variability of chemistry and emissions appears important

for the significance of the O_3-meteorology correlations, and further work is warranted to understand the roles of meteorology, chemistry, and emissions on O_3.

These results answer our original question whether transport, chemistry, or emissions are responsible for the O_3-meteorology relationships, but they also raise the question of which aspect(s) of transport links temperature and humidity to O_3. In the next section we explore the role of the jet stream on surface-level temperature, humidity, and O_3, and we also develop and test hypotheses to link synoptic-scale flow aloft to meteorology and composition at the surface.

4.5.1 The role of the jet stream

In this section we document the response of surface-level O_3, temperature, and humidity to daily changes in ϕ_{jet} across the Northern Hemisphere. Barnes and Fiore (2013) determined that the largest O_3 variability and peak strength of $r(T, O_3)$ are located near ϕ_{jet} in the eastern U.S. These results were further explored by Shen et al. (2015) who found that O_3 responded to seasonal variations in the position of the jet stream and that a poleward shift of the jet increased O_3 concentrations south of the jet.

The position and variability of the jet stream exhibit spatial variability that is important to understand, especially as we document the association between the jet and surface-level O_3, temperature, and humidity. The time-averaged latitude of the jet stream ($\overline{\phi_{jet}}$) is shown by the scatter points in Figure 4.1, and $\overline{\phi_{jet}}$ averaged over the entire hemisphere is 50.1°N. The variability

of the jet, cast in terms of the standard deviation ($\sigma_{\phi_{jet}}$), averaged over the Northern Hemisphere is 10.5°, but its variability is not constant throughout the hemisphere (vertical bars in Figure 4.1). Rather, we the largest variability occurs over continental regions, particularly Eurasia ($\sim$ 20°), and smaller variability over maritime regions, coinciding with the Atlantic and Pacific storm tracks. ϕ_{jet} is only one metric to describe the jet stream, and other jet-related measures exist (e.g., strength of the jet, waviness). Our focus on ϕ_{jet} rather than other metrics is based on Ordóñez et al. (2019) who found that ϕ_{jet} exerts a stronger influence than the strength of the jet on surface-level pollution extremes.

The maximum variability of O_3 (Figure 4.1) and the strength of the O_3-meteorology correlations (Figures 4.3-4.6) peak at or slightly south of ϕ_{jet}, and ϕ_{jet} also separates regions with elevated O_3 concentrations to its south from regions with low ($<$ 30 ppbv) concentrations to its north (Figure 4.1a). These results are consistent with Barnes and Fiore (2013); however, it is worth pointing out a couple of exceptions: (1) In Asia, O_3 variability peaks over a broader latitudinal range, extending from southward to $\sim$ 20°N (Figure 4.1). (2) There are regions with significant positive values of $r(T, O_3)$ such as the Sahel and India that do not coincide with ϕ_{jet} (Figure 4.3a). These results expand upon Barnes and Fiore (2013), who only examined latitudes within $\sim$ 15° of the jet in eastern North America. Our current work also reveals the weak-to-negative correlation between O_3 and humidity or temperature for marine environments and subtropical and high latitude locations.

To further examine the role of the jet stream on the O_3-meteorology relationships, we segregate summer days into two subsets: days when the jet stream is in poleward (PW) and equatorward (EW) positions. Days classified as PW (EW) are days in which ϕ_{jet} exceeds (is less than) the 70th (30th) percentile of all daily ϕ_{jet} at each longitudinal grid cell. We construct composites of O_3, temperature, and humidity by identifying the average value of these fields on days with a PW or EW jet stream and thereafter calculate the difference of these PW and EW composites.

The difference in the PW and EW composites (PW - EW) of O_3, temperature, and humidity are positive in the mid-latitudes over land (Figure 4.7), which indicates that these fields increase when the jet is in a more northerly position. The positive values are generally significant (hatching in Figure 4.7), coincide with the latitudinal band over which the jet stream migrates, and persist $10 - 15^{\circ}$ north and south of its mean position over land. Outside the continental mid-latitudes, the association between the position of the jet and O_3, temperature, or humidity is weak and not statistically significant (Figure 4.7).

In contrast, there is a difference in the response of O_3 to the jet stream versus temperature and humidity over the mid-latitude ocean basins. In the case of O_3, a poleward movement of the jet decreases O_3 (Figure 4.7a), which could reflect asymmetries in the source regions of O_3 precursors between the land and ocean. On the other hand, temperature and humidity increase as the jet shifts poleward, akin to the behavior of these variables over land (Figure 4.7b-c). The impact of the jet stream on O_3, temperature, and humidity outside

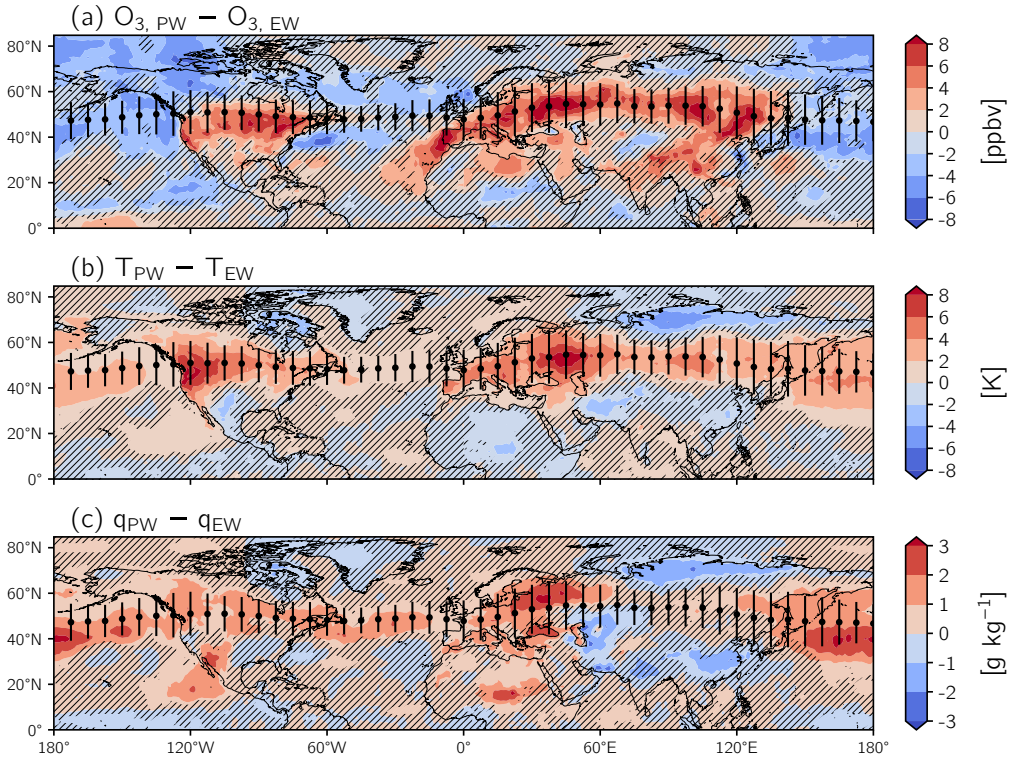

Figure 4.7: The relationships between the position of the jet stream and surface-level O_3 and meteorological variables. Relationships are calculated as the difference in composites of (a) O_3, (b) temperature, and (c) specific humidity on days when the jet is in a PW and EW position. Composites are formed for the PW (EW) case by determining the value of each field in (a-c) averaged over all days when the position of the jet stream (ϕ_{jet}) exceeds the 70th (is less than the 30th) percentile for each longitude. Hatching indicates regions where the correlation between each field and the distance from the jet is statistically non-significant. The distance from the jet, $\phi - \phi_{jet}$, is defined as the difference, in degrees, between the local latitude and the latitude of the jet. Scatter points and vertical bars in (a-c) specify the mean position and variability of the jet stream, respectively.

of the mid-latitudes is largely not statistically significant (Figure 4.7).

For completeness, maps of the correlation of jet distance with the variables

in Figure 4.7 are shown in Figure 4.8. We note that the strength of the correlation between ϕ_{jet} and O_3 and meteorology is weaker than $r(T, O_3)$ and $r(q, O_3)$, and the spatial extent of areas with significant correlations is smaller (compare Figures 4.3 and 4.8).

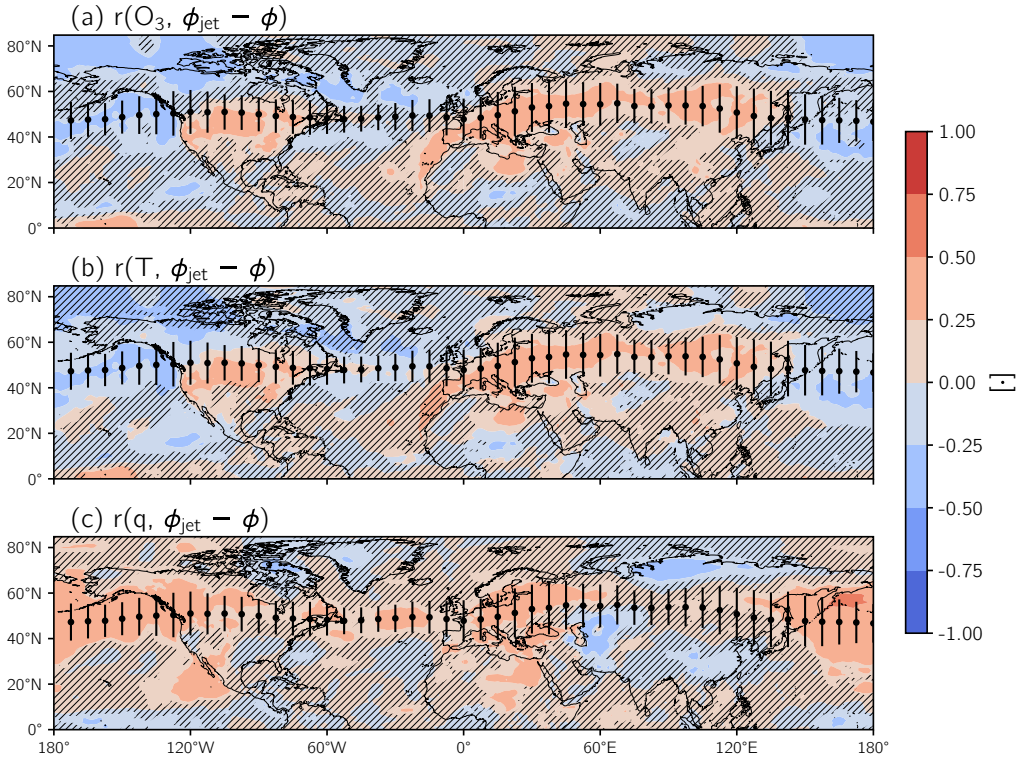

Figure 4.8: Colored shading shows the correlation coefficient (r) calculated between distance from the eddy-driven jet and (a) O_3, (b) temperature (T), and (c) specific humidity (q). Hatching is the same as in Figure 6, and scatterpoints, and vertical bars are the same as in Figure 3.

While the response of O_3 and meteorological fields to the meridional movement of the jet stream is consistent in its sign in the mid-latitudes over land, there are some regions outside of the continental mid-latitudes where

jet movement leads to increases of one variable and decreases of another. China is an example of this. As the jet migrates poleward, O_3 significantly increases, as it does throughout the mid-latitudes; however, temperature remains more or less constant, and humidity slightly decreases (Figures 4.7, 4.8). This discrepancy and others evident in Figures 4.7 and 4.8, particularly those at lower latitudes and over the oceans, are beyond the scope of this study, but future studies should further examine and address regions where O_3, temperature, and humidity are decoupled from the jet in this manner.

Having uncovered the dominant role of transport and the connections with the jet, we next explore transport-related processes that might be responsible for the relationships among surface-level O_3, the jet stream, and meteorology. As cyclones are commonly-invoked to explain O_3 variability, we begin by showing the impact of the jet stream on cyclone frequency and, in turn, the effect of cyclones on O_3. We then show and discuss the how the jet stream affects the mean meridional circulation and commensurate fluxes of O_3, heat, and moisture.

4.5.2 Cyclones

Mid-latitude baroclinic cyclones follow a storm track dictated by the jet stream, and changes in ϕ_{jet} affect the location of this storm track (e.g., Shen et al., 2015). To assess the dependence of cyclone frequency on ϕ_{jet}, we show the spatial distribution of the climatological frequency of cyclones detected by MCMS (Section 4.2.4.3) in Figure 4.9a. The highest frequency of mid-latitude cyclone detections largely follows ϕ_{jet} and is offset north of the jet by $\sim 10^{\circ}$ over North

America. In other regions such as eastern Asia, the peak cyclone frequency occurs in a broader latitudinal band, extending north and south of ϕ_{jet} by $\sim 15°$ (Figure 4.9a).

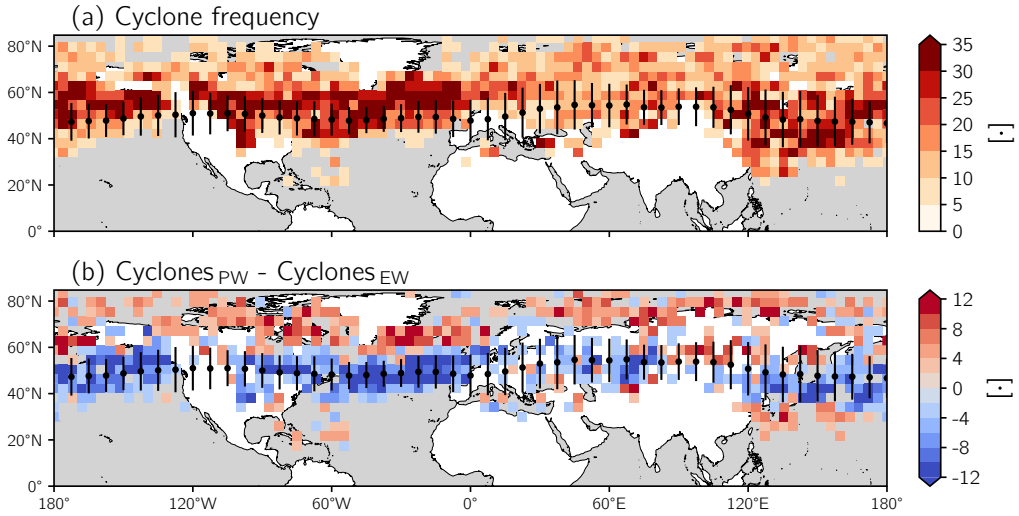

Figure 4.9: (a) Total number of cyclones detected by MCMS on sub-daily (six-hourly) time scales binned to a $\sim 4° \times 4°$ grid. (b) The difference in the total number of cyclones calculated between days when the jet is in a PW and EW position. Scatter points and vertical bars in (a-b) specify the mean position and variability of the jet stream, respectively.

We identify the subset of days with a poleward-shifted or equatorward-shifted jet using the 70th and 30th percentiles of the daily latitudes of the jet stream, as previously described, to determine the dependence of cyclones on ϕ_{jet}. We thereafter determined the frequency of cyclones on these subsets of days and found the difference (Figure 4.9b). The meridional movement of the jet affects cyclones in two different ways. First, the total number of cyclones on days when the jet is in a poleward position is 15% less than on days when the jet is equatorward. Second, the preferred location of cyclones ("storm track")

shifts alongside the jet, and cyclones are more highly concentrated about ϕ_{jet} when the jet is equatorward compared to when it is poleward (Figure 4.9b).

The decrease and latitudinal shift in cyclone frequency with meridional movements of the jet stream could be the transport-related mechanism responsible for the above O_3-meteorology relationships. The cold fronts associated with mid-latitude cyclones have been suggested as a mechanism for the ventilation of the eastern U.S. (Mickley, 2004). Furthermore, Knowland et al. (2015) and Jaeglé et al. (2017) demonstrated how cyclones redistribute O_3, its precursors, and other pollutants vertically and horizontally in the atmosphere. We assess the impact of cyclones on surface-level O_3 by further filtering the cyclones from the MCMS dataset (Section 4.2.4.3), requiring that a particular cyclone (1) occurs over land and (2) is detected for ≥ 2 six-hourly time steps to allow us to calculate the direction of propagation. We then rotate cyclones following Knowland et al. (2015) and Knowland et al. (2017) such that they propagate to the right of Figure 4.10 to account for the impact of different ascending and descending airstreams within the cyclones. Applying these filters to cyclones in summers $2008 - 2010$ yields ~ 730 cyclones with an average lifetime of ~ 54 hours. The mean direction of cyclone propagation is east-southeast ($\sim 120^\circ$, where 0° is north). Though we have only considered cyclones occurring over land in this analysis, compositing all land- and ocean-based cyclones produces O_3 anomalies of similar magnitude.

We observe that the largest negative O_3 anomaly occurs in the "cold sector" of the cyclone, whereas a positive anomaly occurs in the "warm sector," but these positive and negative anomalies cancel each other when averaged over

the footprint of the cyclones leading to a net ~ 0 ppbv change in O_3 (Figure 4.10). Comparing our results with conceptual models of baroclinic cyclones (e.g., Polvani and Esler, 2007) hints that the positive anomalies occur near the warm conveyor belt, while negative anomalies occur near the dry intrusion where there is likely an influence of air from the free troposphere or lower stratosphere.

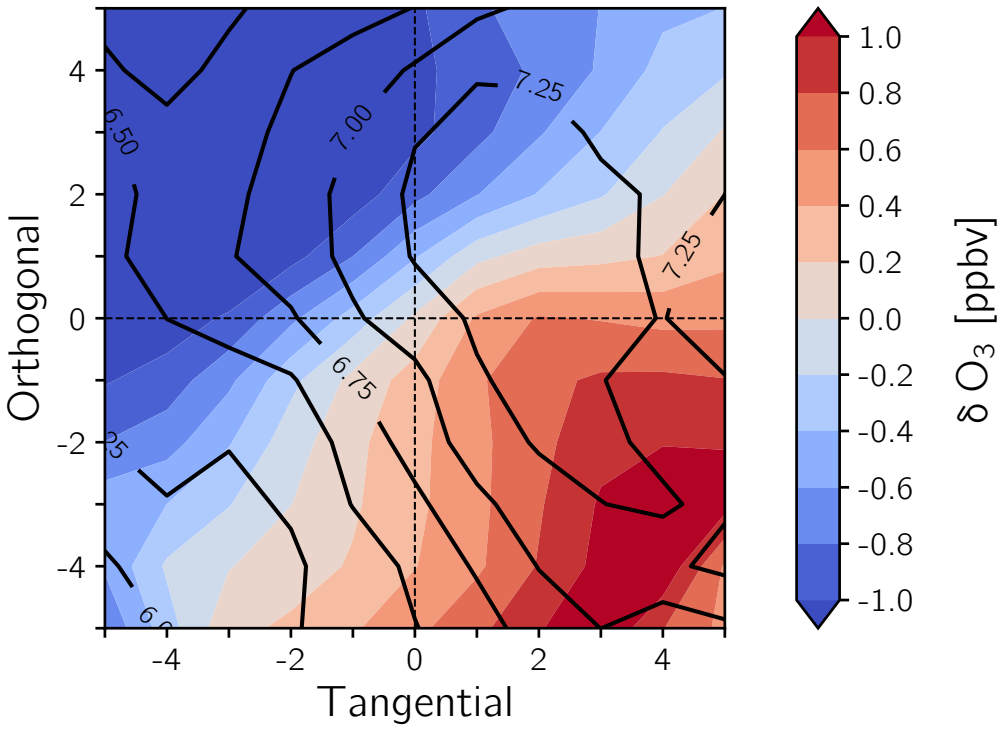

Figure 4.10: The impact of cyclones on surface-level O_3. From the cyclones shown in Figure 4.9, we consider cyclones occurring over land and detected for ≥ 2 time steps and subsequently rotate the cyclones following the direction of their propogation such that they move to the right of the figure. We thereafter calculate the average O_3 anomaly (colored shading) and standard deviation of the anomalies (solid black contours) within five grid cells ($\sim 5°$) of the position of theses cyclones. Dashed black lines divide the cyclone composites into quadrants.

If cyclones were the mechanism that linked ϕ_{jet} to surface-level O_3, we might expect that the cyclones-driven impact on O_3 would be > 6 ppbv in the mid-latitudes, similar to the impact that ϕ_{jet} has on O_3 (Figure 4.7a). However, our analysis in Figure 4.10 indicates that, on average, cyclones have a much weaker effect on surface-level O_3, despite the connections between cyclones and the jet stream (Figure 4.9b). We do note that there is substantial variability among individual cyclones (the standard deviation of the O_3 anomaly is a factor of ~ 6 greater than the largest anomaly; Figure 4.10), so some cyclones might be effective at reducing surface-level O_3, but this is far from the case for all cyclones.

Other studies support the small role of cyclones on surface-level O_3. Knowland et al. (2015) showed that the surface-level O_3 anomaly associated with springtime cyclones in the North Atlantic and Pacific is small (i.e., $-5 < \delta O_3 < 5$ ppbv); however, they found a larger impact when examining the mid- to upper-level O_3 anomalies. Moreover, Leibensperger et al. (2008) found a negative correlation between the number of O_3 pollution events and the number of mid-latitude cyclones passing through the southern climatological storm track ($\sim 40 - 50^{\circ}$N) over eastern North America on interannual timescales, but Turner et al. (2012) demonstrated that this correlation is weak, and cyclone frequency explains less than 10% of the variability of O_3 pollution events in the region.

In summary, while the storm track dictating the preferred location of baroclinic cyclones shifts with the jet (Figure 4.9b), cyclones are likely not the

key mechanism controlling O_3 variability in the Northern Hemisphere mid-latitudes as they only explain a small fraction of the changes of O_3 associated with daily migrations of the jet (Figure 4.10).

4.5.3 Zonal mean meridional transport

An analysis of PBLH, near-surface zonal flow, and near-surface total wind are either not significantly influenced by ϕ_{jet} or cannot explain the magnitude of jet-related changes in O_3 (Section 4.7.1-4.7.2 and Figures 4.11-4.12). In contrast, the increase in the near-surface meridional flow (V_{10}) as the jet shifts poleward (Section 4.7.2; Figures 4.11c, 4.12c) accompanied by increases in O_3, temperature, and humidity (Figures 4.7-4.8) suggest that changes in the mean meridional flow may play a major role in the relationships among the jet stream, O_3, and meteorology. To examine this further, we next calculate the meridional fluxes of O_3, heat, and moisture; the contributions from the zonal mean and eddy components; and how the jet influences these fluxes.

To distinguish contributions from the eddy and the mean components of the total flux, we decompose the total flux of a given field X into deviations from its time and zonal means. The time mean is denoted by $\overline{X}$, and deviations from the time mean are denoted X', such that $X = \overline{X} + X'$. We denote the zonal mean by $[X]$, and deviations from the zonal mean are given by X^*, so that $X = [X] + X^*$ (e.g., Peixoto and Oort, 1992; Kaspi and Schneider, 2013). The time-averaged zonal mean O_3 flux by the near-surface meridional wind

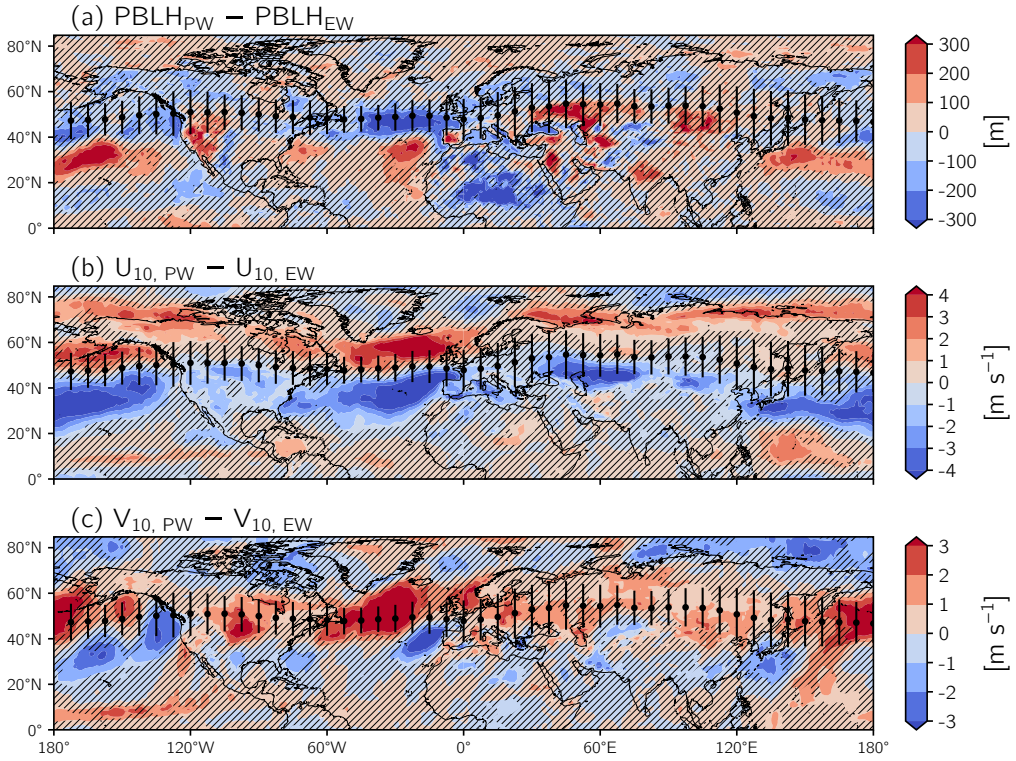

Figure 4.11: Same as Figure 6 in the main text but for (a) PBLH, (b) U_{10}, and (c) V_{10}.

can be expressed by

$$[\overline{V_{10}\,O_3}] = [\overline{V_{10}}][\overline{O_3}] + [\overline{V_{10}^*\,O_3^*}] + [\overline{V_{10}'\,O_3'}], \tag{4.1}$$

where the terms on the righthand side of Equation 4.1 represent the contributions from the mean meridional circulation, stationary eddies, and transient eddies, respectively. Similar expressions can be derived for temperature and humidity. Note that in our analysis, we sum the contributions from the stationary and transient eddies and refer to them as the "eddy" contribution.

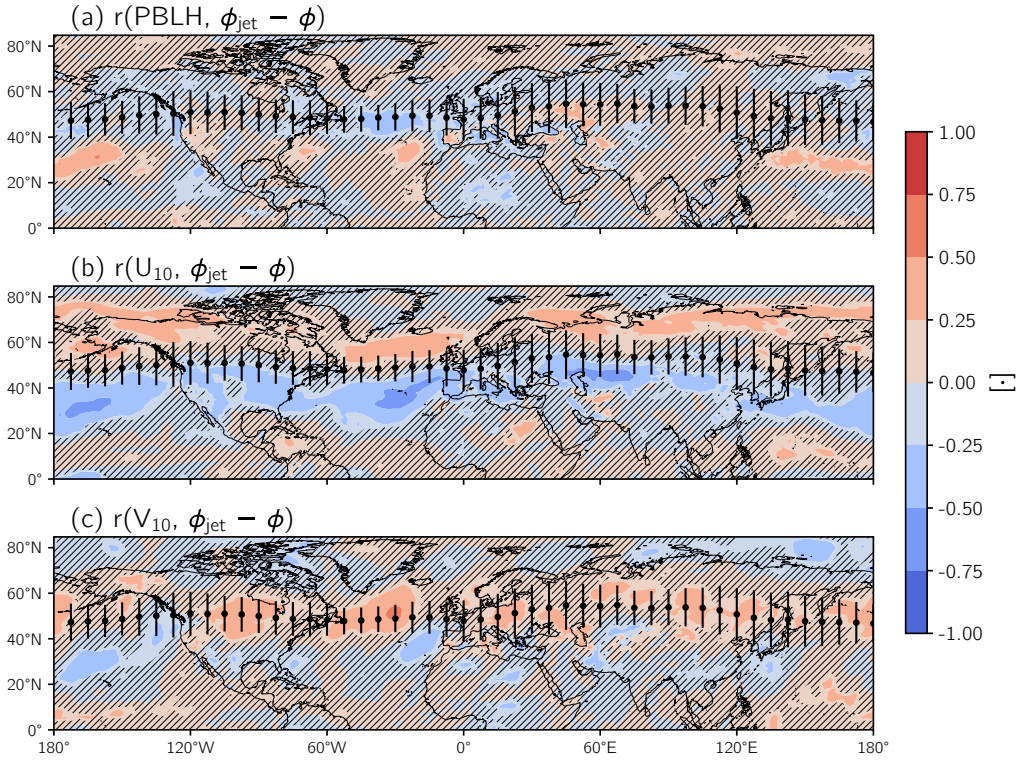

Figure 4.12: Same as Figure 4.8 but for (a) PBLH, (b) U_{10}, and (c) V_{10}.

In the zonal mean, the contribution from eddies and the mean meridional circulation for O_3 and temperature on all days are qualitatively similar (Figure 4.13a, d). For these fields, eddies play a small role, regardless of latitude, while the mean meridional circulation leads to a equatorward (poleward) O_3 and heat flux for $\phi < 40°$N ($\phi > 40°$N). Eddies play a larger role in shaping the total flux of humidity for $\phi < 45°$N than for temperature or O_3 (compare Figure 4.13g with Figure 4.13a, d), but the eddies make a negligible contribution to the total moisture flux at higher latitudes (Figure 4.13g). While

heat transport in the Northern Hemisphere mid-latitudes is often attributed to eddies, this only holds for boreal winter or annual means, not boreal summer (Hartmann, 2007).

If we recalculate the fluxes for the subsets of days when the jet is PW and EW, a striking feature is revealed: there is a large difference in the sign and magnitude of O_3, temperature, and humidity flux by the mean meridional circulation (Figure 4.13b-c, e-f, h-i). The relatively small total flux of these fields in the mid-latitudes on all days (Figure 4.13a, d, g) can be viewed as the cancellation of a large positive (poleward) flux on days when the jet is PW (Figure 4.13b, e, h) and large negative (equatorward) flux on days when the jet is EW (Figure 4.13c, f, i). There is a consistent contribution from the eddy component whether all days or days when the jet is PW or EW are considered. Although we only have shown the flux of O_3, temperature, and humidity using surface-level fields here, using fields averaged over the lower troposphere (1000 − 800 hPa) does not change our conclusions.

In the mid-latitudes over land, V_{10} and the flux of O_3, temperature, and humidity by the mean meridional circulation responds to changes in the position of the jet stream such that when the jet is PW, increased northerly flow transports O_3, heat, and moisture northward (Figures 4.11c, 4.12c, 4.13). This yields positive relationships among O_3, meteorology, and the jet stream.

Over the mid-latitude oceans, O_3 does not have the monotonically decreasing latitudinal gradient as it does over land (Figure 4.1a); rather, O_3 increases slightly increases with latitude in the vicinity of the North Atlantic and North Pacific storm tracks ($\sim 50 - 60^{\circ}$N), potentially reflecting transient

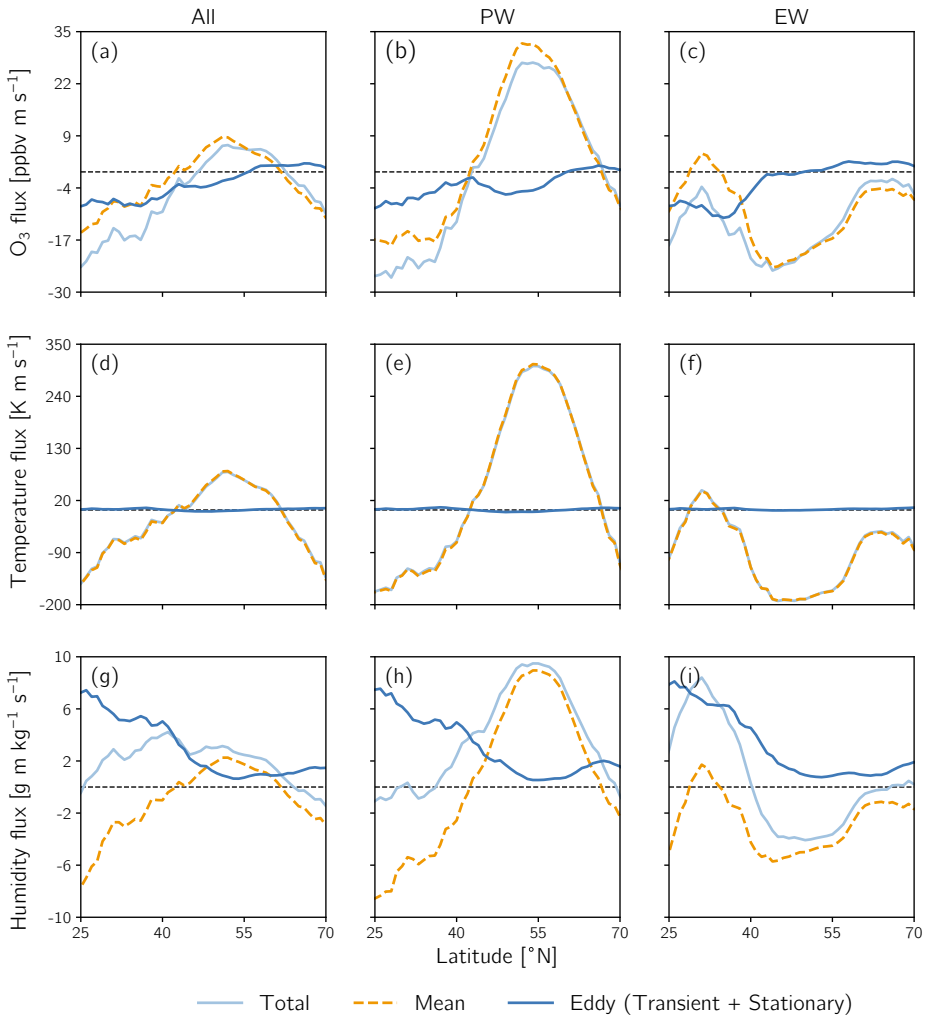

Figure 4.13: The zonally-averaged total flux of (a-c) O_3, (d-f) temperature, and (g-i) specific humidity and the contributions from the mean and eddy components. Calculations of the total flux and its components are done for all days (first column; a, d, g), days when the jet is in a PW position (second column; b, e, h), and days when the jet is in a EW position (third column; c, f, i).

baroclinic cyclones ventilating continental regions and sweeping O_3 (and its precursors) to sea. Increased poleward meridional flow when the jet migrates

north over the oceans (Figure 4.11c, 4.12c) could advect *lower* concentrations of O_3 poleward (Figure 4.7a), while advecting *higher* temperature and humidity poleward (Figure 4.7b-c). This mismatch in sign between O_3 and temperature or humidity could contribute to the negative O_3-meteorology-jet relationships over the oceans. While this can explain some of the negative correlation of O_3 with temperature and humidity over the oceans in the mid-latitudes, it cannot explain the widespread negative O_3-meteorology relationships over all ocean basins.

Outside of the mid-latitudes, ϕ_{jet} is not linked to changes in the eddy versus zonal mean contributions to the total flux of O_3, heat, and moisture. Accordingly, the relationships among O_3, the jet stream, and temperature or humidity have mixed strength and sign outside the mid-latitudes (Figures 4.3, 4.7, 4.13).

It is important to note that the eddy contribution to the total flux (Equation 4.1, Figure 4.13) encompasses more than just transient baroclinic cyclones. Implicit in this term are contributions from stationary centers of action such as the Bermuda High and Pacific High. Additionally, processes occurring within these systems such as stratospheric-tropospheric exchanges are included within our calculation of the eddy fluxes.

We have also conducted a similar decomposition of the fluxes of O_3 precursors such as NO_x and CO (not shown) and found that these species respond similarly to changes in ϕ_{jet}. Thus, we cannot explicitly rule out whether the O_3-meteorology-jet relationships are solely the result of the transport of O_3 versus the transport of its precursor species leading to subsequent chemical

production.

The connection between the mean meridional circulation and O_3 variability has been the subject of a recent study by Lu et al. (2019b). This study related increasing trends in Southern Hemisphere tropospheric O_3 with changes in the mean meridional circulation (i.e., the Southern Hemisphere Hadley Cell). Specifically, it was suggested that changes in extratropical stratospheric-to-tropospheric transport, associated with the Hadley Cell, can foster the transport of O_3-rich air to the troposphere and redistribute O_3 precursors (Lu et al., 2019b).

4.6 Conclusions

The primary intent of this study was to document the relationships among surface-level O_3, temperature, and humidity and explore the cause(s) of these relationships. Both observations and the GMI CTM support substantial spatial variations in $r(T, O_3)$ and $r(q, O_3)$. In continental regions of the mid-latitudes ($\sim 35 - 60°$N), the O_3-meteorology relationships are significantly positive (Figures 4.3-4.5), but outside of the mid-latitudes and over the oceans, $r(T, O_3)$ and $r(q, O_3)$ are either not significant or significantly anticorrelated (Figure 4.3).

Our transport-only GMI CTM simulation indicates that the O_3-temperature and O_3-humidity relationships are largely the product an indirect association with transport across the Northern Hemisphere (Figure 4.6). This result is consistent with previous work by Kerr et al. (2019) and Porter and Heald (2019), which showed that a majority of the O_3-temperature relationship in

the U.S. and Europe derived from meteorological phenomena.

The variability of surface-level O_3, temperature, and humidity are linked to the meridional movement of the jet stream in the Northern Hemisphere mid-latitudes. This result extends previous work focusing on the eastern U.S. (e.g., Barnes and Fiore, 2013; Shen et al., 2015) to the entire Northern Hemisphere. Over land in the mid-latitudes, a poleward (equatorward) shift of the jet is associated with increased (decreased) surface-level O_3, temperature, and humidity (Figures 4.7-4.8). Over the oceans, temperature and humidity respond to this meridional movement of the jet in the same fashion as over land, but the poleward (equatorward) movement of the jet decreases (increases) O_3. Changes in cyclone frequency, PBLH, and strength of the near-surface winds are either not connected with movements of the jet or do not result in substantial changes in surface O_3 (Figures 4.9-4.12).

We ultimately find that the jet influences these surface-level fields by means of changes in the mean meridional circulation. On days when the jet is in a poleward (equatorward) position, the mean meridional circulation is responsible for a large poleward (equatorward) flux of heat, moisture, and O_3 in the mid-latitudes (Figure 4.13). While this result holds in the zonal mean, we have shown clear land-ocean differences in the relationships among O_3, temperature or specific humidity, and the jet stream (Figures 4.3, 4.7-4.8). These differences could stem from differences in meridional gradients of O_3 and its precursors between the continental and marine regions of the Northern Hemisphere (e.g., Figure 4.1b). Our future work will elucidate how the source region of emissions impacts the relationship between the jet stream

and surface-level composition and investigate why the land-ocean differences exist.

Establishing the spatial variations of the O_3-meteorology relationships is a prerequisite to understand which regions could experience an "O_3-climate penalty" (Wu et al., 2008) under future climatic changes. As the O_3-meteorology relationships in the present-day climate are far from uniform in both magnitude and sign, it is unlikely that future changes in the climate will affect O_3 uniformly. Furthermore, as the relationships among O_3, temperature, and humidity are driven by an indirect association with transport, caution should be used when applying any measures of the current sensitivity of O_3 to meteorological variables (e.g., dO_3/dT or dO_3/dq from Figure 4.4) to future climatic changes.

Overall, our results demonstrate the importance of the position of the jet stream and mean meridional circulation on O_3 variability in the Northern Hemisphere, both of which will be affected by the future climate (e.g., Barnes and Polvani, 2013; Shaw and Voigt, 2015; Grise et al., 2019). A robust poleward displacement of the jet stream is expected in the twenty-first century, while changes to other properties of the jet (i.e., variations in speed; north-south movement) will exhibit spatial heterogeneity (Barnes and Polvani, 2013). The effect of these changes on surface-level O_3 needs to be explored.

4.7 Appendix

4.7.1 Planetary boundary layer (PBL) dynamics

Variations in the PBLH could connect the jet to surface-level O_3, temperature, and humidity. PBLH determines vertical mixing and the dilution of surface-level pollutants (Dawson et al., 2007) and responds directly to the flux of heat into the PBL. Previous studies have used both PBLH and mixing height to assess the impact of PBL dynamics on surface-level pollutants (e.g., Jacob and Winner, 2009; Reddy and Pfister, 2016), and here we use daily mean MERRA-2 PBLH, detailed in Section 4.2.3. MERRA-2 has been used to understand the behavior of observed PBL height (Molod et al., 2015). These authors found that the MERRA-2 PBLH compared well to observed values with the sign of the (MERRA-2 - observation) bias dependent on cloud cover.

An analysis of the (PW - EW) composites shows that the daily north-south movement of the jet stream is not significantly associated with PBLH variability over a majority of the continental regions of the Northern Hemisphere (Figures 4.11a, 4.12a). Over the oceans, northward movement of the jet stream tends to be associated with a more shallow boundary layer; but, in general, there is a no consistent sign associated with the variability of the jet with PBLH (Figure 4.11a, 4.12a). This result is robust whether daily mean PBLH is used as we have here, or if the jet-PBLH relationship is derived using PBLH averaged over subsets of the day (e.g., daytime, afternoon)

Although there is no jet-PBLH relationship, it is possible that PBLH may influence ozone independent of the jet stream. To examine this we evaluate the

correlation between PBLH and O_3. The sign of this correlation is varied, and its strength is largely not statistically significant across the mid-latitudes (not shown). There are some regions where $r(PBLH, O_3)$ is significant positively, but this implies that a deeper PBL results in higher O_3, which goes against simple dilution arguments. These findings agree with other studies: Jacob and Winner (2009) pointed out that the effect of mixing depth on O_3 is weak or variable (while the effect of mixing depth on $PM_{2.5}$ is consistently negative).

4.7.2 Near-surface winds

Another possible mechanism for the jet-O_3 relationship is changes in near-surface flow. We form additional (PW - EW) composites but for near-surface eastward (U_{10}) and northward (V_{10}) winds (Figure 4.11b-c). In a $\sim 20^\circ$ latitudinal band north (south) of $\overline{\phi_{jet}}$, the poleward (equatorward) movement of the jet significantly increases (decreases) U_{10} by up to 4 m/s (Figure 4.11a). Figure 4.11b asserts that V_{10} increases by up to 3 m/s as the jet migrates north throughout the mid-latitudes. It is worth noting the largest areal extent of changes (both increases and decreases) in U_{10} are centered over the oceans, while increases in V_{10} occur throughout the mid-latitudes over both land and oceans (Figure 4.11b-c).

The spatial structure of the change in V_{10} is qualitatively similar to the impact of the jet stream on other fields (e.g., O_3, temperature, and humidity in Figure 6 of the main text), but we note that there are some marine regions the windward side of continents where V_{10} has a negative relationship with the jet stream. Outside of the mid-latitudes the sign and significance of the

relationship of the jet with U_{10} and V_{10} is varied.

The composites in Figure 4.11b-c are less meaningful unless placed in the context of the time-averaged direction and magnitude of U_{10} and V_{10}, and we next discuss this. The time-averaged U_{10} is generally positive (eastward) over both land and ocean in the mid-latitudes ($40 - 60°$N) with a speed of ~ 1 m/s, while V_{10} in this latitudinal band is varied and generally weak ($-0.5 < V_{10} < 0.5$ m/s) (not shown). Thus, given the average speed and magnitude of U_{10} and V_{10}, the differences in V_{10} over land given the meridional vacillation of the jet (Figure 4.11c) represent much larger percentage changes than the jet-associated changes in U_{10}.

We also analyze the correlation between and U_{10} or V_{10} (Figure S3b-c). This analysis further supports that the ϕ_{jet} is linked to changes in near-surface flow in the mid-latitudes and that V_{10} strengthens as the jet migrates poleward.

We investigated the relationship among ϕ_{jet} and the total near-surface wind ($|U_{10}|$), a proxy for stagnation (not shown). Differences in $|U_{10}|$ between days with a poleward- versus equatorward-shifted jet were weak and variable in sign, and the correlation was not statistically significant across virtually the entire hemisphere. As we did with PBLH, we considered the impact that $|U_{10}|$ has on O_3 independent of the jet, as weak flow can inhibit the ventilation of the PBL (Mickley, 2004). We found that O_3 and $|U_{10}|$ were generally anticorrelated in the mid-latitudes; however, these correlations were weak and not statistically significant. There were also parts of the mid-latitudes with positive correlations between O_3 and $|U_{10}|$, implying that higher wind speeds and therefore increased ventilation are associated with higher

concentrations of O_3.

References

Barnes, Elizabeth A. and Arlene M. Fiore (2013). "Surface ozone variability and the jet position: Implications for projecting future air quality". In: 40.11, pp. 2839–2844. DOI: 10.1002/grl.50411.

Barnes, Elizabeth A. and Lorenzo Polvani (2013). "Response of the midlatitude jets, and of their variability, to increased greenhouse gases in the CMIP5 models". In: *J. Clim.* 26.18, pp. 7117–7135. DOI: 10.1175/JCLI-D-12-00536.1.

Barrett, Bradford S., Graciela B. Raga, Armando Retama, and Christopher Leonard (2019). "A multiscale analysis of the tropospheric and stratospheric mechanisms leading to the March 2016 extreme surface ozone event in Mexico City". In: *J. Geophys. Res.* 124.8, pp. 4782–4799. DOI: 10.1029/2018JD029918.

Bauer, Mike and Anthony D. Del Genio (2006). "Composite Analysis of Winter Cyclones in a GCM: Influence on Climatological Humidity". In: *J. Clim.* 19.9, pp. 1652–1672. DOI: 10.1175/jcli3690.1.

Bauer, Mike, George Tselioudis, and William B. Rossow (2016). "A New Climatology for Investigating Storm Influences in and on the Extratropics". In: *J. Appl. Meteorol. Climatol.* 55.5, pp. 1287–1303. DOI: 10.1175/jamc-d-15-0245.1.

Bosilovich, Michael, Santha Akella, Lawrence Coy, Richard Cullather, Clara Draper, Ronald Gelaro, et al. (2015). *MERRA-2: Initial evaluation of the climate, NASA/TM-2015-104606*, 139 pp.

Brown-Steiner, B., P.G. Hess, and M.Y. Lin (2015). "On the capabilities and limitations of GCCM simulations of summertime regional air quality: A diagnostic analysis of ozone and temperature simulations in the US using CESM CAM-Chem". In: 101, pp. 134–148. DOI: 10.1016/j.atmosenv.2014.11.001.

Camalier, Louise, William Cox, and Pat Dolwick (2007). "The effects of meteorology on ozone in urban areas and their use in assessing ozone trends". In: 41.33, pp. 7127–7137. DOI: 10.1016/j.atmosenv.2007.04.061.

Cooper, Owen R., Ru-Shan Gao, David Tarasick, Thierry Leblanc, and Colm Sweeney (2012). "Long-term ozone trends at rural ozone monitoring sites across the United States, 1990-2010". In: 117, p. D22307. DOI: 10.1029/2012JD018261.

Crippa, M., D. Guizzardi, M. Muntean, E. Schaaf, F. Dentener, J. A. van Aardenne, et al. (2018). "Gridded emissions of air pollutants for the period 1970-2012 within EDGAR v4.3.2". In: *Earth Syst. Sci. Data* 10.4, pp. 1987–2013. DOI: 10.5194/essd-10-1987-2018.

Dawson, John P., Peter J. Adams, and Spyros N. Pandis (2007). "Sensitivity of ozone to summertime climate in the eastern USA: A modeling case study". In: *Atmos. Environ.* 41.7, pp. 1494–1511. DOI: 10.1016/j.atmosenv.2006.10.033.

Dee, D. P., S. M. Uppala, A. J. Simmons, P. Berrisford, P. Poli, S. Kobayashi, et al. (2011). "The ERA-Interim reanalysis: Configuration and performance of the data assimilation system". In: *Q. J. R. Meteorol. Soc.* 137.656, pp. 553–597. DOI: 10.1002/qj.828.

Derwent, Richard G., Claire S. Witham, Steven R. Utembe, Michael E. Jenkin, and Neil R. Passant (2010). "Ozone in central England: The impact of 20 years of precursor emission controls in Europe". In: *Environ. Sci. Policy* 13.3, pp. 195–204. DOI: 10.1016/j.envsci.2010.02.001.

Duncan, B. N., S. E. Strahan, Y. Yoshida, S. D. Steenrod, and N. Livesey (2007). "Model study of the cross-tropopause transport of biomass burning pollution". In: 7.14, pp. 3713–3736. (Visited on 10/09/2017).

Duncan, B. N., J. J. West, Y. Yoshida, A. M. Fiore, and J. R. Ziemke (2008). "The influence of European pollution on ozone in the Near East and northern Africa". In: *Atmos. Chem. Phys.* 8.8, pp. 2267–2283. DOI: 10.5194/acp-8-2267-2008.

ECCC (2017). *National Air Pollution Surveillance Program*. https://open.canada.ca/data/en/dataset/1b36a356-defd-4813-acea-47bc3abd859b.

EPA (2019). *Air Quality System Data Mart*. http://www.epa.gov/ttn/airs/aqsdatamart.

Fiore, Arlene M., Vaishali Naik, and Eric M. Leibensperger (2015). "Air Quality and Climate Connections". In: 65.6, pp. 645–685. DOI: 10.1080/10962247.2015.1040526.

Gelaro, Ronald, Will McCarty, Max J. Suarez, Ricardo Todling, Andrea Molod, Lawrence Takacs, et al. (2017). "The Modern-Era Retrospective Analysis for Research and Applications, Version 2 (MERRA-2)". In: 30.14, pp. 5419–5454. DOI: 10.1175/JCLI-D-16-0758.1.

Grise, Kevin M., Sean M. Davis, Isla R. Simpson, Darryn W. Waugh, Qiang Fu, Robert J. Allen, et al. (2019). "Recent Tropical Expansion: Natural Variability or Forced Response?" In: *J. Clim.* 32.5, pp. 1551–1571. DOI: 10.1175/jcli-d-18-0444.1.

Guo, Jean J., Arlene M. Fiore, Lee T. Murray, Daniel A. Jaffe, Jordan L. Schnell, Charles T. Moore, and George P. Milly (2018). "Average versus high surface ozone levels over the continental USA: Model bias, background influences, and interannual variability". In: *Atmos. Chem. Phys.* 18.16, pp. 12123–12140. DOI: 10.5194/acp-18-12123-2018.

Han, Han, Jane Liu, Lei Shu, Tijian Wang, and Huiling Yuan (2020). "Local and synoptic meteorological influences on daily variability of summertime surface ozone in eastern China". In: *Atmos. Chem. Phys.* Pp. 203–222. DOI: 10.5194/acp-20-203-2020.

Hartmann, Dennis L. (2007). "The Atmospheric General Circulation and Its Variability". In: *J. Meteorol. Soc. Jpn. Ser. II* 85B, pp. 123–143. DOI: 10.2151/jmsj.85b.123.

He, H., J. W. Stehr, J. C. Hains, D. J. Krask, B. G. Doddridge, K. Y. Vinnikov, et al. (2013). "Trends in emissions and concentrations of air pollutants in the lower troposphere in the Baltimore/Washington airshed from 1997 to 2011". In: 13.15, pp. 7859–7874. DOI: 10.5194/acp-13-7859-2013.

Hegarty, Jennifer, Huiting Mao, and Robert Talbot (2007). "Synoptic controls on summertime surface ozone in the northeastern United States". In: *J. Geophys. Res.* 112.D14. DOI: 10.1029/2006JD008170.

Hjellbrekke, Anne-Gunn and Sverre Solberg (2019). *Ozone measurements 2017*. EMEP/CCC-Report 2/2019. Kjeller, Norway: EMEP Co-operative Programme for Monitoring and Evaluation of the Long-range Transmission of Air Pollutants in Europe. URL: https://projects.nilu.no//ccc/reports/cccr2-2019_Ozone.pdf.

Jacob, Daniel J. and Darrell A. Winner (2009). "Effect of climate change on air quality". In: 43.1, pp. 51–63. DOI: 10.1016/j.atmosenv.2008.09.051.

Jaeglé, Lyatt, Robert Wood, and Krzysztof Wargan (2017). "Multiyear composite view of ozone enhancements and stratosphere-to-troposphere transport in dry intrusions of Northern Hemisphere extratropical cyclones". In: *J. Geophys. Res.* 122.24, pp. 13436–13457. DOI: 10.1002/2017jd027656.

Kaspi, Yohai and Tapio Schneider (2013). "The Role of Stationary Eddies in Shaping Midlatitude Storm Tracks". In: *J. Atmos. Sci.* 70.8, pp. 2596–2613. DOI: 10.1175/jas-d-12-082.1.

Kavassalis, Sarah C. and Jennifer G. Murphy (2017). "Understanding ozone-meteorology correlations: A role for dry deposition". In: 44.6, pp. 2922–2931. DOI: 10.1002/2016GL071791.

Kerr, Gaige Hunter and Darryn W Waugh (2018). "Connections between summer air pollution and stagnation". In: 13.8, p. 084001. DOI: 10.1088/1748-9326/aad2e2.

Kerr, Gaige Hunter, Darryn W. Waugh, Stephen D. Steenrod, Sarah A. Strode, and Susan E. Strahan (2019). "Disentangling the Drivers of the Summertime Ozone-Temperature Relationship Over the United States". In: 124.19, pp. 10503–10524. DOI: 10.1029/2019jd030572.

Kerr, Gaige Hunter, Darryn W. Waugh, Sarah A. Strode, Stephen D. Steenrod, Luke D. Oman, and Susan E. Strahan (2020). "Surface ozone-meteorology relationships: Spatial variations and the role of the jet stream". In: *Submitted to J. Geophys. Res. Atmos.*

Kim, S.-W., A. Heckel, S. A. McKeen, G. J. Frost, E.-Y. Hsie, M. K. Trainer, et al. (2006). "Satellite-observed U.S. power plant NO_x emission reductions and their impact on air quality". In: *Geophys. Res. Lett.* 33.22. DOI: 10.1029/2006GL027749.

Knowland, K. E., R. M. Doherty, and K. I. Hodges (2015). "The effects of springtime mid-latitude storms on trace gas composition determined from the MACC reanalysis". In: *Atmos. Chem. Phys.* 15.6, pp. 3605–3628. DOI: 10.5194/acp-15-3605-2015.

Knowland, K. Emma, Ruth M. Doherty, Kevin I. Hodges, and Lesley E. Ott (2017). "The influence of mid-latitude cyclones on European background surface ozone". In: 17.20, pp. 12421–12447. DOI: 10.5194/acp-17-12421-2017.

Landrigan, Philip J, Richard Fuller, Nereus J R Acosta, Olusoji Adeyi, Robert Arnold, Niladri Basu, et al. (2018). "The Lancet Commission on pollution and health". In: *Lancet* 391.10119, pp. 462–512. DOI: 10.1016/s0140-6736(17)32345-0.

Lefohn, Allen S., Christopher S. Malley, Luther Smith, Benjamin Wells, Milan Hazucha, Heather Simon, et al. (2018). "Tropospheric ozone assessment report: Global ozone metrics for climate change, human health, and crop/ecosystem research". In: *Elem. Sci. Anth.* 6.1, p. 28. DOI: 10.1525/elementa.279.

Leibensperger, Eric M., Loretta J. Mickley, and Daniel J. Jacob (2008). "Sensitivity of US air quality to mid-latitude cyclone frequency and implications of 1980-2006 climate change". In: 8.23, pp. 7075–7086.

Li, Ke, Daniel J. Jacob, Hong Liao, Lu Shen, Qiang Zhang, and Kelvin H. Bates (2019). "Anthropogenic drivers of 2013-2017 trends in summer surface ozone in China". en. In: *Proc. Natl. Acad. Sci. U.S.A.* 116.2, pp. 422–427. DOI: 10.1073/pnas.1812168116.

Lin, Meiyun, Larry W. Horowitz, Richard Payton, Arlene M. Fiore, and Gail Tonnesen (2017). "US surface ozone trends and extremes from 1980 to 2014: Quantifying the roles of rising Asian emissions, domestic controls, wildfires, and climate". In: *Atmos. Chem. Phys.* 17.4, pp. 2943–2970. DOI: 10.5194/acp-17-2943-2017.

Lu, Xiao, Lin Zhang, Youfan Chen, Mi Zhou, Bo Zheng, Ke Li, Yiming Liu, Jintai Lin, Tzung-May Fu, and Qiang Zhang (2019a). "Exploring 2016-2017 surface ozone pollution over China: Source contributions and meteorological influences". en. In: *Atmos. Chem. Phys.* 19.12, pp. 8339–8361. DOI: 10.5194/acp-19-8339-2019. (Visited on 07/31/2019).

Lu, Xiao, Lin Zhang, Yuanhong Zhao, Daniel J. Jacob, Yongyun Hu, Lu Hu, et al. (2019b). "Surface and tropospheric ozone trends in the Southern Hemisphere since 1990: Possible linkages to poleward expansion of the Hadley circulation". In: *Sci. Bull.* 64.6, pp. 400–409. DOI: 10.1016/j.scib.2018.12.021.

Meehl, Gerald A, Claudia Tebaldi, Simone Tilmes, Jean-Francois Lamarque, Susan Bates, Angeline Pendergrass, and Danica Lombardozzi (2018). "Future heat waves and surface ozone". In: 13.6, p. 064004. DOI: 10.1088/1748-9326/aabcdc.

Mickley, L. J. (2004). "Effects of future climate change on regional air pollution episodes in the United States". In: *Geophys. Res. Lett.* 31.24. DOI: 10.1029/2004GL021216.

Molod, A., H. Salmun, and M. Dempsey (2015). "Estimating Planetary Boundary Layer Heights from NOAA Profiler Network Wind Profiler Data". In: *J. Atmos. Ocean Tech.* 32.9, pp. 1545–1561. DOI: 10.1175/jtech-d-14-00155.1.

Mudelsee, Manfred (2003). "Estimating Pearson's Correlation Coefficient with Bootstrap Confidence Interval from Serially Dependent Time Series". In: *Math. Geol.* 35.6, pp. 651–665. DOI: 10.1023/b:matg.0000002982.52104.02.

Mudelsee, Manfred (2014). *Climate Time Series Analysis: Classical Statistical and Bootstrap Methods*. 2nd. Cham, Heidelberg, New York, Dordrecht, London:

Springer International Publishing. ISBN: 9780123850225. DOI: 10.1007/978-3-319-04450-7.

Ordóñez, Carlos, David Barriopedro, and Ricardo García-Herrera (2019). "Role of the position of the North Atlantic jet in the variability and odds of extreme PM_{10} in Europe". In: *Atmos. Environ.* 210, pp. 35–46. DOI: 10.1016/j.atmosenv.2019.04.045.

Otero, N, J Sillmann, J L Schnell, H W Rust, and T Butler (2016). "Synoptic and meteorological drivers of extreme ozone concentrations over Europe". In: 11.2, p. 024005. DOI: 10.1088/1748-9326/11/2/024005.

Parrish, D. D., K. S. Law, J. Staehelin, R. Derwent, O. R. Cooper, H. Tanimoto, et al. (2012). "Long-term changes in lower tropospheric baseline ozone concentrations at northern mid-latitudes". In: *Atmos. Chem. Phys.* 12.23, pp. 11485–11504. DOI: 10.5194/acp-12-11485-2012.

Peixoto, J. P. and A. H. Oort (1992). *Physics of climate*. 2nd. New York: Am. Inst. Phys., 520 pp.

Phalitnonkiat, Pakawat, Peter G. M. Hess, Mircea D. Grigoriu, Gennady Samorodnitsky, Wenxiu Sun, Ellie Beaudry, et al. (2018). "Extremal dependence between temperature and ozone over the continental US". In: *Atmos. Chem. Phys.* 18.16, pp. 11927–11948. DOI: 10.5194/acp-18-11927-2018.

Polvani, L. M. and J. G. Esler (2007). "Transport and mixing of chemical air masses in idealized baroclinic life cycles". In: *J. Geophys. Res.* 112.D23, p. D23102. DOI: 10.1029/2007JD008555. (Visited on 04/29/2019).

Porter, W. C., C. L. Heald, D. Cooley, and B. Russell (2015). "Investigating the observed sensitivities of air-quality extremes to meteorological drivers via quantile regression". In: *Atmos. Chem. Phys.* 15.18, pp. 10349–10366.

Porter, William C. and Colette L. Heald (2019). "The mechanisms and meteorological drivers of the ozone-temperature relationship". In: pp. 13367–13381. DOI: 10.5194/acp-2019-140.

Pusede, Sally E., Allison L. Steiner, and Ronald C. Cohen (2015). "Temperature and Recent Trends in the Chemistry of Continental Surface Ozone". In: 115.10, pp. 3898–3918. DOI: 10.1021/cr5006815.

Rasmussen, D. J., A.M. Fiore, V. Naik, L.W. Horowitz, S.J. McGinnis, and M.G. Schultz (2012). "Surface ozone-temperature relationships in the eastern US: A monthly climatology for evaluating chemistry-climate models". In: 47, pp. 142–153. DOI: 10.1016/j.atmosenv.2011.11.021.

Rasmussen, D. J., Jianlin Hu, Abdullah Mahmud, and Michael J. Kleeman (2013). "The ozone-climate penalty: Past, present, and future". In: 47.24, pp. 14258–14266. DOI: 10.1021/es403446m.

Reddy, Patrick J. and Gabriele G. Pfister (2016). "Meteorological factors contributing to the interannual variability of midsummer surface ozone in Colorado, Utah, and other western U.S. states". In: *J. Geophys. Res.* 121.5, pp. 2434–2456. DOI: 10.1002/2015JD023840.

Sadiq, Mehliyar, Amos P. K. Tai, Danica Lombardozzi, and Maria Val Martin (2017). "Effects of ozone-vegetation coupling on surface ozone air quality via biogeochemical and meteorological feedbacks". In: *Atmos. Chem. Phys.* 17.4, pp. 3055–3066. DOI: 10.5194/acp-17-3055-2017.

Schnell, J. L., C. D. Holmes, A. Jangam, and M. J. Prather (2014). "Skill in forecasting extreme ozone pollution episodes with a global atmospheric chemistry model". In: *Atmos. Chem. Phys.* 14.15, pp. 7721–7739. DOI: 10.5194/acp-14-7721-2014.

Shaw, T. A. and A. Voigt (2015). "Tug of war on summertime circulation between radiative forcing and sea surface warming". In: *Nature Geosci.* 8.7, pp. 560–566. DOI: 10.1038/ngeo2449.

Shen, L., L. J. Mickley, and A. P. K. Tai (2015). "Influence of synoptic patterns on surface ozone variability over the eastern United States from 1980 to 2012". In: 15.19, pp. 10925–10938. DOI: 10.5194/acp-15-10925-2015.

Simon, Heather, Adam Reff, Benjamin Wells, Jia Xing, and Neil Frank (2015). "Ozone trends across the United States over a period of decreasing NOx and VOC emissions". In: 49.1, pp. 186–195. DOI: 10.1021/es504514z.

Strahan, S. E., A. R. Douglass, and P. A. Newman (2013). "The contributions of chemistry and transport to low arctic ozone in March 2011 derived from Aura MLS observations". In: 118.3, pp. 1563–1576. DOI: 10.1002/jgrd.50181.

Strahan, S. E., B. N. Duncan, and P. Hoor (2007). "Observationally derived transport diagnostics for the lowermost stratosphere and their application to the GMI chemistry and transport model". In: 7.9, pp. 2435–2445. (Visited on 10/09/2017).

Strode, Sarah A., Jose M. Rodriguez, Jennifer A. Logan, Owen R. Cooper, Jacquelyn C. Witte, Lok N. Lamsal, et al. (2015). "Trends and variability in surface ozone over the United States". In: 120.17, pp. 9020–9042. DOI: 10.1002/2014JD022784.

Sun, Wenxiu, Peter Hess, and Chengji Liu (2017). "The impact of meteorological persistence on the distribution and extremes of ozone". In: 44, pp. 1545–1553. DOI: 10.1002/2016GL071731.

Tai, Amos P.K. and Maria Val Martin (2017). "Impacts of ozone air pollution and temperature extremes on crop yields: Spatial variability, adaptation

and implications for future food security". In: 169, pp. 11–21. DOI: 10.1016/j.atmosenv.2017.09.002.

Tai, Amos P.K., Loretta J. Mickley, and Daniel J. Jacob (2010). "Correlations between fine particulate matter ($PM_{2.5}$) and meteorological variables in the United States: Implications for the sensitivity of $PM_{2.5}$ to climate change". In: 44.32, pp. 3976–3984. DOI: 10.1016/j.atmosenv.2010.06.060.

Tarasick, David, Ian E. Galbally, Owen R. Cooper, Martin G. Schultz, Gerard Ancellet, Thierry Leblanc, et al. (2019). "Tropospheric Ozone Assessment Report: Tropospheric ozone from 1877 to 2016, observed levels, trends and uncertainties". In: *Elem. Sci. Anth.* 7.1, p. 39. DOI: 10.1525/elementa.376.

Tawfik, Ahmed B. and Allison L. Steiner (2013). "A proposed physical mechanism for ozone-meteorology correlations using land-atmosphere coupling regimes". In: 72, pp. 50–59. DOI: 10.1016/j.atmosenv.2013.03.002. (Visited on 10/08/2018).

Turner, A. J., A. M. Fiore, L. W. Horowitz, V. Naik, and M. Bauer (2012). "Summertime cyclones over the Great Lakes storm track from 1860-2100: Variability, trends, and association with ozone pollution". In: *Atmos. Chem. Phys.* 12.8, pp. 21679–21712. DOI: 10.5194/acpd-12-21679-2012.

Varotsos, K. V., M. Tombrou, and C. Giannakopoulos (2013). "Statistical estimations of the number of future ozone exceedances due to climate change in Europe". In: *J. Geophys. Res.* 118.12, pp. 6080–6099. DOI: 10.1002/jgrd.50451.

Wilks, D. S. (1997). "Resampling Hypothesis Tests for Autocorrelated Fields". In: *J. Clim.* 10.1, pp. 65–82. DOI: 10.1175/1520-0442(1997)010<0065:rhtfaf>2.0.co;2.

Wilks, Daniel S. (2011). *Statistical methods in the atmospheric sciences*. Elsevier Academic Press. ISBN: 9780123850225.

Woollings, Tim, Abdel Hannachi, and Brian Hoskins (2010). "Variability of the North Atlantic eddy-driven jet stream". In: *Q. J. R. Meteorol. Soc.* 136.649, pp. 856–868. DOI: 10.1002/qj.625. (Visited on 12/16/2019).

Wu, Shiliang, Loretta J. Mickley, Eric M. Leibensperger, Daniel J. Jacob, David Rind, and David G. Streets (2008). "Effects of 2000-2050 global change on ozone air quality in the United States". In: 113.D6. DOI: 10.1029/2007JD008917.

Zhang, Yuzhong and Yuhang Wang (2016). "Climate-driven ground-level ozone extreme in the fall over the southeast United States". In: *Proc. Natl. Acad. Sci. U.S.A.* 113.36, pp. 10025–10030. DOI: 10.1073/pnas.1602563113.

Zhao, Shunliu, Amanda J. Pappin, S. Morteza Mesbah, J. Y. Joyce Zhang, Nicole L. MacDonald, and Amir Hakami (2013). "Adjoint estimation of ozone climate penalties". In: *Geophys. Res. Lett.* 40.20, pp. 5559–5563. DOI: 10.1002/2013GL057623.

Zhao, Zijian and Yuxuan Wang (2017). "Influence of the West Pacific subtropical high on surface ozone daily variability in summertime over eastern China". In: *Atmos. Environ.* 170, pp. 197–204. DOI: 10.1016/j.atmosenv.2017.09.024.

Zhu, Jinhong and Xin-Zhong Liang (2013). "Impacts of the Bermuda High on Regional Climate and Ozone over the United States". In: *J. Clim.* 26.3, pp. 1018–1032. DOI: 10.1175/jcli-d-12-00168.1.

Zhuang, J. (2018). *JiaweiZhuang/xESMF: v0.1.1*. DOI: https://doi.org/10.5281/ZENODO.1134366.

Zwiers, Francis W. and Hans von Storch (1995). "Taking Serial Correlation into Account in Tests of the Mean". In: *J. Clim.* 8.2, pp. 336–351. DOI: 10.1175/1520-0442(1995)008<0336:tsciai>2.0.co;2.

Chapter 5

Jet Stream-surface tracer relationships: Mechanism and sensitivity to source region

The upper-level jet stream has a significant impact on surface-level ozone (O_3), yet the cause of the daily variability and seasonal differences in this relationship remain unclear. We test the possible drivers of the O_3-jet relationship using idealized tracers with different source regions within an atmospheric chemical transport model. All tracers are correlated with the meridional position of the jet stream in the mid-latitudes, but tracers emitted south of the jet increase in the mid-latitudes when the jet is poleward-shifted, while the opposite is true for tracers emitted at high latitudes. The jet stream regulates the near-surface meridional wind, and we find that this coupling together with the meridional tracer gradient can reproduce regions where the jet stream and tracer concentrations are in and out of phase. Our results explain the land-ocean and seasonal differences in the O_3-jet relationship and highlight implications for jet-driven impacts on chemistry-climate connections.

5.1 Introduction and Motivation

There is substantial daily variability in near-surface atmospheric composition due to a combination of variations in emissions, chemistry, and transport. Understanding the cause of this variability is important for interpreting air pollution and its effects on human health (Landrigan et al., 2018) and the impacts of greenhouse gases on the climate system (IPCC, 2013). The upper-level jet stream is closely coupled to surface-level dynamics (Barnes and Polvani, 2013), and several recent studies have connected the the meridional, or north-south, position of the upper-level jet to surface-level ozone (O_3) O_3(Barnes and Fiore, 2013; Shen et al., 2015; Kerr et al., 2020), particulate matter (Ordóñez et al., 2019), and methane (Guha et al., 2018). However, there are many uncertainties in the cause of this connection.

We illustrate the connection between the meridional position of the jet stream (ϕ_{jet}) in Figure 5.1, which shows the temporal correlation (see Section 5.2) between ϕ_{jet} and surface-level O_3 from a chemical transport model (CTM) simulation detailed in Kerr et al. (2020). Ozone and ϕ_{jet} are significantly correlated within the seasonally-dependent range of the jet (Figure 5.1). Within this latitudinal band during boreal summer (JJA), O_3 increases over land and decreases over the oceans when the jet is in a poleward position (Figure 5.1a). During boreal winter (DJF), O_3 predominantly decreases in the mid-latitudes when the jet is poleward, and the DJF relationship lacks the land-ocean contrasts that exist during JJA (Figure 5.1b).

There are several open questions regarding the the jet-O_3 relationship: What is the mechanisms connecting the upper level jet to surface-level O_3?

Why does the sign of the relationship vary between land and ocean and with season? Does this relationship hold for other constituents?

We address these questions by performing CTM simulations of idealized tracers with differing source regions and thereafter examine how the Northern Hemisphere tracer-jet relationships varies with source region and under what condition(s) there are land-ocean or seasonal variations. As transport, not chemistry or emissions, is the leading driver of O_3 variability across the Northern Hemisphere mid-latitudes (Jacob et al., 1993; Kerr et al., 2019; Porter and Heald, 2019; Kerr et al., 2020), idealized tracers can aid in understanding and interpreting the jet stream-driven transport of O_3 while avoiding the complex interplay of non-linear O_3 chemistry and temporally- and spatially-varying precursor emissions (e.g. Orbe et al., 2016).

In Section 5.2, we describe the CTM simulations, reanalysis, and methodology used in this study. We document the relationship of the tracers with the jet in Section 5.3.1 and the impact of the jet on near-surface meridional wind in Section 5.3.2. We find a simple balance between the meridional tracer gradient and the relationship between the position of the jet stream and the near-surface meridional winds provides a satisfying physical explanation to differences in the sign of the O_3-jet and tracer-jet relationships (Sections 5.3.2-5.4).

5.2 Data and Methodology

We use the GEOS-Chem CTM (version 12.0.2) to perform our tracer simulations (Bey et al., 2001; The International GEOS-Chem User Community, 2018,

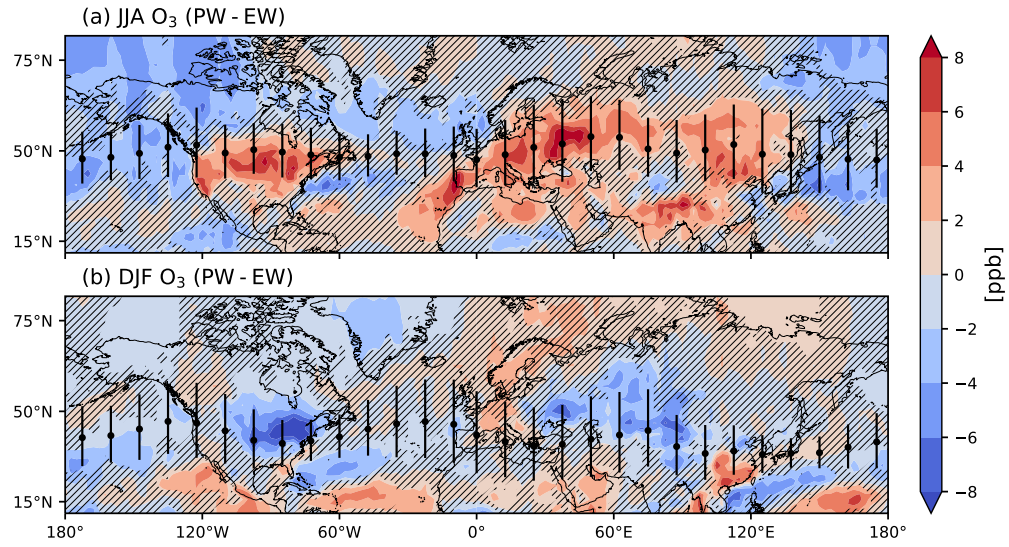

Figure 5.1: The difference in composites of surface-level, mean 1300-1400 hours (local time) O_3 for days with a poleward (PW) and equatorward (EW) jet stream during (a) JJA and (b) DJF 2008-2010. Scatter points and vertical bars in represent the mean position and variability of the jet stream, respectively. Hatching denotes O_3-ϕ_{jet} correlations that are statistically non-significant at the 95% confidence level.

October 10). GEOS-Chem is driven by assimilated meteorology from the Modern Era Retrospective-Analysis for Research and Applications, Version 2 (MERRA-2). Three-dimensional MERRA-2 fields are input to the CTM every three hours, while surface quantities and mixing depths are provided every hour. Specifically, our configuration of GEOS-Chem follows a passive simulation described in Liu et al. (2001). We perform this simulation at 2° latitude x 2.5° longitude resolution with 72 vertical levels ($\sim$ 15 hPa spacing below 800 hPa) for 2007 $-$ 2010, and we discard the first year (2007) for spin up.

We implement a suite of nine passive tracers that differ only in their source

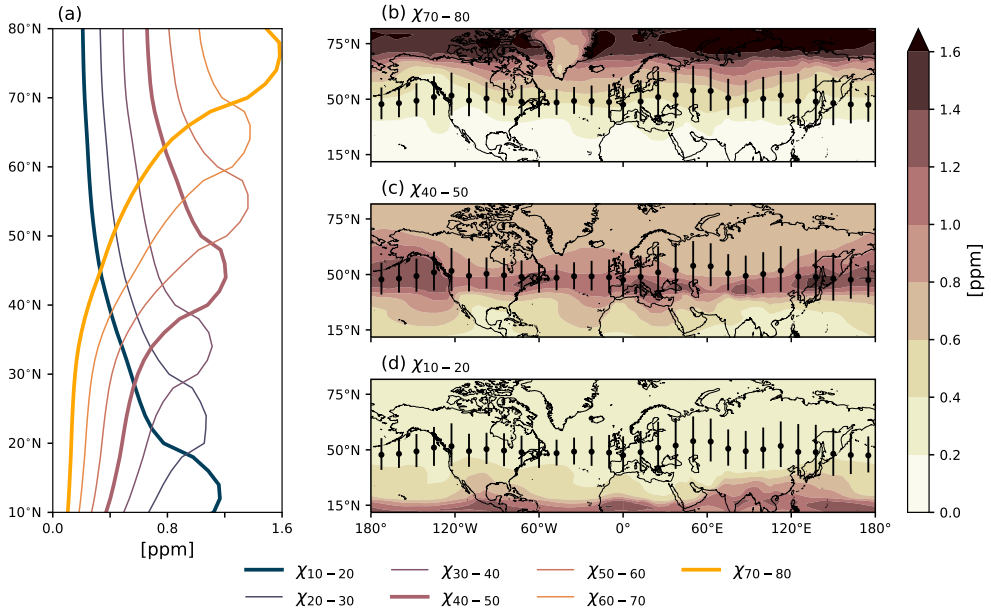

Figure 5.2: (a) Zonally-averaged tracer concentrations in JJA. (b) JJA-averaged concentrations of (b) χ_{70-80}, (c) χ_{40-50}, and (d) χ_{10-20}. Scatter points and vertical bars in (b)-(d) represent the mean position and variability of the jet stream in JJA, respectively. Note that the thicker lines in (a) correspond to the tracers featured in (b)-(d).

regions, which are prescribed as constant flux boundary conditions (i.e., emissions) in zonally-symmetric 10° latitudinal bands. Tracers are herein denoted $\chi_{\phi 1-\phi 2}$, where $\phi 1$ is the latitude corresponding to the southern boundary of the source region and $\phi 2$ is the northern boundary. All tracers decay uniformly at a loss rate of $\tau = 50$ days^{-1}. Tracers with the same loss have been used in prior studies (e.g., Shindell et al., 2008; Orbe et al., 2017; Orbe et al., 2018; Yang et al., 2019). We average hourly near-surface ($1000 - 800$ hPa) tracer concentrations to yield daily mean concentrations.

In addition to driving the GEOS-Chem simulations, we use MERRA-2 to characterize the meteorology responsible for tracer and O_3 variability (McCarty et al., 2016; Gelaro et al., 2017). MERRA-2 is output on a global 0.5° x

0.625° grid with 72 vertical levels. Specifically, we obtain 3-hourly $1000 - 800$ hPa meridional wind (V) and 500 hPa zonal wind (U) from MERRA-2 and average these data to daily mean values, consistent with our treatment of tracers from GEOS-Chem. The horizontal resolution differs between GEOS-Chem and MERRA-2, and we degrade the resolution of MERRA-2 to match that of GEOS-Chem using xESMF, a universal regridder for geospatial data (Zhuang et al., 2020).

Previous studies have demonstrated the accuracy of transport in GEOS-Chem and the assimilated meteorological product, MERRA-2, driving the CTM. Bosilovich et al. (2015) showed that magnitude of MERRA-2 zonal and meridional wind fields as well as the location of wind maxima are well constrained by observations and other reanalyses. GEOS-Chem yields realistic concentrations and seasonal and latitudinal distributions of other tracers (e.g., Pb, Be) with no significant global bias (Liu et al., 2001). However, Yu et al. (2018) recently pointed out that the use of offline CTMs, such as GEOS-Chem, together with an archived assimilated meteorological product can lead to vertical transport errors due, in part, to loss of transient advection motions (resolved convection). While potential biases and errors are important to keep in mind, the extensive body of literature on the validity of GEOS-Chem indicates that it is a reliable framework to address our research questions.

We locate ϕ_{jet} daily at each longitude by finding the latitude (restricted to $20 - 70°$N) of maximum 500 hPa U. A simple convolution-based smoothing is applied to these latitudes using a box-shaped function with width of $\sim 10°$ longitude (Barnes and Fiore, 2013; Kerr et al., 2020).

The temporal correlation between ϕ_{jet} and near-surface tracer concentrations or V is quantified with the Pearson product-moment correlation coefficient, indicated by $r(X, Y)$, where X and Y are the time series of interest. We assess its significance using the non-parametric moving block bootstrapping method, which preserves much of the temporal correlation in the time series and makes no *a priori* assumptions about the time series' distribution. In essence, time series X and Y are randomly reordered by sampling continuous blocks of data with length = 10 days, and $r(X, Y)$ is thereafter recalculated. We conduct 10000 realizations of this reordering, and significance is determined with a two-tailed percentile confidence interval method at the 0.05 significance level (Wilks, 1997; Mudelsee, 2003; Wilks, 2011).

We also generate composites of tracer concentrations and V on days when the jet stream is poleward (PW) and equatorward (EW). The PW (EW) composite is defined locally (i.e., at each longitude) as the average value of the field of interest for days where ϕ_{jet} exceeds (is less than) the 70th (30th) percentile. We define a "positive" relationship to mean that the PW (EW) movement of the jet is associated with increased (decreased) tracer concentrations or V. The opposite is true for a "negative" tracer-jet relationship.

5.3 Results

5.3.1 Relationship between the jet stream and tracers

Zonally-averaged tracer concentrations peak within their source regions and diminish to roughly half of their peak value $\pm 5^\circ$ outside their source regions (Figure 5.2a). Tracers with source regions at latitudes (ϕ) north of 60°N have

higher concentrations within their source regions compared with tracers emitted at lower latitudes (Figure 5.2a). Based on simple geometric effects (i.e., less area for latitude bands closer to the pole), one might expect smaller tracer concentrations at higher latitudes. This is not the case, and our results suggest less efficient pathways to transport these tracers vertically or from the Arctic equatorward, supporting an isolated Arctic lower troposphere and the "polar dome" as a barrier to transport (Law and Stohl, 2007).

Despite zonally-symmetric emissions, there are zonal variations in tracer concentrations (Figure 5.2b-d). The latitudinal range with high tracer concentrations (> 0.8 ppm) is larger over the ocean basins for tracers with high and mid-latitude source regions (e.g., χ_{70-80}, χ_{40-50}; Figure 5.2b-c). These ocean regions coincide with the Atlantic and Pacific storm tracks. The opposite occurs for tracers with source regions in the tropics (e.g., χ_{10-20}): high concentrations are more diffuse over land and more restricted over the tropical ocean (Figure 5.2d).

Within the mid-latitudinal range over which the jet traverses (vertical bars in Figure 5.3), there is a significant tracer-jet relationship during JJA and DJF, regardless of the source region of the tracer (hatching in Figure 5.3). However, the sign of the relationship hinges on the source region of the tracers. Tracers with source regions at low latitudes ($\phi < 40°$N) increase in the mid-latitudes when the jet is PW-positioned (Figure 5.3a-b). Tracers emitted around the latitude of the jet ($40° < \phi < 60°$N) have a spatially-varied relationship in the mid-latitudes with land-ocean differences despite zonally-symmetric emissions (Figure 5.3c-d). Tracers with source regions at

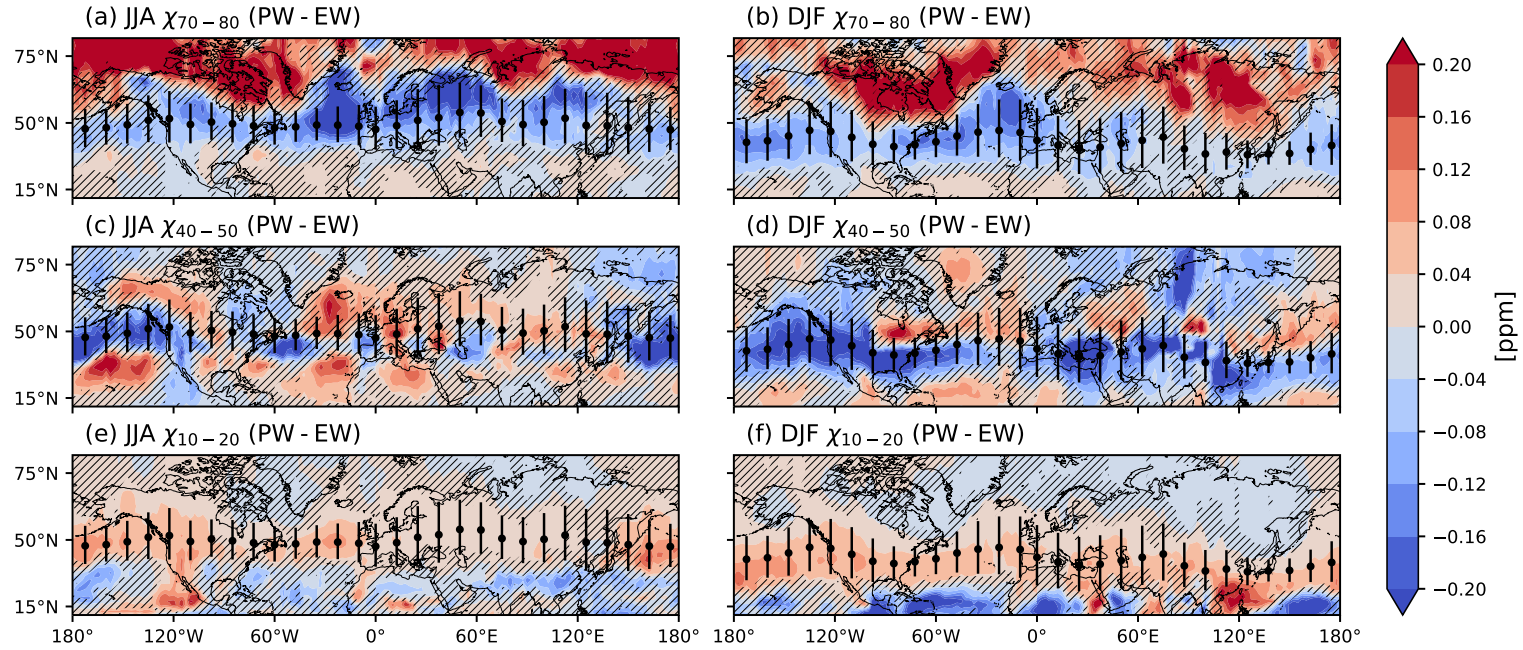

Figure 5.3: The difference in composites of JJA (a) χ_{10-20}, (c) χ_{40-50}, and (e) χ_{70-80} for days with a PW versus EW jet stream. Hatching denotes statistically non-significant tracer-jet correlations. Scatter points and vertical bars represent the mean position and variability of the jet stream in JJA, respectively. (b), (d), and (f) are the same as (a), (c), and (f) but for DJF.

high latitudes ($\phi > 60°$N) decrease in the mid-latitudes when the jet is PW (Figure 5.3e-f).

Beyond the mid-latitudes and these three tracers, impact of source region on the tracer-jet relationships for all the GEOS-Chem tracers can be easily seen in the zonal mean (Figure 5.4a-b). The tracer-jet relationships all exhibit an oscillatory pattern, but tracers with source regions south of the range of the jet are positively correlated with the jet in the mid-latitudes and are flanked by negative correlations outside the mid-latitudes, while tracers with source regions north of the jet have a negative correlation with the jet in the mid-latitudes and positive correlations outside the mid-latitudes (Figure 5.4a-b).

Outside of the mid-latitudes, the correlation of all tracers with ϕ_{jet} is generally statistically non-significant. As it pertains to regions with significant versus statistically non-significant relationships with the jet, both the tracers and O_3 behave similarly (Figure 5.1; Kerr et al., 2020).

In a gross sense, the relationship between the jet stream and our tracers does not change in DJF compared to JJA, but further inspection suggests that there are nuanced differences in the tracer-jet relationships (Figure 5.3). For example, the change in mid-latitude concentrations of χ_{40-50} due to the meridional movement of the jet is varied in sign and strength during JJA, while the DJF change is largely negative (Figures 5.3c-d, 5.4b-c).

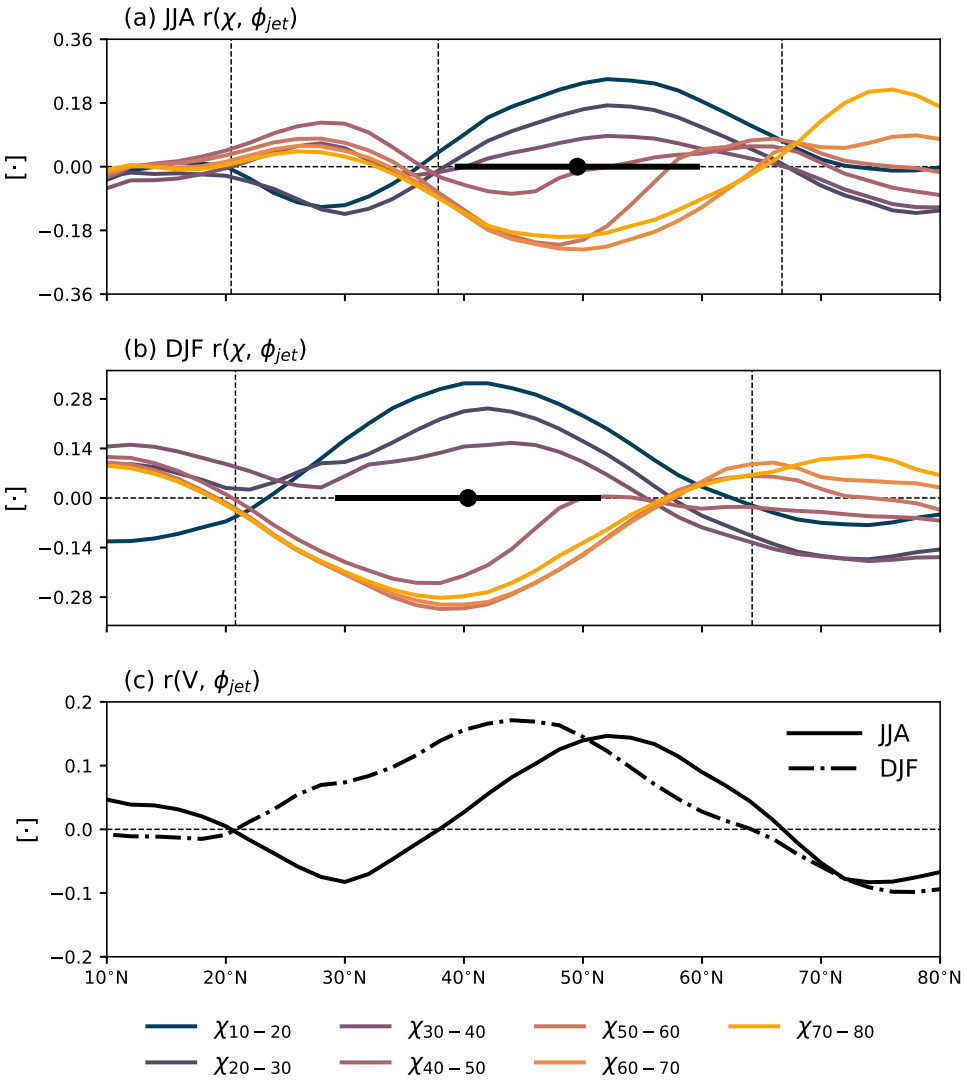

Figure 5.4: The relationship among ϕ_{jet}, V, and tracers. This figure shows (a) Zonally-averaged correlation between ϕ_{jet} and individual tracers in JJA (colors) and the mean position and and variability of the jet stream (scatter point and vertical bars. (b) same as (a) but for DJF. (c) Zonally-averaged $r(V, \phi_{jet})$. Dashed vertical lines in (a)-(b) denote the latitudes where $r(V, \phi_{jet}) = 0$ for each season. Dashed horizontal lines separate positive from negative correlations.

5.3.2 How the meridional wind and tracer gradient affect the tracer-jet relationship

Kerr et al. (2020) suggested that the jet stream affects surface-level O_3 by altering the near-surface meridional flow (V), and we next expand upon these findings and relate them to our tracers. We next examine the V-jet relationship in terms of the correlation coefficient (Figure 5.4c) and (PW - EW) composites (Figure 5.6a-b).

In the zonal mean, the latitudes, or nodes, where $r(\chi, \phi_{jet}) = 0$ are well-aligned with the latitudes where the jet stream and V are not correlated (Figure 5.4). The only node where $r(V, \phi_{jet}) = 0$ does not coincide with $r(\chi, \phi_{jet}) = 0$ occurs during DJF north of the jet (Figure 5.4b). In this case, the latitude where $r(V, \phi_{jet}) = 0$ lies north of $r(\chi, \phi_{jet}) = 0$ by $\sim 5°$, and other processes could be important for the tracer-jet relationships in this region and season. These results support Kerr et al. (2020) and provide strong evidence linking the tracer-jet relationships to (1) the source region of the tracers and (2) the V-jet relationship (Figure 5.4).

Figure 5.4c suggests that southerly flow increased in the mid-latitudes when the jet stream is PW during JJA and DJF; however, it does not show the magnitude. In parts of the mid-latitudes, V increases over 5 m/s when the jet is PW (colored shading in Figure 5.6a-b). This stands in sharp contrast to time-averaged V, which is generally weak ($-2 < V < 2$ m/s) over the vast majority of the mid-latitudes. It is exceedingly rare for time-averaged V to have the same magnitude changes in V linked to the jet (contours in Figure 5.6a-b). Outside the mid-latitudes, the relationship between V and ϕ_{jet}

is largely non-significant and weak (Figure 5.6a-b).

The V-jet relationship is not zonally-symmetric (Figure 5.6a-b). For example, there is a significant negative V-jet relationship windward side of the continents during JJA, but over the continents and the leeward side of the continents (Figure 5.6a).

The jet-induced change in V modifies meridional tracer advection (i.e., $-V \cdot \partial\chi/\partial\phi$). Thus, the impact of a given change in V is expected to depend on the local tracer gradients ($\partial\chi/\partial\phi$). If $\partial\chi/\partial\phi$ is weak, then smaller tracer changes are expected compared with locations with stronger $\partial\chi/\partial\phi$. It also follows that the same change in V operating over $\partial\chi/\partial\phi < 0$ versus $\partial\chi/\partial\phi > 0$ would result in changes of tracer concentrations with different signs.

V is tightly connected with the jet and the mean advective flux generally accounts for most of the total flux (Section 5.5; Figures 5.4c, 5.5). On account of this, we can take into account this dependence building on the advection equation and derive a simple balance. This balance uses $r(V, \phi_{jet})$ and $\partial\chi/\partial\phi$ to approximate the expected sign of the tracer-jet correlation:

$$E[r(\chi, \phi_{jet})] \sim -r(V, \phi_{jet}) \cdot \frac{\partial\chi}{\partial\phi}. \tag{5.1}$$

In practice, this balance implies that the anomalous southerly flow in the mid-latitudes that accompanies a PW-shifted jet ($r(V, \phi_{jet}) > 0$) will advect higher tracer concentrations from lower latitudes if $\partial\chi/\partial\phi < 0$, yielding a positive expected tracer-jet relationship (i.e., $E[r(\chi, \phi_{jet})] > 0$).

The simple balance in Equation 5.1 robustly captures the large-scale differences in the sign of the relationship between the jet and all tracers, confirming

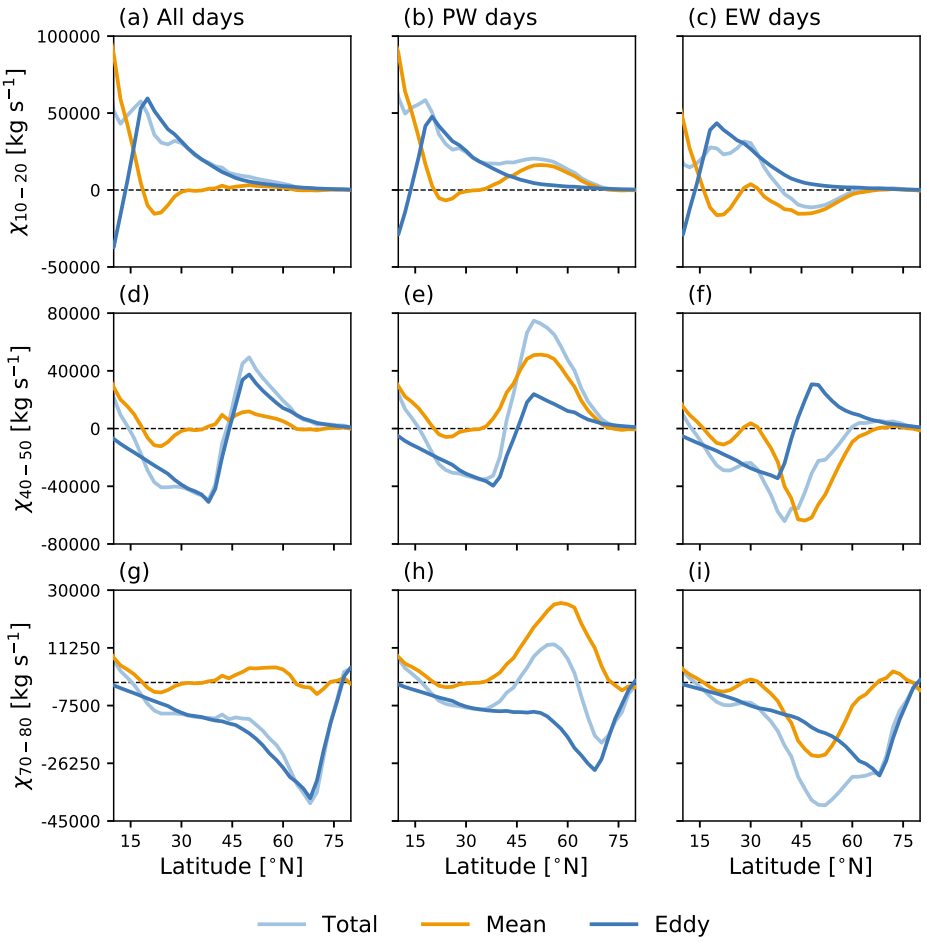

Figure 5.5: The dominant role of the zonal mean flow in linking the ϕ_{jet} to the near-surface V is shown by the zonally-averaged total, mean, and eddy fluxes of (a)-(c) χ_{10-20}, (d)-(f) χ_{40-50}, and (g)-(i) χ_{70-80} vertically integrated over $1000 - 800$ hPa. The left column corresponds to fluxes calculated for all JJA days, and the middle (right) columns corresponds to fluxes on days with a PW-shifted (EW-shifted) jet.

that spatiotemporal variations in the V-jet relationship together with the meridional background gradient are the most important factors to explain the tracer-jet coupling. We illustrate the application of Equation 5.1 for χ_{40-50} in Figure 5.6c-d. Equation 5.1 can explain the widespread negative χ_{40-50}-jet relationship in mid-latitudes during DJF (Figure 5.6d) but also the differences in sign on much smaller spatial scales during JJA (Figure 5.6c). Moreover, we note that Equation 5.1 captures the land-ocean contrasts present in the JJA χ_{40-50}-jet relationship (Figure 5.6c).

The application of Equation 5.1 does not capture the sign of the χ_{40-50}-jet relationship in the vicinity of the Atlantic and Pacific storm tracks (Figure 5.6c-d), and this is the case for other tracers as well (not shown). Since our tracer concentrations are roughly zonally-symmetric (Figure 5.2b-d), the effect of changes in the zonal wind are negligible to first order. However, the jet stream exerts an influence on near-surface U (Woollings et al., 2010), especially near the exit region of the these storm tracks. To account for this, future studies could consider the impact of both the V-jet and U-jet relationships.

We have also isolated the terms in Equation 5.1 by separately fixing each to its zonal mean value and thereafter recalculating $E[r(\chi, \phi_{jet})]$ to gauge which exerts a stronger influence on the tracer-jet relationships (not shown). This analysis indicates that fixing $\partial\chi/\partial\phi$ to its zonal mean value and allowing $r(V, \phi_{jet})$ to vary as in Figure 5.6a-b yields expected tracer-jet relationships with zonal variations that resemble the relationships shown in Figure 5.6c-d. This affirms the importance of the V-jet coupling in driving the tracer-jet relationships.

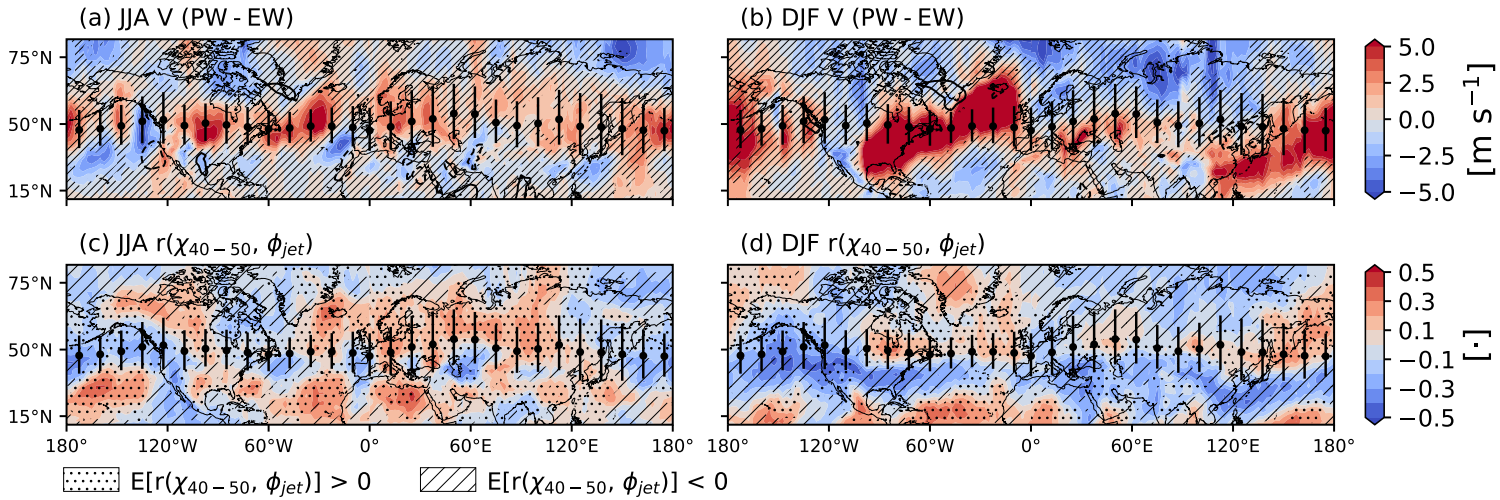

Figure 5.6: (a-b) Differences in composites of V for days with a PW versus EW jet stream (colors). Time-averaged V is illustrated for 5 m/s (solid black contour) and -5 m/s (dashed black contour). Hatching denotes statistically non-significant V-jet correlations. (c-d) Differences in the correlation coefficient calculated between χ_{40-50} and ϕ_{jet} (colors). As denoted in the legend beneath (c), stippling and hatching show the expected sign of the correlation, $E[r(\chi_{40-50}, \phi_{jet})]$, determined using Equation 5.1. Scatter points and vertical bars in all subplots represent the mean position of and variability of the jet stream, respectively.

5.4 Conclusions

Our simulations show that the daily variability of the position of the jet stream has a strong influence on near-surface tracer concentrations within the seasonally-dependent range of the jet. The sign of the tracer-jet relationships varies with source region (Figures 5.3, 5.4a-b). Tracers with source regions at low latitudes have positive tracer-jet relationships in the mid-latitudes, while the opposite is true for tracers with source regions at high latitudes. Tracers with source regions within the latitudinal range of the jet have a varied, zonally-asymmetric relationship with the jet in the mid-latitudes.

We find that the tracer-jet relationships are strongest where the jet exerts the strongest positive influence on near-surface V and that changes in the sign and magnitude of the flux of tracers by the mean flow are key in understanding how the jet stream position influences tracer variability (Figures 5.4, S1). Our proposed mechanism (Equation 5.1) reproduces the main features of the tracer-jet relationships by linking the background tracer gradient with the V-jet relationship.

These results support prior evidence linking daily variations in surface-level O_3 to the mean meridional circulation (e.g., Nikulin and Karpechko, 2005; Lu et al., 2019; Kerr et al., 2020), although we note that not all of these studies strictly focus on surface-level or near-surface O_3. Our findings also importantly relate variations in the near-surface meridional circulation to the position of the jet stream (Figures 5.4c, 5.6a-b). Furthermore, our findings shed light on the O_3-jet relationship discussed in Kerr et al. (2020) and shown in Figure 5.1, specifically answering questions regarding the (1) origin of the

land-ocean differences and (2) why seasonal differences exist.

(1) The land-ocean contrasts in the O_3-jet relationship during JJA are also present for χ_{40-50} (compare Figure 5.1a and Figure 5.3c). Both O_3 and χ_{40-50} have similar latitudinal gradients during JJA, and since the background gradient has a demonstrated effect on the coupling between tracers and the jet (Figure 5.6c-d), species with source regions near the latitude of the jet will have similar land-ocean contrasts. (2) The DJF O_3-jet relationship resembles the DJF χ_{40-50}-jet relationship (compare Figure 5.1b and Figure 5.3d) inasmuch as there are significant negative correlations within the range of the jet and both species have a similar latitudinal gradients (not shown). We therefore attribute the seasonal differences in the O_3-jet relationship to differences in both the V-jet relationship and background gradients.

Though we have considered only O_3 and idealized tracers with zonally-uniform emissions and lifetimes, these results may apply to species with lifetimes that are sufficiently-long to undergo synoptic-scale transport. Future studies should test this and also explore how zonally-asymmetric emissions as well as species' lifetimes affect their relationship with the jet.

Our study has documented a major driver of near-surface composition variability (i.e., transport associated with the jet stream) and linked this driver with the location of emissions. This is especially relevant as the position of the jet stream is expected to migrate poleward with climate change (Barnes and Polvani, 2013) and as emissions are redistributed from the mid-latitudes (developed nations) to low latitudes (developing nations) (Zhang et al., 2016).

Accordingly, the role of the jet stream, the associated meridional wind response, and the location of emissions should be a deliberate consideration of future work on chemistry-climate connections.

5.5 Appendix

To understand how the tracer flux is shaped by the zonal mean flow versus departures from the zonal mean (i.e., eddies), we decompose χ and V into contributions from the Eulerian zonal mean ($\overline{\ }$) and deviations from that zonal mean ($'$) such that $\chi = \overline{\chi} + \chi'$ and $V = \overline{V} + V'$. The total transport of χ by V is given by the factorization of these two expressions and reduces to:

$$\overline{\chi V} = \overline{\chi}\,\overline{V} + \overline{\chi' V'} \tag{5.2}$$

where the terms on the right side correspond to transport by the mean flow and transport by eddies (both stationary and transient), respectively. These terms can be vertically integrated given by:

$$\int_{p_2}^{p_1} \overline{\chi V} \cos(\phi) dp = \int_{p_2}^{p_1} \overline{\chi}\,\overline{V} \cos(\phi) dp + \int_{p_2}^{p_1} \overline{\chi' V'} \cos(\phi) dp \tag{5.3}$$

Here, p_1 and p_2 are 800 hPa and 1000 hPa, respectively. Since tracers emitted at the Earth?s surface decay exponentially with height, and tracer fluxes in the lower troposphere dominate the total tropospheric flux [e.g., Yang et al., 2019], our results are not sensitive to p_1 in Equation 5.3. We scale each term by $(2\pi a r_M)/g$ to yield the tracer mass flow rates, where r_M is the ratio of the molar mass of the tracers (CO-like; 28 g mol^{-1}) to dry air (28.97 g mol^{-1}); a is

the Earth's radius; g is gravitational acceleration

Eddy fluxes are an important contributor to the total flux near the source regions of individual tracers when all days during JJA are examined (Figure 5.5a, d, g). The maximum poleward (equatorward) eddy flux generally resides on the northern (southern) periphery of the source region. The flux of tracers by the mean flow exceeds that from the eddies at low latitudes ($\phi < 15°$N); the mean flux is near-zero for higher latitudes.

We perform the same decomposition and vertically integrated flow rate calculations (Equations 5.2-5.3) for the case of a poleward- and equatorward-shifted jet. Unlike for all JJA days, this analysis reveals that the flux of tracers by the mean flow is critically important to explain differences in tracer concentrations associated with the position of the jet (Figure 5.5). The flux by the mean flow changes sign in the mid-latitudes and clearly dominates the total flux in the zonal mean, leading to a net poleward (equatorward) flux of tracers when the jet is in a PW (EW) position. Eddies play a slightly large role in the equatorward flux of χ_{70-80} and other tracers with source regions at high latitudes compared with tracers with source regions at lower latitudes (Figure 5.5g-i).

We have also analyzed the eddy versus mean contributions to the total flux in DJF (not shown), and while the precise magnitude of the fluxes changes, the relative roles of the mean and eddy fluxes and their connections with the position of the jet stream do not. Moreover, we have examined other GEOS-Chem tracers besides the three shown here, and in all cases the results are similar.

Transient and stationary eddy fluxes of moisture and sensible and latent heat are the primary contributors to the total flux in the mid-latitudes during winter (e.g., Peixóto and Oort, 1983; Liu and Barnes, 2015). However, we have shown that this does not hold for tracer fluxes during boreal winter and summer. Our past work demonstrated that meridional transport of summertime O_3 by the mean advective flux is linked to ϕ_{jet} and dominated the total transport of O_3 in the mid-latitudes (Kerr et al., 2020). Eddies could play a stronger role on moisture and heat transport compared with the transport of a passive tracer, and it would be worthwhile to further investigate this in future studies.

References

Barnes, Elizabeth A. and Arlene M. Fiore (2013). "Surface ozone variability and the jet position: Implications for projecting future air quality". In: 40.11, pp. 2839–2844. DOI: 10.1002/grl.50411.

Barnes, Elizabeth A. and Lorenzo Polvani (2013). "Response of the midlatitude jets, and of their variability, to increased greenhouse gases in the CMIP5 models". In: 26.18, pp. 7117–7135. DOI: 10.1175/JCLI-D-12-00536.1.

Bey, Isabelle, Daniel J. Jacob, Robert M. Yantosca, Jennifer A. Logan, Brendan D. Field, Arlene M. Fiore, et al. (2001). "Global modeling of tropospheric chemistry with assimilated meteorology: Model description and evaluation". In: *J. Geophys. Res. Atmos.* 106.D19, pp. 23073–23095. DOI: 10.1029/2001jd000807.

Bosilovich, Michael, Santha Akella, Lawrence Coy, Richard Cullather, Clara Draper, Ronald Gelaro, et al. (2015). *MERRA-2: Initial evaluation of the climate, NASA/TM-2015-104606*, 139 pp.

Gelaro, Ronald, Will McCarty, Max J. Suárez, Ricardo Todling, Andrea Molod, Lawrence Takacs, et al. (2017). "The Modern-Era Retrospective Analysis for Research and Applications, Version 2 (MERRA-2)". In: 30.14, pp. 5419–5454. DOI: 10.1175/jcli-d-16-0758.1.

Guha, Tania, Yogesh K. Tiwari, Vinu Valsala, Xin Lin, Michel Ramonet, Anoop Mahajan, Amey Datye, and K. Ravi Kumar (2018). "What controls the atmospheric methane seasonal variability over India?" In: *Atmos. Environ.* 175, pp. 83–91. DOI: 10.1016/j.atmosenv.2017.11.042.

IPCC (2013). *Climate Change 2013: The Physical Science Basis. Contribution of Working Group I to the Fifth Assessment Report of the Intergovernmental Panel on Climate Change*. Cambridge University Press, p. 1535. ISBN: ISBN 978-1-107-66182-0. DOI: 10.1017/CBO9781107415324. URL: www.climatechange2013.org.

Jacob, Daniel J., Jennifer A. Logan, Geraldine M. Gardner, Rose M. Yevich, Clarisa M. Spivakovsky, Steven C. Wofsy, et al. (1993). "Factors regulating

ozone over the United States and its export to the global atmosphere". In: 98.D8, p. 14817. DOI: 10.1029/98jd01224.

Kerr, Gaige Hunter, Darryn W. Waugh, Stephen D. Steenrod, Sarah A. Strode, and Susan E. Strahan (2020). "Surface ozone-meteorology relationships: Spatial variations and the role of the jet stream". In:

Kerr, Gaige Hunter, Darryn W. Waugh, Sarah A. Strode, Stephen D. Steenrod, Luke D. Oman, and Susan E. Strahan (2019). "Disentangling the Drivers of the Summertime Ozone-Temperature Relationship Over the United States". In: 124.19, pp. 10503–10524. DOI: 10.1029/2019jd030572.

Landrigan, Philip J, Richard Fuller, Nereus J R Acosta, Olusoji Adeyi, Robert Arnold, Niladri (Nil) Basu, et al. (2018). "The Lancet Commission on pollution and health". In: 391.10119, pp. 462–512. DOI: 10.1016/s0140-6736(17)32345-0.

Law, K. S. and A. Stohl (2007). "Arctic Air Pollution: Origins and Impacts". In: *Science* 315.5818, pp. 1537–1540. DOI: 10.1126/science.1137695.

Liu, Chengji and Elizabeth A. Barnes (2015). "Extreme moisture transport into the Arctic linked to Rossby wave breaking". In: *J. Geophys. Res. Atmos.* 120.9, pp. 3774–3788. DOI: 10.1002/2014jd022796.

Liu, Hongyu, Daniel J. Jacob, Isabelle Bey, and Robert M. Yantosca (2001). "Constraints from ^{210}Pb and ^{7}Be on wet deposition and transport in a global three-dimensional chemical tracer model driven by assimilated meteorological fields". In: *J. Geophys. Res. Atmos.* 106.D11, pp. 12109–12128. DOI: 10.1029/2000jd900839.

Lu, Xiao, Lin Zhang, Yuanhong Zhao, Daniel J. Jacob, Yongyun Hu, Lu Hu, et al. (2019). "Surface and tropospheric ozone trends in the Southern Hemisphere since 1990: Possible linkages to poleward expansion of the Hadley circulation". In: 64.6, pp. 400–409. DOI: 10.1016/j.scib.2018.12.021.

McCarty, Will, Lawrence Coy, Ronald Gelaro, Albert Huang, Dagmar Merkova, Edmond B. Smith, et al. (2016). *MERRA-2 Input Observations: Summary and Assessment*. Technical Report Series on Global Modeling and Data Assimilation, Volume 46. Greenbelt, MD, USA: National Aeronautics and Space Administration.

Mudelsee, Manfred (2003). "Estimating Pearson's Correlation Coefficient with Bootstrap Confidence Interval from Serially Dependent Time Series". In: 35.6, pp. 651–665. DOI: 10.1023/b:matg.0000002982.52104.02.

Nikulin, G. and A. Karpechko (2005). "The mean meridional circulation and midlatitude ozone buildup". In: *Atmos. Chem. Phys.* 5.11, pp. 3159–3172. DOI: 10.5194/acp-5-3159-2005.

Orbe, Clara, Darryn W. Waugh, Paul A. Newman, and Stephen Steenrod (2016). "The Transit-Time Distribution from the Northern Hemisphere Midlatitude Surface". In: *J. Atmos. Sci.* 73.10, pp. 3785–3802. DOI: 10.1175/jas-d-15-0289.1.

Orbe, Clara, Darryn W. Waugh, Huang Yang, Jean-Francois Lamarque, Simone Tilmes, and Douglas E. Kinnison (2017). "Tropospheric transport differences between models using the same large-scale meteorological fields". In: *Geophys. Res. Lett.* 44.2, pp. 1068–1078. DOI: 10.1002/2016gl071339.

Orbe, Clara, Huang Yang, Darryn W. Waugh, Guang Zeng, Olaf Morgenstern, Douglas E. Kinnison, et al. (2018). "Large-scale tropospheric transport in the Chemistry-Climate Model Initiative (CCMI) simulations". In: *Atmos. Chem. Phys.* 18.10, pp. 7217–7235. DOI: 10.5194/acp-18-7217-2018.

Ordóñez, Carlos, David Barriopedro, and Ricardo García-Herrera (2019). "Role of the position of the North Atlantic jet in the variability and odds of extreme PM_{10} in Europe". In: 210, pp. 35–46. DOI: 10.1016/j.atmosenv.2019.04.045.

Peixóto, José P and Abraham H Oort (1983). "The atmospheric branch of the hydrological cycle and climate". In: *Variations in the global water budget*. Springer, pp. 5–65.

Porter, William C. and Colette L. Heald (2019). "The mechanisms and meteorological drivers of the ozone-temperature relationship". In: pp. 13367–13381. DOI: 10.5194/acp-2019-140.

Shen, L., L. J. Mickley, and A. P. K. Tai (2015). "Influence of synoptic patterns on surface ozone variability over the eastern United States from 1980 to 2012". In: 15.19, pp. 10925–10938. DOI: 10.5194/acp-15-10925-2015.

Shindell, D. T., M. Chin, F. Dentener, R. M. Doherty, G. Faluvegi, A. M. Fiore, et al. (2008). "A multi-model assessment of pollution transport to the Arctic". In: *Atmos. Chem. Phys.* 8.17, pp. 5353–5372. DOI: 10.5194/acp-8-5353-2008.

The International GEOS-Chem User Community (2018, October 10). *geoschem/geos-chem: GEOS-Chem 12.0.2 release (Version 12.0.2)*. URL: http://doi.org/10.5281/zenodo.1455215.

Wilks, D. S. (1997). "Resampling Hypothesis Tests for Autocorrelated Fields". In: 10.1, pp. 65–82. DOI: 10.1175/1520-0442(1997)010<0065:rhtfaf>2.0.co;2.

Wilks, Daniel S. (2011). *Statistical methods in the atmospheric sciences*. Elsevier Academic Press. ISBN: 9780123850225.

Woollings, Tim, Abdel Hannachi, and Brian Hoskins (2010). "Variability of the North Atlantic eddy-driven jet stream". In: 136.649, pp. 856–868. DOI: 10.1002/qj.625.

Yang, Huang, Darryn W. Waugh, Clara Orbe, Guang Zeng, Olaf Morgenstern, Douglas E. Kinnison, et al. (2019). "Large-scale transport into the Arctic: The roles of the midlatitude jet and the Hadley Cell". In: *Atmos. Chem. Phys.* 19.8, pp. 5511–5528. DOI: 10.5194/acp-19-5511-2019.

Yu, Karen, Christoph A. Keller, Daniel J. Jacob, Andrea M. Molod, Sebastian D. Eastham, and Michael S. Long (2018). "Errors and improvements in the use of archived meteorological data for chemical transport modeling: An analysis using GEOS-Chem v11-01 driven by GEOS-5 meteorology". In: *Geosci. Model Dev.* 11.1, pp. 305–319. DOI: 10.5194/gmd-11-305-2018.

Zhang, Yuqiang, Owen R. Cooper, Audrey Gaudel, Anne M. Thompson, Philippe Nédélec, Shin-Ya Ogino, and J. Jason West (2016). "Tropospheric ozone change from 1980 to 2010 dominated by equatorward redistribution of emissions". In: *Nat. Geosci.* 9.12, pp. 875–879. DOI: 10.1038/ngeo2827.

Zhuang, Jiawei, Raphael Dussin, André Jüling, and Stephan Rasp (2020). *JiaweiZhuang/xESMF: v0.3.0 Adding ESMF.LocStream capabilities*. DOI: 10.5281/ZENODO.1134365. URL: https://zenodo.org/record/1134365.

Chapter 6

Conclusions

6.1 Summary

This thesis presents four studies that investigate surface-level O_3 and its covariance with temperature and humidity over the Northern Hemisphere through observations and CTM simulations. Elucidating the drivers of O_3 variability and the relationship of O_3 with meteorology is important not only for basic research but also for understanding the impacts of O_3 on human health, the climate, and ecosystems. Our work has uncovered the dominant role of transport in causing day-to-day variations in O_3 and the O_3-meteorology relationships.

Throughout the thesis, we show the skill of the GMI CTM in simulating O_3. As reliable observations are sparse outside of populated regions within developed nations, the use of CTMs like the GMI CTM is necessary to understand O_3 where observations are not available as well as to isolate specific processes responsible for O_3 variability, which cannot be done through observations alone. Our extensive documentation of the model against *in-situ* observations

support its use both for our present work and future tropospheric O_3 studies.

In Chapter 2, we use a suite of sensitivity simulations of the GMI CTM to disentangle the roles of anthropogenic emissions, chemistry, and transport in driving the O_3-temperature relationship. We find excellent agreement between observations and our model simulations. The O_3-temperature relationship is positive and strong in the north of the contiguous U.S., but the strength of the relationship decreases to near-zero values in southern parts of the U.S.. In regions where the O_3-temperature relationship is strongly positive, our sensitivity simulations indicate that $\sim$ 60% of the variability of O_3 and its relationship with temperature is driven by an indirect association with transport. Anthropogenic emissions and processes related to chemistry contribute $\sim$ 10% and $\sim$ 30%, respectively, to the O_3-temperature relationship.

Temperature is linked to O_3 via chemistry and emissions in a direct fashion, rather than the indirect association that connects transport with O_3 and temperature. Thus, suggesting that O_3 will increase (or decrease) in the future based on the historical O_3-temperature relationship together with projected temperature changes is not advised due to the indirect nature of the temperature-transport-O_3 pathway.

In Chapter 3, we investigate a particular transport-related feature, stagnation, that is commonly-invoked as the meteorological prerequisite leading to pollution events and could be responsible for linking temperature and humidity with O_3. Conceptually, stagnation is characterized by a lack of ventilation in the PBL under clear sky conditions, often concurrent with a slow-moving anticyclone. In practice, stagnation is defined with the ASI. We document the

correspondence among temperature, O_3 and $PM_{2.5}$, and the ASI through both their day-to-day correlation and the fraction of concurrent events.

Throughout most of the contiguous U.S., we find a weak correspondence of stagnation with both pollutant and temperature extremes. For example, in the northeastern U.S., 78% (66%) of $PM_{2.5}$ (O_3) events occur under non-stagnant conditions. Similar relationships hold for the rest of the U.S. with the exception of the southeastern U.S., where extreme pollution and stagnation events co-occur with greater likelihood. Chapter 3 indicates that there is a small increase in $PM_{2.5}$ and O_3 concentrations on stagnant days as well as a correspondence on interannual timescales, thus reconciling our study with past work. However, we show that the magnitude of this correspondence is small compared to daily variations in pollutant concentrations and interannual variability. Overall, our results indicate stagnation is not the transport feature that connects the ambient meteorology to O_3 (or $PM_{2.5}$).

We broaden our focus from the U.S. to the entire Northern Hemisphere in Chapter 4 and document the O_3-temperature and O_3-humidity relationships. Positive relationships among O_3, temperature, and humidity hold only in continental mid-latitude regions. At high and low latitudes as well as over the oceans, the O_3-meteorology relationships are weakly positive or even negative, although often statistically insignificant. We return to the sensitivity simulations detailed in Chapter 2 and show that the O_3-meteorology relationships in the Northern Hemisphere stem from an indirect association with transport.

The covariance of O_3 with temperature and humidity is linked to the meridional position of the mid-latitude jet stream. Specifically, when the jet

stream is in a poleward (equatorward) position, there is a significant increase (decrease) of temperature, humidity, and O_3 over the land in the mid-latitudes. Over the oceans, O_3 and the meteorological variables decrease when the jet is poleward, and at high and low latitudes there is generally a weak, insignificant relationship among the jet stream, O_3, and the meteorological variables. We examine a variety of surface-level transport-related features and whether they are (1) connected to the meridional position of the jet stream and (2) important for explaining the daily variability of O_3. Variations in the PBLH, cyclone frequency, and the magnitude of near-surface winds either are not connected to the jet, do not significantly affect surface-level O_3, or both. However, we find the jet stream position affects the O_3-meteorology relationships by altering the near-surface mean meridional flow. When the jet is poleward (equatorward), the mean meridional circulation transports heat, moisture, and O_3 poleward (equatorward). Regions with positive O_3-meteorology relationships (e.g., the continental mid-latitudes) can be viewed as regions where temperature and O_3 or humidity and O_3 respond to jet-induced changes in the mean meridional circulation with the same sign.

While Chapter 4 showed the connections between the jet stream and surface-level O_3-meteorology relationships and hypothesized that changes in the mean meridional circulation were responsible for these relationships, it left several open questions. Why does the sign of the relationships vary between land and oceans and with season? Does the coupling of the jet stream with surface-level O_3 hold for other constituents? Accordingly, Chapter 5 serves as a follow-up to Chapter 4 and answers these questions by simulating a suite of

idealized tracers with different source regions within a CTM.

We find that near-surface concentrations of our idealized tracers and the position of the jet stream are significantly correlated in the mid-latitudes; however, the sign of this correlation in the mid-latitudes depends on the source region. Tracers with source regions $< 40°$N ($> 60°$N) are positively (negatively) correlated with the jet in the mid-latitudes. The relationship between the jet and tracers with source regions at or near the mean position of the jet ($40° < \phi < 60°$N) varies between the land and oceans in the mid-latitudes. As with O_3, near-surface tracer variability is linked to jet-induced changes in the mean meridional circulation. We find that we can interpret spatiotemporal differences in the jet-tracer coupling by relating the background gradient of the tracer with the relationship between the jet and near-surface meridional flow. This chapter answers our original questions regarding the source of the O_3-jet relationship, showing that variations in this relationship are largely due to the latitudinal gradient of O_3 (and its precursors) and the jet's effect on meridional winds at the surface.

6.2 Future Directions

We have identified several outstanding questions that are natural extensions to the research documented in this thesis and should be the attention of future studies:

(1) Part of the attractiveness of the ASI is characterizing air pollution with simple, commonly-measured meteorological parameters. While we ultimately found that the ASI could not explain day-to-day changes in O_3 and $PM_{2.5}$

concentration (Chapter 3), it would be worthwhile to develop an index that could be used to understand historical air pollution variability as well as forecast future air pollution events.

The ASI is based, in part, on the absolute wind speed at 500 hPa. We diagnosed the position of the jet stream by examining winds at this level (i.e., 500 hPa) and found that the jet stream's position was linked to O_3 variability. Building a new index based on this component together with a characterization of the near-surface meridional wind might be promising. In doing so, this new index's relationship with O_3 and $PM_{2.5}$ should be properly vetted to understand the region(s) and season(s) for which it holds.

(2) Although day-to-day variations in anthropogenic NO_x emissions and stagnation cannot explain variations in O_3 or extreme O_3 events, we found that stagnation and NO_x emissions were positively correlated with O_3 on interannual timescales (Chapter 2-3). It is unknown why these variables are connected on interannual timescales but not on daily timescales, and future work could explore this and investigate how interannual variations in stagnation frequency and NO_x are impactful for O_3.

(3) In Chapter 5 we hypothesized that the tracer-jet and O_3-jet relationship could extend to other species with lifetimes that are long enough to undergo synoptic-scale transport. A few potential candidates that meet this criterion are CH_4, CO, and N_2O. If the position of the jet stream is correlated with the daily variability of these other species, it could help to interpret the daily variability in observations and constrain remotely-sensed data.

(4) By uncovering the drivers of historical O_3 variability through GMI

CTM hindcast simulations, we have set the stage to study how the transport features responsible for O_3 variability (i.e., the roles of the jet stream and mean meridional circulation) change in the future. With our findings, future work should focus on how these mechanisms are expected to change throughout the twenty-first century, leveraging climate model output.

Gaige Hunter **Kerr**

PhD Candidate · Air Quality and Atmospheric Sciences

301 Olin Hall, 3400 N. Charles Street, Baltimore, MD 21218

(+1) 920-285-5177 | gaige.kerr@jhu.edu | gaigekerr | @weathergaige

Education

Johns Hopkins University, Department of Earth & Planetary Sciences — *Baltimore, MD*

Ph.D., M.A.; Earth & Planetary Sciences — *2015–2020*

Advisor: Darryn Waugh

Cornell University, Department of Earth and Atmospheric Sciences — *Ithaca, NY*

B.Sc. (*cum laude* with distinction); Atmospheric Sciences — *2011–2015*

Advisors: Art DeGaetano, Gang Chen

Experience

George Washington University, Department of Environmental and Occupational Health — *Washington, DC*

Postdoctoral Scientist — *July 2020–Present*

Advisor: Susan Anenberg

NASA Goddard Space Flight Center — *Greenbelt, MD*

Student research collaborator — *June 2017–Present*

Université de Sherbrooke, Département de géomatique appliquée — *Sherbrooke, QC, Canada*

Intern — *May 2014–Aug 2014*

Advisor: Norm O'Neill

Writing

Refereed

[4] Kerr, G. H., Waugh, D. W., Steenrod, S. D., Strode, S. A., & Strahan, S. E. (submitted), Surface ozone-meteorology relationships: Spatial variations and the role of the jet stream, *J. Geophys. Res.*

[3] Kerr, G. H., Waugh, D. W., Strode, S. A., Steenrod, S. D., Oman, L. D., & Strahan, S. E. (2019), Disentangling the drivers of the summertime ozone-temperature relationship over the United States, *J. Geophys. Res.*, doi.org/10.1029/2019JD030572.

[2] Kerr, G. H., & Waugh, D. W. (2018), Connections between summer air pollution and stagnation, *Environ. Res. Lett.*, *13*(8), 084001, doi:10.1088/1748-9326/aad2e2.

[1] Kerr, G. H., DeGaetano, A. T., Stoof, C. R., & Ward, D. (2018), Climate change effects on wildland fire risk in the Northeastern and Great Lakes states predicted by a downscaled multi-model ensemble, *Theor. Appl. Climatol.*, *131*, 625–639, doi:10.1007/s00704-016-1994-4.

Non-Refereed

[4] Krocak, M. J., Kerr, G. H., & Flournoy, M. D. (2019), Diversity, equity, and inclusion in the atmospheric sciences. An interview with Kevin Petty *Bull. Amer. Meteor. Soc.*, *100*(6), 1126.

[3] Flournoy, M. D., Krocak, M. J., & Kerr, G. H. (2018), An introvert's guide to networking, *Bull. Amer. Meteor. Soc.*, *99*(11), 2379.

[2] Kerr, G. H., Krocak, M. J., Flournoy, M. D., & Knox, J. A. (2018), Weathering together: Building a climate of diverse community perspectives, *Bull. Amer. Meteor. Soc.*, *99*(10), 2150.

[1] Kerr, G. H. (2015), Climate change effects on fire risk in the U. S. Northeast (Honors thesis). Ithaca, NY: Cornell University.

Presentation

Oral

[9] Kerr, G. H., Waugh, D. W. (2020). *Connections between the surface-Level ozone-temperature relationship and the eddy-driven jet stream* Paper presented at the 22nd Conference on Atmospheric Chemistry, American Meteorological Society, Boston, MA.

[8] Kerr, G. H. (2019). *What controls the ozone-temperature relationship? Results from the GMI CTM over the United States.* Paper presented at CCM Meeting, NASA Goddard Space Flight Center, Greenbelt, MD (invited).

[7] Kerr, G. H., Waugh, D. W., Steenrod, S. D., & Strode, S. A. (2019). *Sensitivity of surface-level ozone to temperature-related processes.* Paper presented at the 21st Conference on Atmospheric Chemistry, American Meteorological Society, Phoenix, AZ.

[6] Kerr, G. H., & Waugh, D. W. (2018). *Impacts of emission variability on CTM pollutant representation.* Paper presented at 20th Joint Conference on the Applications of Air Pollution Meteorology with the A&WMA, American Meteorological Society, Austin, TX.

[5] Kerr, G. H., & Waugh, D. W. (2017). *Connections between air pollution and stagnation.* Paper presented at Fall Meeting of the American Geophysical Union, New Orleans, LA.

[4] Kerr, G. H., & Waugh, D. W. (2017). *Modeling of regional air pollution events.* Paper presented at Meteorology And Climate–Modeling for Air Quality Conference, Davis, CA.

[3] Kerr, G. H., & Waugh, D. W. (2017). *Air pollution in the Northeastern United States: Elucidating drivers of $PM_{2.5}$ and O_3 events.* Paper presented at 19th Conference on Atmospheric Chemistry, American Meteorological Society, Seattle, WA.

[2] Kerr, G. H., & DeGaetano, A. T. (2016). *Climate change effects on wildland fire risk in the Northeastern United States and Great Lakes region.* Paper presented at 28th Conference on Climate Variability and Change, American Meteorological Society, New Orleans, LA.

[1] Kerr, G. H., DeGaetano, A. T., & Flannigan, M. D. (2015). *Climate change effects on fire risk in the Northeast U.S.* Paper presented at Northeastern Storms Conference, Saratoga Springs, NY.

Poster

[3] Kerr, G. H., & Waugh, D. W. (2019). *What causes the observed surface ozone-temperature relationship? Effect of the eddy-driven jet on surface-level transport.* Paper presented at Meteorology And Climate–Modeling for Air Quality Conference, Davis, CA.

[2] Kerr, G. H., & Waugh, D. W. (2018). *Temperature-dependent drivers of summer surface-level ozone: Insights from a chemical transport model within the Eastern United States.* Paper presented at iCACGP-IGAC Science Conference, Takamatsu, Kagawa, Japan.

[1] Kerr, G. , Chaubey, J. P., O'Neill, N. T., Hayes, P., & Atkinson, D. E. (2014). *Identification of absorbing organic (brown carbon) aerosols through sun photometry: Results from AEROCAN/AERONET stations in high Arctic and urban locations.* Paper presented at Fall Meeting of the American Geophysical Union, San Francisco, CA.

Honors & Awards

2020	**ASP Postdoctoral Fellowship**, NCAR (declined)
2020	**Earth Institute Postdoctoral Fellowship**, Columbia University (declined)
2018	**Best Student Presentation ($2000)**, Department of Earth & Planetary Sciences, Johns Hopkins University
2018	**J. Brien Key Travel Award ($500)**, Johns Hopkins University
2018	**Jay Fein Scholarship ($1000)**, American Meteorological Society
2017	**Travel Award ($400)**, UC Davis Air Quality Research Center/California Air Resources Board
2017	**Committee on Atmospheric Chemistry Travel Award ($750)**, American Meteorological Society
2016–2018	**Water, Climate, and Health Integrative Graduate Education and Research Traineeship (IGERT) Program**, NSF

Teaching and Outreach

Johns Hopkins Teaching Academy. Completed a three-phase professional development program to learn an overview of pedagogy, acquire teaching and assessment skills, and served as an apprentice with faculty mentors (August 2018–April 2019).

Engineering FUNdamentals. Developed and taught an intensive, two-week curriculum reviewing Algebra, Physics, Trigonometry, and Computer Science for ∼20 Baltimore City high school students (Summers 2016–2019).

Oceans & Atmospheres (AS.270.224): Taught six 50-minute lectures on atmospheric chemistry and tropical meteorology, drafted and graded problem sets, led review sessions and office hours for ∼20 students (Spring 2019).

Introduction to Global Environmental Change (AS.270.103): Held office hours, led review sessions, and compiled relevant supplementary materials for ∼50 students (Fall 2018).

Climate Change and Global Warming (EAS 2680): Graded problem sets and exams (Spring 2015).

Atmospheric Thermodynamics and Hydrostatics (EAS 3410): Integrated key concepts from lectures into weekly problem sets, corrected problem sets and developed grading schemes, and individually met with students needing additional help (Fall 2014).

Chesapeake Climate Action Network: Conducted research on emissions from local incineration facilities and canvassed neighborhoods to amass community support of city-wide bill on fossil fuel transport (2016–present).

Engineers Week: Gave interactive demonstrations on air quality monitoring to middle school students through the Barclay Hopkins STEM partnership (2017).

Leadership

- **Student Member**: AMS Board on Women and Minorities (2017–present)
- **Co-Organizer**: American Meteorological Society (AMS) Student Conference (responsible for organizing a two-day conference for 800+ students and overseeing a budget of ~$120,000; 2018–2020)
- **Member**: AMS Task Force on Professional Conduct (2019–2020)
- **Student Member**: AMS Committee on Meteorological Aspects of Air Pollution (2016–2019)
- **Judge**: AMS Student Conference poster session (2019)
- **Member**: AMS Charles Anderson Award Committee (2019)

Skills

Programming	Python (and data visualization packages; e.g., cartopy, matplotlib, basemap), MatLab, GIS, LaTeX, R
Atmospheric Models	GEOS-Chem, BOXMOX
Languages	English (native), German (proficient), French (basic)

Interests

traveling, hiking, and backpacking • cooking • genealogy • houseplants • classical piano and pipe organ